

# **Investigations on Colloidal Synthesis of Copper Nanoparticles in a Two-phase Liquid-liquid System**

by

**Nafiseh Dadgostar**

A thesis  
presented to the University of Waterloo  
in fulfillment of the  
thesis requirement for the degree of  
Master of Applied Science  
in  
Chemical Engineering

Waterloo, Ontario, Canada, 2008

©Nafiseh Dadgostar 2008

## **AUTHOR'S DECLARATION**

I hereby declare that I am the sole author of this thesis. This is a true copy of the thesis, including any required final revisions, as accepted by my examiners.

I understand that my thesis may be made electronically available to the public.

## Abstract

Synthesis of copper nanoparticles by a colloidal recipe in a two-phase liquid-liquid mixture (toluene/water) was investigated. The synthesis recipe used in this work was originally applied for the fabrication of alkylamine-capped gold nanoparticles. This method involves transferring metal cations from the aqueous layer to the organic one by the phase transfer reagent, tetraoctylammonium bromide, followed by reduction with sodium borohydride in the presence of oleylamine, which was used as the stabilising ligand.

Several modifications were made to the original recipe to produce copper nanoparticles with high degrees of purity and stability. These particles are potentially applicable in various industries and are considered as an alternative for expensive metal nanoparticles, such as gold, silver, and platinum. Due to the high tendency of copper for oxidation, all of the synthesis experiments were carried out in a glove box under the flow of an inert gas ( $N_2$  or Ar). The concentration of  $Cl^-$  was initially increased to form anionic complexes of copper that could later react with the cationic phase transfer reagent. This modification was followed to enhance the efficiency of the transferring step; however, the presence of anion,  $Cl^-$ , at the surface of the synthesized particles was reported to change their properties, as their UV-visible spectra did not show any significant peak including the plasmon absorption band for copper at 560 nm. Moreover, the results of trials, in which the phase transfer reagent was added to the aqueous solution of copper chloride, show that tetraoctylammonium bromide transfers copper cations into the organic phase to some extent even when they are present in the form of cationic complexes. The same observation was reported previously in the literature for silver nanoparticles synthesized by this technique, though the mechanism of this transfer has not been clarified yet. Thus, increasing chloride concentration was eventually ignored.

The decanting of two phases prior to the reduction step was also investigated to examine whether the site of the reduction reaction could be limited to cores of reverse micelles. Discarding the aqueous phase, in order to get rid of copper cations that remained in this layer, resulted in losing excess surfactant; therefore, clusters of agglomerated nanoparticles were produced.

The aggregated nanoparticles, which were fabricated by reducing the decanted organic phase, were heated after the synthesis at  $150^\circ C$  for 30 minutes to obtain a light green solution of nanoparticles. TEM images demonstrated that the result of post-synthesis heating was separated nanoparticles with an average size of about 5 nm. However, further characterization was not possible due to the hydrocarbon impurities. Dodecane, which was employed as the solvent for post-synthesis heating procedure, is

believed to result in these impurities. FTIR-spectroscopy was applied in this work to study the bonding at the surface of the synthesized nanoparticles. Neither the spectra of nanoparticles produced by reducing the decanted organic solution nor those of post-synthesis heated particles showed N-H bands, meaning that they were not capped with the oleylamine hydrophilic head. In spite of the FTIR results, the UV-visible spectra of the heated nanoparticles illustrate that they are stable for more than an hour. Further investigation is required to explain the mechanism by which post-synthesis heating facilitates nanoparticle stabilization.

Duplication of the original recipe for copper in an inert atmosphere resulted in a mixture of assembled layers of separated copper nanocrystals with an average size of  $\sim 5$  nm and aggregated clusters of cubic copper (I) oxide nanoparticles. The possible mechanism for this division is believed to be the presence of the phase transfer reagent capped to the surface of a portion of synthesized particles leading to their metastability. Based on FTIR and UV-visible spectra of the product, the bonding between N-H and the surface of copper nanoparticles did not seem to be strong enough to avoid oxidation and stabilize nanoparticle for a long time. Additional post-synthesis treatments such as heating may affect the stability of these nanoparticles.

## Acknowledgements

I would like to express my gratitude to Professor Dale E. Henneke, my supervisor, for his guidance and financial support throughout the course of my graduate program. I am also grateful to the readers of my thesis, Professor Alexander Penlidis and Professor Neil McManus for their valuable suggestions. Special thanks go to Professor Alexander Penlidis for his encouragement and kind consideration during the hard days of research.

I am glad to get to know two amazing technicians when I started to analyze my samples: Dale Weber at the Biology Department of the University of Waterloo, who trained me to work with TEM, and Fred Pearson at the Canadian Centre for Electron Microscopy (CCEM), who helped me a lot to gather many important data. I appreciate their contribution to my thesis and guidance and sense of humor they offered while working together. I would also like to thank Dr. Ravindra Reddy, who patiently helped me with the FTIR spectroscopy.

I wish to acknowledge all of my friends who supported me along these two years with their kindness and generosity. My special thanks go to Afsaneh Nabifar, my wonderful roommate, and Parisa Sadatmousavi for being great listeners and encouraging me whenever I felt disappointed. I also thank Parisa for her guidance with the UV-visible spectroscopy at Professor Pu Chen's laboratory.

I am deeply indebted to my family for all their love and supports. I would like to thank my parents for their financial assistance. I am incredibly lucky to have such parents who care about their children's education more than anything in their lives. Many thanks to my sisters and brother for their emotional support.

Most importantly, I would like to thank my husband and true love, Roham. He fulfills my life with unconditional love, constant patience, and great deal of understanding. I am extremely grateful for his devotion to our life so that both of us could successfully finish our graduate studies in spite of being far from each other. To Roham, I dedicate this thesis to thank him for everything that he did for me in these two years of our life.

## **Dedication**

*To my husband, Roham.*

## Table of Contents

List of Figures.....	ix
List of Tables.....	xiii
Chapter 1 : Introduction.....	1
1.1 Background for the Study of Copper Nanoparticles.....	1
1.2 Remarkable Properties of Nanoparticles .....	1
1.2.1 Immense Surface Area to Volume Ratio .....	2
1.2.2 Superplasticity of Nanocrystalline Materials.....	2
1.2.3 Enhanced Hardness and Strength for Nanostructured films.....	3
1.2.4 Quantum Confinement Effects .....	3
1.2.5 Optical Properties of Metal Nanoparticles.....	4
1.3 Methods for Producing Copper Nanoparticles .....	4
1.3.1 Vacuum Vapor Deposition (VVD).....	5
1.3.2 Chemical Reduction.....	6
1.3.3 Discharge of Copper Rod Electrodes in a Surfactant Solution: a Combination of Physical and Chemical Processes .....	8
1.4 Agglomeration .....	10
1.5 Properties of the Capping Agent used in this Work .....	12
1.6 Metal Oxidation in Synthesis of Copper Nanoparticles .....	13
1.7 Objectives and Overview of the Thesis .....	14
Chapter 2 : Literature Review.....	16
2.1 Microemulsion (colloidal) synthesis of metal nanoparticles .....	16
2.2 Synthesis of copper nanoparticles in reverse micelles with controlled water content (w) .....	21
2.3 Colloidal Synthesis of metal nanoparticles in a two–phase liquid–liquid system .....	25
Chapter 3 : Experimental Methods .....	29
3.1 Materials .....	29
3.2 Copper Nanoparticle Synthesis.....	29
3.2.1 Original Recipe for Gold Nanoparticles .....	29
3.2.2 Modified Synthesis Procedures .....	31
3.3 Characterization Techniques.....	33
3.3.1 High-Resolution Transmission Electron Microscopy.....	33

3.3.2 Energy-Dispersive X-ray Spectroscopy (EDS).....	36
3.3.3 Ultra Violet – Visible Spectroscopy (UV-Vis).....	37
3.3.4 FTIR Spectroscopy .....	38
Chapter 4 : Results and Discussion.....	39
4.1 Addition of HCl .....	39
4.2 Studies of Cu Reduction in a Glove Box .....	42
4.3 Substituting KCl for HCl .....	43
4.3.1 Procedure .....	43
4.3.2 Characterization Results (TEM image and EDS spectra).....	45
4.4 Decanting the Aqueous Phase prior to the Reduction Step.....	48
4.4.1 Procedure .....	48
4.4.2 Characterization Techniques.....	49
4.5 Post-synthesis Heating .....	59
4.5.1 Principles and Procedure.....	59
4.5.2 Characterization Techniques.....	61
4.6 Duplicating the Colloidal Recipe by Leff and co-workers for Copper .....	75
4.6.1 Procedure .....	75
4.6.2 Characterization Techniques.....	77
Chapter 5 : Conclusions and Recommendations.....	90
5.1 Conclusions.....	90
5.2 Recommendations for Future Work.....	92
References.....	94

## List of Figures

<b>Figure 1.3.1:</b> TEM image showing a section of a long Cu nanowire which exceeds 20 $\mu$ m in length. Scale bar: 2 $\mu$ m (Liu and Bando 2003).....	6
<b>Figure 1.3.2:</b> TEM image of copper nanocubes synthesized by a simple one-pot solution-phase method proposed by Wang <i>et al.</i> (at 140°C, in the presence of PVP and ascorbic acid) (Wang, Chen and Liu 2006).....	7
<b>Figure 1.3.3:</b> SEM image of copper nanoparticles prepared using a procedure similar to that of figure 1.3.2 except reaction system was kept at 25°C for 24h (Wang, Chen and Liu 2006). ....	7
<b>Figure 1.3.4:</b> TEM image (a) and XRD pattern (b) of the spindle-like Cu <sub>2</sub> O/CuO nanostructures produced from copper arc-discharge in deionized water (●:Cu <sub>2</sub> O, ■: CuO) (Xie et al. 2004).....	8
<b>Figure 1.3.5:</b> TEM image (a) and XRD pattern (b) of the products from discharge of Cu in the presence of ascorbic acid (Xie et al. 2004).....	9
<b>Figure 1.3.6:</b> TEM image of an individual spherical nanostructure self-assembled from Cu nanoparticles (Xie et al. 2004). ....	10
<b>Figure 1.4.1:</b> Agglomerated copper nanoparticles using dodecanethiol as the surfactant. ....	11
<b>Figure 1.4.2:</b> Flocculated copper nanoparticles in the presence of oleylamine. ....	12
<b>Figure 2.1.1:</b> Phase diagram of the water – surfactant – oil microemulsion system demonstrating various surfactant aggregate geometries consisting of 1. Spherical micelles. 2. Rod-like micelles. 3. Irregular bicontinuous phase. 4. Reverse cylindrical micelles. 5. Reverse micelles. 6. Hexagonal phase. 7. Cubic phase. 8. Lamellar phase. 9. Reverse cubic phase. 10. Reverse hexagonal phase (Zhang 2003). ....	17
<b>Figure 2.1.2:</b> A Reverse micelle formed by AOT surfactant molecules. Nano-sized water droplets are colloidally dispersed in the organic phase by the surfactant molecules in this form to decrease the free energy of the microemulsion (Salzemann et al. 2004). ....	18
<b>Figure 2.1.3:</b> Illustration of the mechanism for the synthesis of metal nanoparticles in reverse micelles. ....	19
<b>Figure 2.1.4:</b> Mechanism for intermicellar exchange of the water cones of the reverse micelles that were formed by AOT surfactant molecules. This process facilitates the chemical reaction between water soluble reactants A and B to produce C (Kitchens 2004). ....	20
<b>Figure 2.2.1:</b> Molecular structure of Aerosol OT (= AOT = Sodium di-2-ethylhexylsulfosuccinate), used as the surfactant in Pileni et al.'s work (Pileni and Lisiecki 1993; Pileni and Tanori 1995a; Pileni and Tanori 1995b). The dotted lines show the inverted cone geometry of this surfactant (Kitchens 2004).	22

**Figure 2.2.2:** Reaction mechanism for the synthesis of copper nanoparticles upon chemical reduction of AOT-derivatised copper ions followed by particle growth as a result of the dynamic intermicellar exchange of the contents of reverse micelles cores (Kitchens 2004)..... 23

**Figure 2.3.1:** Diagram shows two steps of the colloidal synthesis technique that was first established for synthesizing thiol-stabilised gold nanoparticles in a two-phase liquid/liquid system (modified image of Swami *et al.*'s work(Swami et al. 2004))..... 26

**Figure 3.3.1:** Abbe's theory of image formation in a one-lens transmission electron microscope. This theory is for a general optical system in TEM (Wang 2000)..... 35

**Figure 3.3.2:** Schematic diagrams showing how the waves leaving the specimen in the same direction (or angle  $\theta$  with the optic axis) are brought together by the objective lens at a point on the back focal plane (Wang 2000)..... 35

**Figure 3.3.3:** Signals generated when high energy electrons interact with a thin specimen. The directions shown for these signals schematically represent the regions at which the signals are relatively stronger and detected (Gai and Boyes 2003). ..... 37

**Figure 4.2.1:** Schematic view of the oxidation mechanism during the synthesis of copper nanoparticles when the system was exposed to air during the reduction step..... 43

**Figure 4.3.1:** TEM results for the modified version of the Leff *et al.*'s recipe in which KCl was added to form anionic complex of copper. Scale bar: 20 nm. .... 46

**Figure 4.3.2:** EDS data for the synthesized nanoparticles that are apparently copper. Using the phase transfer reagent,  $N(C_8H_{17})_4Br$ , allows Br to be traced in this diagram..... 46

**Figure 4.3.3:** A cluster of agglomerated copper nanoparticles formed as the result of inefficient transformation of cations into the organic phase. Leff *et al.*'s recipe was followed with using dodecanethiol ( $C_{12}H_{25}SH$ ) as the surfactant. The phase that first turned dark was the aqueous one... 48

**Figure 4.4.1:** Clusters of copper nanoparticles synthesized by reducing the decanted organic phase.51

**Figure 4.4.2:** A part of a cluster that is mostly made of agglomerated copper nanoparticles. Few nanoparticles, however, are not diffused to the neighboring particles and are isolated..... 51

**Figure 4.4.3:** FTIR spectra of neat oleylamine and copper nanoparticles synthesized by reducing the decanted organic phase. .... 52

**Figure 4.4.4:** UV-visible absorption spectra of reaction mixture at various times of oxidation accompanying a change in particle morphology of the  $Cu_2O$  nanocrystals: (a) 30, (b) 60, (c) 90, (d) 120, (e) 150, (f) 180, and (g) 210 min and (h) after aging for 3 days (Ng and Fan 2006)..... 54

<b>Figure 4.4.5:</b> UV-visible absorption spectra of the nanoparticles synthesized by reducing the decanted organic layer: (a) just after the toluene solution of the particles was exposed to air, after (b) 45 min, and (c) 90 min of exposure to air.....	55
<b>Figure 4.4.6:</b> (a) TEM image of Cu <sub>2</sub> O triangular nanoplates synthesized by Ng <i>et al.</i> 's method for oxidation time = 210 min. (b) Single triangular nanoplates (Ng and Fan 2006).....	56
<b>Figure 4.4.7:</b> Absorption spectrum of copper particles synthesized in nonionic water-in-oil microemulsions by reducing CuCl <sub>2</sub> with NaBH <sub>4</sub> (Qi, Ma and Shen 1997).....	57
<b>Figure 4.5.1:</b> Schematic view of the post-synthesis heating step in which the synthesized copper nanoparticles become more stable after uncapped surfactant molecules have had the chance to bind to the nanoparticle surface by their hydrophilic head.....	60
<b>Figure 4.5.2:</b> TEM images of copper nanoparticles after half an hour post-synthesis heating at 150 °C showing how arrays of separated nanoparticles were formed (a). The particles were almost spherical, with an average size ~ 5 nm (b).....	62
<b>Figure 4.5.3:</b> The result of gas chromatography (GC) for hexane used as the solvent for the post-synthesis heated nanoparticles.....	63
<b>Figure 4.5.4:</b> The overall TEM image of the post-synthesis heated sample taken by HRTEM microscope (a) and the EDS spectrum of nanoparticles (b) prior to the charge cloud built-up.....	64
<b>Figure 4.5.5:</b> TEM image taken by HRTEM microscope of the post-synthesis heated nanoparticles after the formation of the charge cloud (a) and EDS spectrum of the black area (charge cloud) caused by the hydrocarbon impurities (dodecane) on the surface of the specimen (b).....	65
<b>Figure 4.5.6:</b> HRTEM image of a single copper nanocrystal that was heated after the synthesis in dodecane at 150 °C for half an hour (a) and the histogram that facilitates the measurement of the <i>d</i> spacing corresponds to the particle crystalline structure (b).....	69
<b>Figure 4.5.7:</b> HRTEM image of a single copper nanocrystal (a) and the histogram of the white box area shown in the image (b).....	70
<b>Figure 4.5.8:</b> SAED pattern obtained for the sample of the post-synthesis heating procedure.....	71
<b>Figure 4.5.9:</b> FTIR spectra of oleylamine and copper nanoparticles that were heated after the synthesis in dodecane at 150°C for half an hour.....	72
<b>Figure 4.5.10:</b> FTIR spectra of dodecane and nanoparticles that were dissolved in dodecane and heated after the synthesis.....	72
<b>Figure 4.5.11:</b> UV-visible absorption spectra of post-synthesis heated nanoparticles (a) just after the hexane solution of nanoparticles was exposed to air and (b) after 100 min of exposure to air.....	74

**Figure 4.6.1:** TEM image of copper nanoparticles synthesized by duplicating Leff et al.'s recipe in an inert atmosphere (N<sub>2</sub> or Ar). ..... 78

**Figure 4.6.2:** (a) A self-assembled layer of fairly separated copper nanoparticles. (b) A closer view of these particles shows that the result was spherical nanoparticles with an average particle size of ~ 5 nm. .... 79

**Figure 4.6.3:** (a) TEM image of agglomerated copper nanoparticles after being stored for two weeks in the liquid nitrogen dewar. (b) EDS spectroscopy of the cluster of aggregated nanoparticles. .... 81

**Figure 4.6.4:** (a) HRTEM image of one of few separated copper nanoparticles with no case of agglomeration after two weeks of storage in the liquid nitrogen dewar. (b) EDS spectroscopy of the same area. .... 82

**Figure 4.6.5:** (a) HRTEM image of a separated copper nanoparticle. The nanocrystal is shown with a circle. (b) Histogram of the area "a" shown in the HRTEM image. .... 84

**Figure 4.6.6:** (a) HRTEM image of a cluster of aggregated nanocrystals. (b) Histogram of the area "A" shown with a circle in the HRTEM image. .... 85

**Figure 4.6.7:** FTIR spectra of copper nanoparticles synthesized by duplicating Leff et al.'s recipe in an inert atmosphere. .... 86

**Figure 4.6.8:** FTIR spectra of pure oleylamine in 1000-3500 cm<sup>-1</sup> region (Shukla et al. 2003). The bands corresponding to N-H are marked. .... 87

**Figure 4.6.9:** UV-visible spectra of the copper nanoparticles synthesized by duplicating the Leff et al.'s method in an inert atmosphere: (a) just after the hexane solution of the nanoparticles exposed to air and (b) after 45 min exposure to air. .... 89

## List of Tables

<b>Table 1-1:</b> Physical properties and chemical structure of oleylamine. ....	13
<b>Table 4-1:</b> Concentration of chemical reagents used for the modified recipe with HCl.....	40
<b>Table 4-2:</b> Concentrations of the chemical reagents used for the modified recipe with KCl.....	44
<b>Table 4-3:</b> Miller indices and interplanar spacings of face-centred cubic copper (Andrews, Dyson and Keown 1971) .....	66
<b>Table 4-4:</b> Miller indices and interplaner spacings of cubic copper (I) oxide (Cu <sub>2</sub> O) (Chiang et al. 2000) .....	67
<b>Table 4-5:</b> Concentrations of the chemical reagents used in duplicating Leff <i>et al.</i> 's recipe. ....	76



# Chapter 1: Introduction

## 1.1 Background for the Study of Copper Nanoparticles

Metal and semiconductor nanoparticles have drawn lots of attention throughout recent decades due to their size and shape-dependent physical and chemical properties. The atomic properties of a particular material may differ considerably from those of the bulk solid state (Petit et al. 1999). Due to the quantum effect, the properties of nanoparticles are tunable by both the particle size and the surface morphology (Chen and Sommers 2001; Haberland 1994; Hayat, M. A. (ed.) 1989; Schmid 1994; Turton 1995). Therefore, nanoparticles can be thought as members of a material transition region.

Metals constitute a wide class of catalysts, and since surface area is a critical factor in catalysis, metallic nanoparticles with immense surface area to volume ratio have been intensely investigated (Lisiecki and Pileni 1993). Among them, copper and its alloy in nanometric sizes have been applied more often in catalysis (e.g., water – gas shift catalysts and gas detoxification catalysts (Barrabés et al. 2006; Mott et al. 2007; Ressler et al. 2005; Vukojević et al. 2005). Controlling the size, shape, and surface property of nanoparticles is crucial to exploring copper-based catalysis (Hoover et al. 2006; Niu and Crooks 2003). Copper nanoparticles have also been considered (Hoover et al. 2006; Niu and Crooks 2003) as an alternative for gold, silver and platinum nanoparticles in many other areas, such as thermal conducting and microelectronics (Eastman et al. 2001; Lu, Sui and Lu 2000). For instance, in the microfabrication of conductive features such as electrodes, conductive lines, and interconnects, ink-jet printing technology has recently been applied as a promising alternative to traditional lithography. So far, noble metals such as gold and silver have mainly been utilized in printing highly conductive elements in electronic devices. Considering the high cost of these metals, copper as a cheap and conductive material is more favorable for this approach (Jeong et al. 2008).

## 1.2 Remarkable Properties of Nanoparticles

Nanoparticles exhibit many unique properties, for which they are intensely being studied in a number of research fields. For example, they have very high surface area to volume ratio compared to bulk material. Room-temperature superplasticity in nanocrystalline metals facilitates the fabrication process for producing components with complex shapes. Nanoparticles can also enhance strength and uniformity of composite materials. Lastly, they show quantum confinement effects that form the basis in developing high technology devices.

### 1.2.1 Immense Surface Area to Volume Ratio

Materials in nanometric sizes have an extremely high surface area to volume ratio. If we assume that these particles are spherical, the surface area to volume ratio can be derived from the following equation:

$$\frac{S}{V} = \frac{4\pi r^2}{\frac{4}{3}\pi r^3} = \frac{3}{r} \quad 1.2.1$$

Therefore,  $\frac{S}{V} \propto \frac{1}{r}$ , and decreasing the particle radius increases the surface area to volume ratio. As we get to the nanometer regime, a significant increase in the surface area is observed. For instance, 1 cm<sup>3</sup> of 1 nm particles would have an active surface area around 100 m<sup>2</sup> (Ichinose et al. 1988). In applications in which surface area plays a key role, such as catalysis and thermal conducting, nanoparticles can offer several benefits over current technologies. Maxwell's model (Maxwell 1904) predicts that the effective thermal conductivity of suspensions containing spherical particles increases with the volume fraction of the solid particles. Since heat transfer takes place at the surface of the particles, it is preferable to use particles with a large surface area to volume ratio. Thus, if nanometer-sized particles could be suspended in traditional heat transfer fluids, a new class of engineered fluids with high thermal conductivity, called "nanofluids", could be fabricated (Choi 1995; Eastman et al. 2001). Eastman et al. (2001) showed that nanofluids containing copper nanoparticles further improve thermal conductivity enhancements when compared to nonparticles-containing fluids or nanofluids containing metal oxide particles (i.e. CuO, Al<sub>2</sub>O<sub>3</sub>).

### 1.2.2 Superplasticity of Nanocrystalline Materials

Plastic deformation occurs at higher temperatures when atomic diffusivity is significantly increased either at grain boundaries or inside the lattice. As a result, diffusion creep becomes a dominant mechanism. The diffusion creep rate ( $\dot{\epsilon}$ ), which is dominated by grain boundary diffusion, is related to grain size by the following equation:

$$\dot{\epsilon} = \frac{B\Omega\sigma\delta D_{gb}}{d^3 kT}; \quad 1.2.2$$

where  $\sigma$  is tensile stress,  $\Omega$  is atomic volume,  $d$  is average grain size (diameter),  $B$  is a numerical constant,  $D_{gb}$  is grain boundary diffusivity,  $\delta$  is grain boundary thickness, and  $k$  is Boltzmann's constant.

Based on this relation, we can say that diffusion creep may be enhanced when grain size is reduced and/or grain boundary diffusivity is enhanced (Lu et al. 2000). A decade ago, different studies resulted in a prediction that we would possibly have high creep rates and large-scale deformation for nanocrystalline materials, in which the crystallite size is in the nanometer regime, at much lower homologous temperatures (Chokshi et al. 1989; Karch et al. 1987). Consequently, ductile ceramics and diffusional creep of pure metals would be feasible even at room temperatures (Chokshi et al. 1989). In agreement with these studies, Lu *et al.* (2000) reported an extreme extensibility (elongation exceeds 5000%) without a strain hardening effect at room temperature for a bulk nanocrystalline pure copper with high density, which was synthesized by electrodeposition. Innovating material processing techniques by means of superplastic deformation of nanocrystalline metals will be beneficial in many fields such as micromachining and electronics.

### **1.2.3 Enhanced Hardness and Strength for Nanostructured films**

Nanostructured films have very low residual stress due to their fine grain structure. Grain boundaries, the interfaces between single crystal grains, are high-energy sites that act as irregularities in the surfaces between grains. Nanosized grains provide considerably more grain boundaries per unit volume than conventional films. Grain boundaries are effective barriers to crack propagation and dislocation motion, which result in material failure (Henneke 2001). Therefore, as we decrease the size of crystalline material from micro to nano regime, significant increases in hardness and strength will be achieved. Interestingly enough, it has been found that sometimes the strength of nanocrystalline material is five times greater than that of microcrystalline material (Weertman 1993). Nanoparticles can be applied to produce a new class of ceramics that are stronger, more ductile, and less brittle (Siegel and Fougere 1994).

### **1.2.4 Quantum Confinement Effects**

Metal and semiconductor nanoparticles may show quantum confinement effects, which arise because in such small particles, the electronic energy levels do not form a continuous set but are discrete in nature (Chakravorty and Giri 1993). If we excite electrons in nanoparticles, the emitted light would have a size-dependent frequency. For smaller nanoparticles, we get higher-frequency light. Behaving like quantum dots, nanoparticles can be used in a variety of technologies including sensors, memory applications, and electronics (Wang and Gao 2007).

### **1.2.5 Optical Properties of Metal Nanoparticles**

An interesting aspect of metal nanoparticles is that their optical properties depend strongly on the particle size and shape. As an example, bulk gold looks yellowish in reflected light, while thin gold films look blue in transmission. This blue color steadily changes to orange as the particle size is decreased to  $\sim 3$  nm. These effects are the result of changes in the surface plasmon resonance (Kreibig and Vollmer 1996), the frequency at which conduction electrons oscillate in response to the alternating electric field of incident electromagnetic radiation. Nevertheless, only metals with free electrons such as Au, Ag, Cu, and alkali metals have plasmon resonance in the visible spectrum, which causes such intense colors (Liz-Marzán 2004). The oscillation wavelength depends on a number of factors, including particle size and shape and the nature of the surrounding medium (Mulvaney 1996). The average distance between neighboring metal nanoparticles is also important (Ung et al. 2001). Accordingly, the spectral features of isolated particles are different from those of closely packed nanoparticles. These linear optical properties of metal nanoparticles have been widely applied in optical filters and sensors.

### **1.3 Methods for Producing Copper Nanoparticles**

Copper nanoparticles have been synthesized via various techniques, typically categorized as physical and chemical processes (Feldheim and Foss 2002; Siegel et al. 1999). Physical methods, such as proton irradiation (García-Santibañez et al. 2000), laser ablation (Yeh et al. 1999), vacuum vapor deposition (Liz-Marzán 2004), and radiation methods (Joshi et al. 1998) are capable of producing a wide range of metal nanoparticles with little effort being required to modify them for each material; however, the quality of produced particles is not as high as chemically synthesized ones. These physical methods usually require expensive vacuum systems to generate plasmas.

In chemical synthesis techniques, we can control the growth and assembly of metal nanoparticles by optimizing reaction parameters, such as temperature and the concentration of surfactant, capping agent, solvent, and precursor (Xie et al. 2004). Thus, the synthesized nanoparticles would have narrow size distribution. Chemical routes seem to be appropriate for lab-scale studies because scaling up these methods is not considered to be economical. Microemulsion (colloidal) techniques (Lisiecki and Pileni 1993; Pileni et al. 1999), sonochemical reduction (Kumar et al. 2001), and chemical reduction (Wang et al. 2006; Wu and Chen 2004) are examples of the chemical approach.

The following sections provide detailed examples of each approach, and the colloidal synthesis techniques are further discussed in Chapter 2.

### 1.3.1 Vacuum Vapor Deposition (VVD)

Due to its high electrical conductivity, copper wire is most commonly used; no other metal can be assumed to play such a vital role in various electronic applications, from electric power leads to interconnect in electronic circuits. As the size of electronic devices is rapidly decreasing, copper nanorods and nanowires may play an essential role in the future generation of electronic nanodevices. So far, copper nanorods and nanowires have been synthesized by reducing copper compounds (Pileni and Tanori 1995a; Tanori and Pileni 1997) and electrochemical deposition (Molares et al. 2001a; Molares et al. 2001b). The main disadvantages of these methods are low yield and producing defected nanoparticles. Vacuum vapor deposition (VVD), pioneered by Liu and Bando (2003), is a one-step procedure that only involves copper vapor generation and re-deposition on a substrate under very low pressure or vacuum conditions. The copper nanorods and nanowires produced by this method are free of defects and uniform in diameter. Moreover, these nanoparticles can be synthesized in large quantities (high yield).

This novel approach was discovered during in-situ observation in a transmission electron microscope (TEM), when a copper grid was heated using a Gatan TEM holder. Although the melting point of copper is 1083°C, copper starts to evaporate at around 800°C under very low pressure (Liu et al. 2002). The copper vapor generated eventually deposits and grows into the shape of a rod at a relatively low temperature area, such as amorphous carbon film in the absence of any catalyst. As can be seen in Figure 1.3.1, the diameter of the copper nanorods is in the range of 50-100 nm and they are defect-free.

A carbon film seems to be a proper substrate for copper vapor deposition and re-nucleation. Liu and Bando (2003) found that favourite sites for copper deposition and re-nucleation are at the edges of the holes in the carbon film where the rough surface might have assisted the nucleation. This method can be applied to synthesize nanorods and nanowires of other metals, such as silver and gold, metal alloys, and even semiconductors.

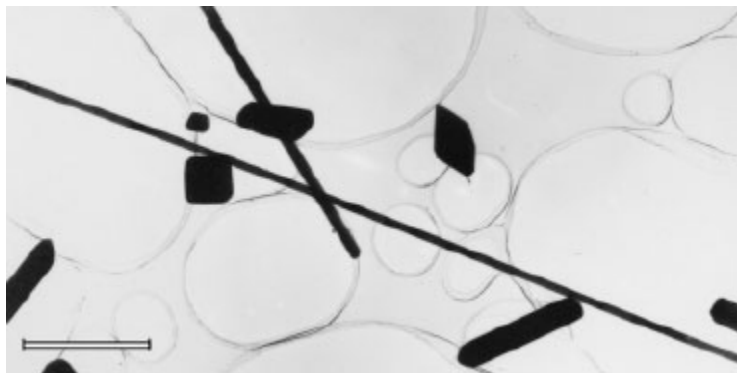


**Figure 1.3.1** TEM image showing a section of a long Cu nanowire which exceeds 20 $\mu\text{m}$  in length. Scale bar: 2 $\mu\text{m}$  (Liu and Bando 2003).

### 1.3.2 Chemical Reduction

In contrast to microemulsion systems, nanoparticles are synthesized in one phase in which the metal salt was initially dissolved. This method is a simple one-pot solution-phase method for synthesis of a variety of metal nanoparticles, including copper nanocrystals. Copper salt and reducing agent are injected in the same solvent in the presence of a stabilizer. Wang *et al.* (2006) reported synthesis of copper nanocubes with an edge length in the range of  $100 \pm 25$  nm. These particles were produced by using ascorbic acid as a reducing agent and poly(vinylpyrrolidone) (PVP) as a capping agent. The solvent used during the procedure was ethylene glycol (EG) because of its relatively high boiling point as the reaction temperature was set at 140°C. To avoid copper oxidation, a small amount of the ascorbic acid was added into the mixture, while cooling the final reddish brown solution to 80°C. Based on these studies, the reaction temperature and additives are the factors affecting on the shape of copper nanoparticles.

High reaction temperature is required to provide enough energy for the growth of nanocubes. Both the dissolution of small Cu nanoparticles and the diffusion of Cu atoms on the surface of Cu nanoparticles call for a relatively high temperature. Figure 1.3.2 shows Cu nanocubes fabricated at 140°C with a size of  $100 \pm 25$  nm, while most of synthesized nanoparticles at 25°C were smaller than 30 nm (Figure 1.3.3).

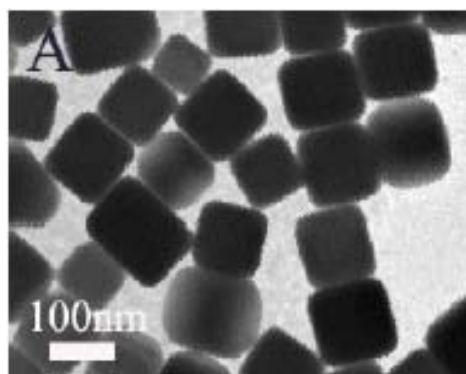


**Figure 1.3.2** TEM image of copper nanocubes synthesized by a simple one-pot solution-phase method proposed by Wang *et al.* (2006) at 140°C, in the presence of PVP and ascorbic acid.

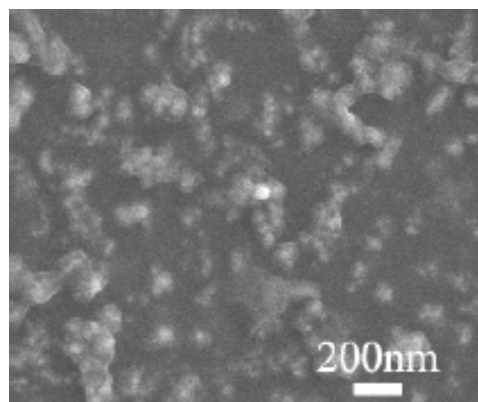


**Figure 1.3.3** SEM image of copper nanoparticles prepared using a procedure similar to that of figure 1.3.2 except reaction system was kept at 25°C for 24h (Wang *et al.* 2006).

The surface-regulating polymer (PVP) is considered not only as a stabilizer but also as the shape controller. The selective interaction of particles with PVP may lead to the formation of copper nanocubes. Wang *et al.* (2006) suggested that the introduction of PVP to the system could have enhanced the growth rate along the [001] direction and/or reduced the growth rate along the [111] direction so that PVP played a key role in nanocube formation. Shape-controlled synthesis of copper nanoparticles in one-phase liquid systems can also be partially achieved by this method.

### 1.3.3 Discharge of Copper Rod Electrodes in a Surfactant Solution: a Combination of Physical and Chemical Processes

Combinations of physical and chemical processes have been developed as new flexible methods that take advantage of simultaneous co-existence of both physical and chemical approaches during nanoparticle synthesis. Submerging discharged electrodes into liquid (also called arc-discharge in liquid phase) is considered a promising technique in this field. This method was used to fabricate various metal nanoparticles. For example, Ag nanowires were produced in a discharge between silver nitrate solution and silver electrode placed slightly above the liquid surface (Zhou et al. 1999).

Xie *et al.* (2004) applied this process and synthesized 10-15 nm Cu particles by discharging bulk rod in water or aqueous cetyltrimethylammonium bromide (C-TAB)/ascorbic acid solution under non-vacuum conditions. Two copper rods were used as electrode and reactant for nanoparticle production. When an alternating electrical source was applied to these electrodes, pulsed arc-discharge appeared at the gap between the ends of two electrodes in the liquid phase. Although copper has a melting point of 1083°C, it was transformed from bulk to nanometer scale in the pure water at room temperature by arc-discharge. Nanoparticles are formed in the plasma zone in the electrode gap surrounded by gas bubbles (Sano et al. 2002). The gas bubbles that are formed by the liquid vaporization under arc-discharge high temperature (around 4000 K) condition act as microwater-cooling reaction chambers. The main role of these chambers is enabling rapid quenching of the Cu plasma vapor produced in the arc-discharge to synthesize nanoparticles. Xie *et al.* (2004) also investigated the role of each liquid in this process. In the absence of ascorbic acid, spindle-like nanostructures of CuO/Cu<sub>2</sub>O were produced (see TEM and XRD results in Figure 1.3.4) because the surface of fresh copper nanoclusters was reactive and subject to oxidation. Ascorbic acid, as protective agent, was added to avoid oxidation, and the XRD pattern in Figure 1.3.5 proves that the horned nanostructures were pure Cu. However, after 10 days of aging in the air, Cu nanostructures would be gradually oxidized and their colloidal color changed from red to black.

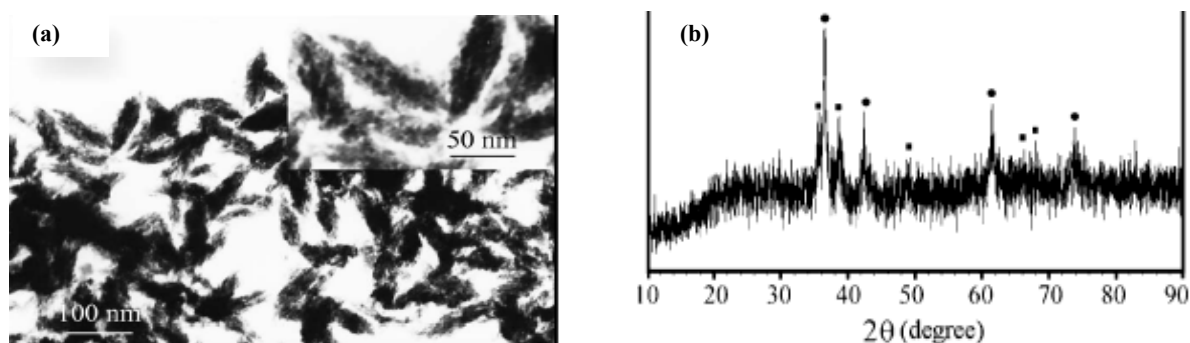


**Figure 1.3.4** TEM image (a) and XRD pattern (b) of the spindle-like Cu<sub>2</sub>O/CuO nanostructures produced from copper arc-discharge in deionized water (●:Cu<sub>2</sub>O, ■: CuO) (Xie et al. 2004).

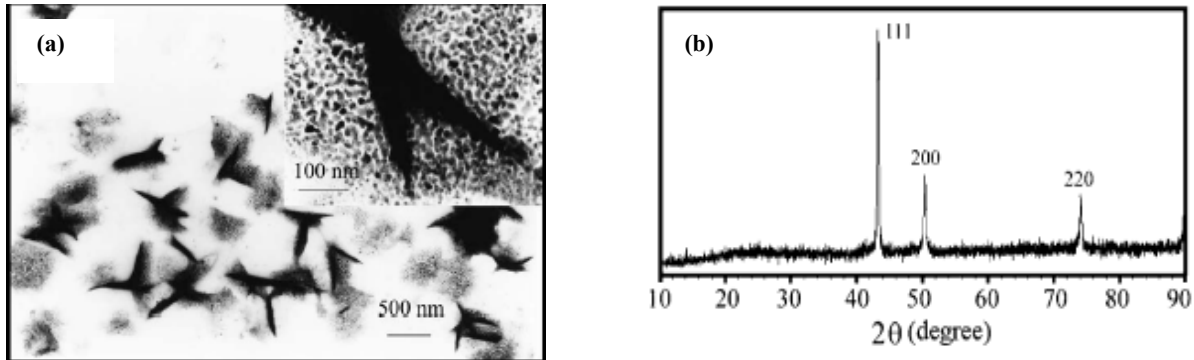


**Figure 1.3.5** TEM image (a) and XRD pattern (b) of the products from discharge of Cu in the presence of ascorbic acid (Xie et al. 2004).

Self-assembly of copper nanoparticles in this process was investigated by replacing the deionized water with a traditional surfactant, e.g. CTAB, which has been greatly utilized for controllable growth of metal nanomaterials with different shapes (Jana et al. 2001; Tanori and Pileni 1997). In the presence of CTAB, the surface of fresh copper nanostructures, which was subject to coalescence due to unsaturated valences, would be covered with a CTAB layer to lower the surface tension and stabilize the unstable nanoclusters (Chen et al. 2002; Chen and Carroll 2002). This stability is provided by the strong hydrophobic interactions between long alkyl chains on neighboring particles in an assembled structure. Figure 1.3.6 shows the TEM image of one of the synthesized nanostructures, which were in the range of 700 nm to 1  $\mu\text{m}$ . This self-assembled structure is made of 5-35 nm pure copper nanoparticles.

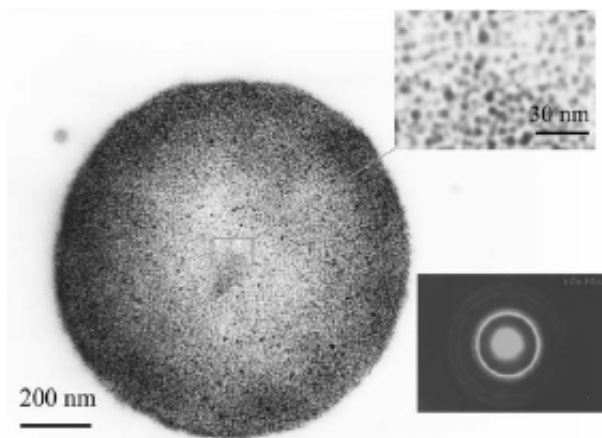


**Figure 1.3.6** TEM image of an individual spherical nanostructure self-assembled from Cu nanoparticles (Xie et al. 2004).

Synthesis and self-assembly of three-dimensional (3D) structures of metal nanoparticles have been mostly approached via chemical routes (Naka et al. 2002; Selvan et al. 1998; Vidoni et al. 1999). Following this technique, 3D copper spherical structures can be fabricated by means of Cu arc-discharge in liquid, a method that has a combination of properties from both physical arc-discharge and chemical solution reaction.

#### **1.4 Agglomeration**

An important challenge in any nanofabrication technique is agglomeration. Agglomeration is an irreversible fusing of individual nanoparticles when they are free to contact each other, which leads to formation of fractal aggregates. This phenomenon should be avoided since most of desirable properties of nanoparticles are destroyed after they become agglomerated. One way to impede agglomeration is by providing a steric barrier by introducing a capping molecule to the surface of the nanoparticle before agglomeration can occur. Well-capped nanoparticles are no longer at risk of agglomeration. The properties of the capping agent used in this research can be found in Section 1.5.

Another typical phenomenon during nanoparticle synthesis is flocculation. Capped nanoparticles may get fairly close to each other and form clusters, called “flocs”. In this case, individual nanoparticles are insulated from each other by the capping agent, but they are close enough to be considered as a group. “Flocculents” or “flocs” can be re-dispersed, while agglomerated nanoparticles are permanently fused and can no longer be separated. Flocculation can be applied to sediment nanoparticles in colloidal solutions. To differentiate between agglomerated and flocculated nanoparticles, Figure 1.4.1 and Figure

1.4.2 should be contrasted. In Figure 1.4.1, agglomerated copper nanoparticles synthesized by a microemulsion recipe that was reported by Leff *et al.* (1996) when using dodecanethiol as surfactant are shown. An image of flocculated copper nanoparticles synthesized by the same method in the presence of oleylamine as surfactant can be seen in Figure 1.4.2.

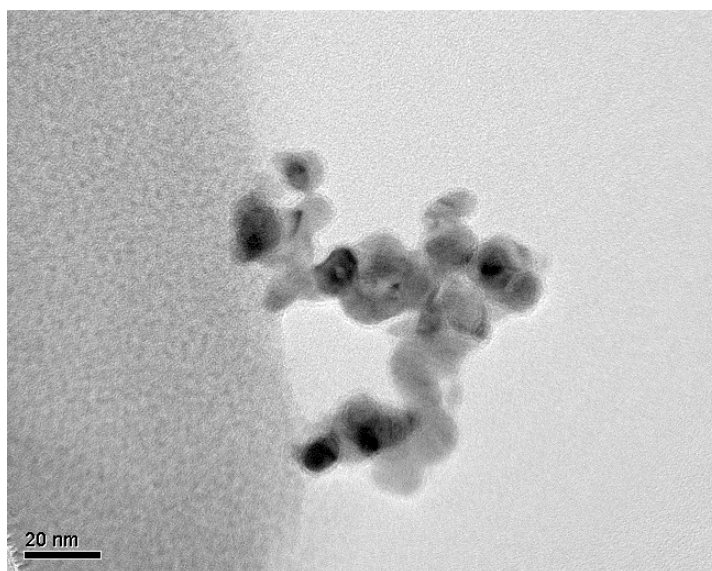


**Figure 1.4.1** Agglomerated copper nanoparticles using dodecanethiol as surfactant.

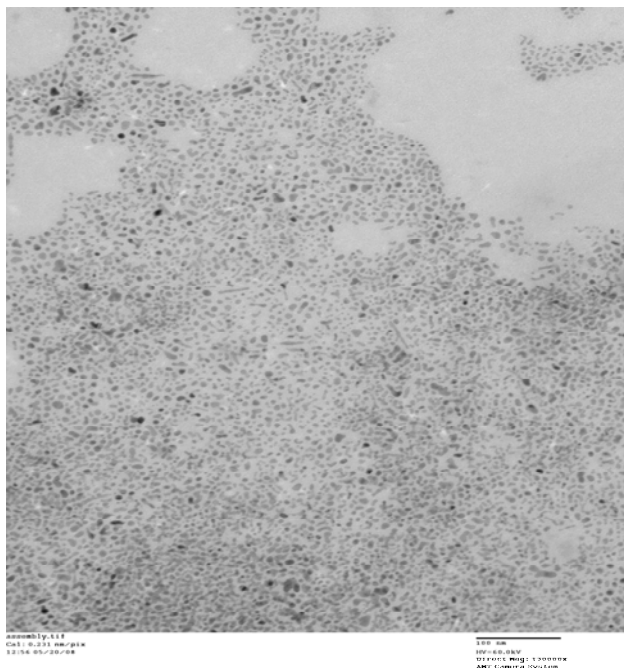


**Figure 1.4.2** Flocculated copper nanoparticles in the presence of oleylamine.

### **1.5 Properties of the Capping Agent used in this Work**

A large group of surfactants has been applied in various nanosynthesis recipes to provide the steric barrier. Any sufficiently large, quasi-polar, organic molecule can play the capping role in producing nanoparticles. However, the type of nanoparticles changes the performance of different surfactants due to the strength of the bonding between the surface of the nanoparticle and one end of the surfactant (Leff et al. 1996). Surfactants are amphiphilic compounds, meaning that they have a hydrophilic head and a hydrophobic tail. The head produces an image charge on the nanoparticle surface, while the hydrophobic tail provides the steric repulsion to stop agglomeration.

We used oleylamine, a linear alkylamine, to synthesize non-agglomerated copper nanoparticles. The chemical structure of oleylamine and its physical properties are listed in Table 1-1.

Table 1-1 Physical properties and chemical structure of oleylamine.

Property	Value
Molecular Weight	267.49 [g/mol]
Boiling Point	348-350 °C
Melting Point	18-26 °C
Density at 25°C	0.813 [g/ml]
Viscosity	N/A
Solubility	alcohols and chloroform
Chemical Structure:	

## 1.6 Metal Oxidation in Synthesis of Copper Nanoparticles

Although copper is one of the most widely used materials in various applications, its synthesis in nano sizes is challenging due to its high tendency for oxidation. Unlike gold and silver, copper is extremely sensitive to air, and the oxide phases are thermodynamically more stable (Jeong *et al.* 2008). Therefore, the formation of a surface oxide layer on copper nanoparticles is inevitable. The presence of copper oxides on the surface of nanoparticles is not desirable for many industries, such as electronics that count on copper as a good alternative for current expensive metals. The electrical conductivity of copper nanoparticles decreases dramatically if they become impure with oxide phases. One can rarely find a method in literature that produces pure copper nanoparticles, unless the whole procedure was done under an inert atmosphere (Chen and Sommers 2001; Mott *et al.* 2007; Salzemann *et al.* 2004). Khanna *et al.* (2007) described their achievement in synthesis of pure copper nanoparticles by reducing copper salt with sodium formaldehyde sulfoxylate (SFS) in the presence of carboxylic acids or their salts as the surfactant. However, they did not investigate the stability of these prepared nanoparticles after they were exposed to air for several days. Moreover, it is unclear by what mechanism carboxylic acid is preventing oxidation when, by contrast, a protecting polymer such as poly(vinyl alcohol) results in the formation of a mixture of Cu<sub>2</sub>O and Cu under the same experimental conditions.

Another approach for dealing with metal oxidation is controlling the thickness of the surface oxide layer. This novel preparation technique, introduced by Jeong *et al.* (2008), reduces surface oxidation during Cu

nanoparticle synthesis through the use of polymeric capping agents, and provides a great control on the thickness of this layer by setting the molecular weight of the polymer. Polymers with a higher molecular weight are more densely packed on the surface of copper nanoparticles; hence, a thinner oxide layer forms.

In this work, the whole nanoparticle fabrication was performed in a glove box using an inert gas (N<sub>2</sub> or Ar) to avoid oxidation during synthesis. The prepared copper nanoparticles were immediately stored in a liquid nitrogen dewar so that they were kept away from oxygen for a longer time. However, for different analytical methods, they were usually exposed to air. Characterization and properties of these copper nanoparticles will be discussed further in Chapter 4.

## 1.7 Objectives and Overview of the Thesis

Copper nanoparticles are potentially applicable in many different industries and if one can synthesize these particles with high degree of stability and purity, they can be cheap alternatives for noble and expensive metal nanoparticles such as gold, silver, and platinum. Among various synthesis techniques proposed for copper, microemulsion (colloidal) techniques are most frequently investigated because of their many advantages for growing single crystalline metal nanoparticles while controlling their size and shape. Also, these methods are less likely to produce agglomerated nanoparticles since they are surfactant-routed. In some cases, the presence of a proper surfactant helps to avoid (Khanna et al. 2007) or control (Jeong et al. 2008) oxidation.

In this work, we investigated the possibility of producing alkylamine-capped copper nanoparticles. The recipe we used as the starting point for this work had been originally reported for gold nanoparticles by Leff *et al.* (1996) as a modified version of the synthesis technique by Brust *et al.* (1994). Modifications were made to make this method feasible for copper nanoparticles. After each modification step, prepared nanoparticles were characterized to determine the most efficient scheme to follow for synthesizing them.

General background for nanoparticles, their properties, different approaches to fabricating them, and the main challenges in producing them are given in Chapter 1. The great motivation behind copper nanoparticle studies is described by emphasis on many applications that these particles have in a number of industries.

In Chapter 2, principles of colloidal synthesis techniques and two pioneering studies on the fabrication of metal nanoparticles by these methods are presented. The parameters affecting the size and shape of nanoparticles in these techniques, including water content, steric stabilization, surfactant concentration,

and temperature, are discussed. Moreover, the phenomenon of self-assembly of nanoparticles produced by a colloidal synthesis technique is introduced as a new class of nanostructure fabrication.

The chemicals used in the experimental procedures of this work and a description of the preparation scheme and its modified versions are presented in Chapter 3. Moreover, various characterization techniques that were applied to analyze prepared copper nanoparticles are described.

In Chapter 4, the results for each modified recipe are given, followed by comparison between these results so that we can examine the effectiveness of each modification. Also, physical measurements that were done for synthesized nanoparticles are presented to offer more insight on their characterization and properties.

Concluding remarks and recommendations for future studies are presented in Chapter 5. A tentative experimental design for colloidal synthesis of nanoparticles is among these suggestions. It is proposed that a screening design be run first in order to attain more knowledge of the factors affecting either size or shape of prepared metal nanoparticles.

## Chapter 2: Literature Review

### 2.1 Microemulsion (colloidal) synthesis of metal nanoparticles

Microemulsion synthesis techniques for producing metal nanoparticles were accurately summarized by Kitchens (2004). Thus, this section of the literature background is mainly based on his review of work conducted so far on the colloidal synthesis of metal nanoparticles. Selective important studies in this area not covered by Kitchens are included and referred to specifically.

An emulsion forms when an amphiphilic molecule (e.g., surfactant) is introduced to a two-phase liquid-liquid system such as water and oil. These two liquids are essentially immiscible; however, upon the addition of surfactant, the interfacial tension between them reduces and they become emulsified. As was mentioned before, the surfactant has an amphiphilic molecular structure: a hydrophilic head group, which prefers aqueous environments and a hydrophobic tail group, which prefers organic environments. This characteristic structure enables the surfactant to reside in both polar and non-polar liquids such as water and oil.

In a microemulsion, which is also called a colloid, a dispersed phase reaches a size of less than 1 $\mu$ m. Being transparent, spontaneously self-assembled, and more stable regarding phase separation, microemulsions (colloids) are distinct from other emulsions. Furthermore, microemulsions consist of surfactant aggregates that are in the length scale of less than 100 nm. The geometry of these aggregates in the microemulsion system depends on the location in the water – surfactant – oil phase diagram illustrated in Figure 2.1.1. In an oil-in-water microemulsion (o/w), shown in the bottom left corner of the diagram, water is the bulk fluid with small amounts of surfactant. In this system, oil and surfactant self-assemble into a form of aggregates, known as micelles, to minimize free energy. Micelles are nano-scale oil droplets with the hydrophobic surfactant tails pointing to the “centre” of the aggregates, while the hydrophilic head groups are exposed to the aqueous bulk solvent. The water-in-oil (w/o) microemulsion in the bottom right corner of the phase diagram includes an organic solvent or oil as the bulk solvent. Thermodynamically stable aggregates that are assembled in this mixture are called reverse micelles. The reverse micelle has a small water pool at its core that is surrounded by a surfactant monolayer where the hydrophilic head groups organize themselves at the water surface and the hydrophobic tails are extended into the bulk organic phase. A typical view of the reverse micelle formed by AOT surfactant is given in Figure 2.1.2. Colloidal dispersion of these nano-sized water droplets in the organic phase by the

surfactant molecules in the form of reverse micelles results in a decrease in the free energy of the microemulsion (Salzemann et al. 2004).

One important property of the reverse micelles is the water content, defined as  $w = [\text{H}_2\text{O}]/[\text{Surfactant}]$  (Kitchens 2004; Salzemann et al. 2004). The size and number of reverse micelles dispersed in the bulk organic phase depend mainly on the concentrations of water and surfactant and their molar ratio, expressed as the water content,  $w$ . We further discuss the role of the water content in determining the size of the AOT reverse micelle in the following section.

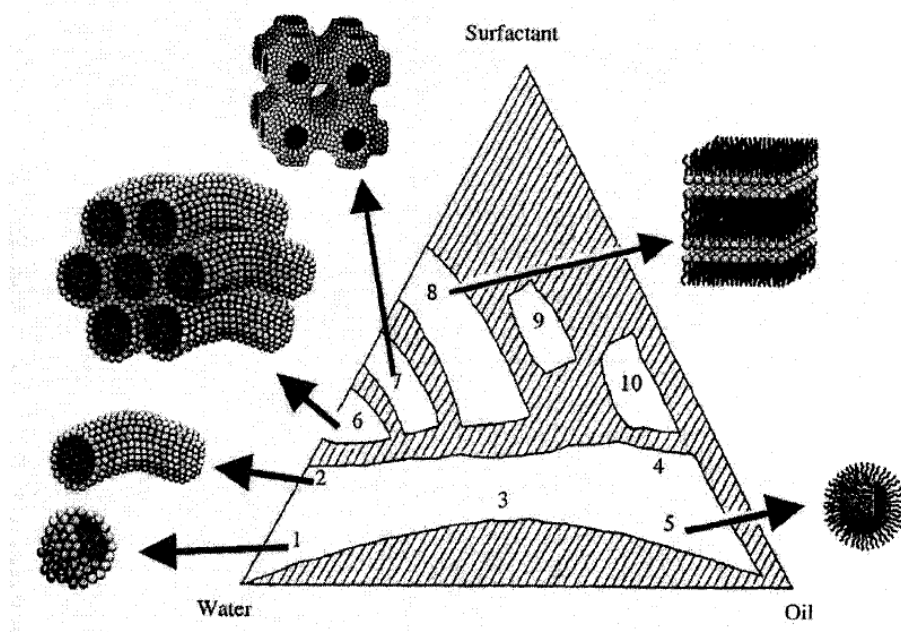


**Figure 2.1.1** Phase diagram of the water – surfactant – oil microemulsion system demonstrating various surfactant aggregate geometries consisting of 1. Spherical micelles. 2. Rod-like micelles. 3. Irregular bicontinuous phase. 4. Reverse cylindrical micelles. 5. Reverse micelles. 6. Hexagonal phase. 7. Cubic phase. 8. Lamellar phase. 9. Reverse cubic phase. 10. Reverse hexagonal phase (Zhang 2003).

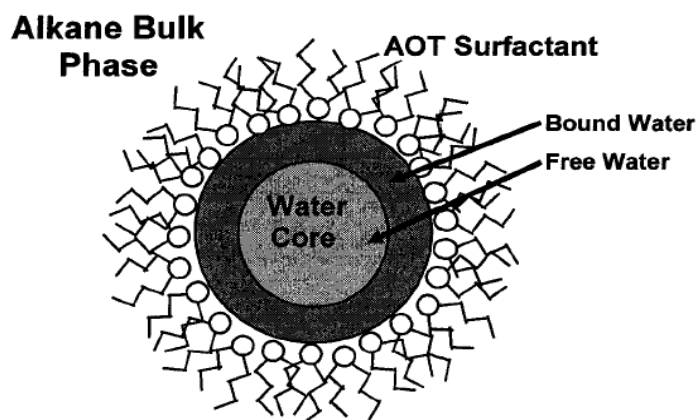


**Figure 2.1.2** A reverse micelle formed by AOT surfactant molecules (Kitchens 2004).

The surfactant concentration at which the spherical reverse micelles can be generated is known as the critical micelle concentration, CMC, which is the minimum surfactant concentration required to produce reverse micelles. Various properties of the reverse micelle system, such as the interactions between the hydrocarbon chains and the bulk phase, the geometry of the surfactant, and the temperature affect the CMC. As the concentration of the surfactant rises above the CMC, the system reaches a point where the reverse micelles start to aggregate into larger compounds and flocculation starts.

The reduction reaction in which metal nanoparticles are synthesized occurs in the core of the reverse micelle. Among several mechanisms proposed for explaining micellar kinetics, the most accepted one is illustrated in Figure 2.1.3. Reverse micelles randomly collide because of thermal Brownian motion; therefore, a fraction of droplets transforms into the form of short-lived dimers where the intermicellar exchange of the aqueous contents of two different reverse micelles proceeds (Fletcher et al. 1987; Pileni 1993). These dimers then separate to generate surfactant-capped metal nanoparticles. The intermicellar exchange process facilitates the chemical reaction between water soluble reactants to form the final product (Kitchens 2004). This process has been investigated by various techniques, such as laser flash photolysis, spectrophotometry, NMR, and electrochemistry (Atik and Thomas 1981; Blitz et al. 1988; Charlton and Doherty 2000; Eicke et al. 1976; Fletcher et al. 1987; Howe et al. 1987). Fletcher *et al.* (1987) investigated the micelle kinetics for a water/alkane/AOT system by applying laser flash photolysis and a stopped flow where two reverse micelles including reactants were mixed, as shown in Figure 2.1.4, and the reaction progress was monitored in order to estimate the intermicellar exchange rate constant,  $k_{ex}$ . This study was focused on determining the effect of the bulk liquid alkane fluid, water content, AOT concentration, and temperature on  $k_{ex}$ . The results demonstrated that  $k_{ex}$  decreases with increasing water

content for  $w = 10, 15, 20,$  and  $30$ ;  $k_{ex}$  is independent of AOT and reactant concentrations;  $k_{ex}$  increases with increasing temperature; and  $k_{ex}$  is dependent on the alkane molecular structure, meaning that an increase in the carbon number of the alkane solvent from pentane through dodecane slightly raises  $k_{ex}$ , while a significant decrease in  $k_{ex}$  was observed for cyclic compounds, specifically for cyclohexane. In addition to  $k_{ex}$ , thermodynamic and physical properties such as critical micelle concentration, phase separation, diffusion, microemulsion stability, interaction forces, and solvent effects play an important role in reverse micelle synthesis (Kitchens 2004).

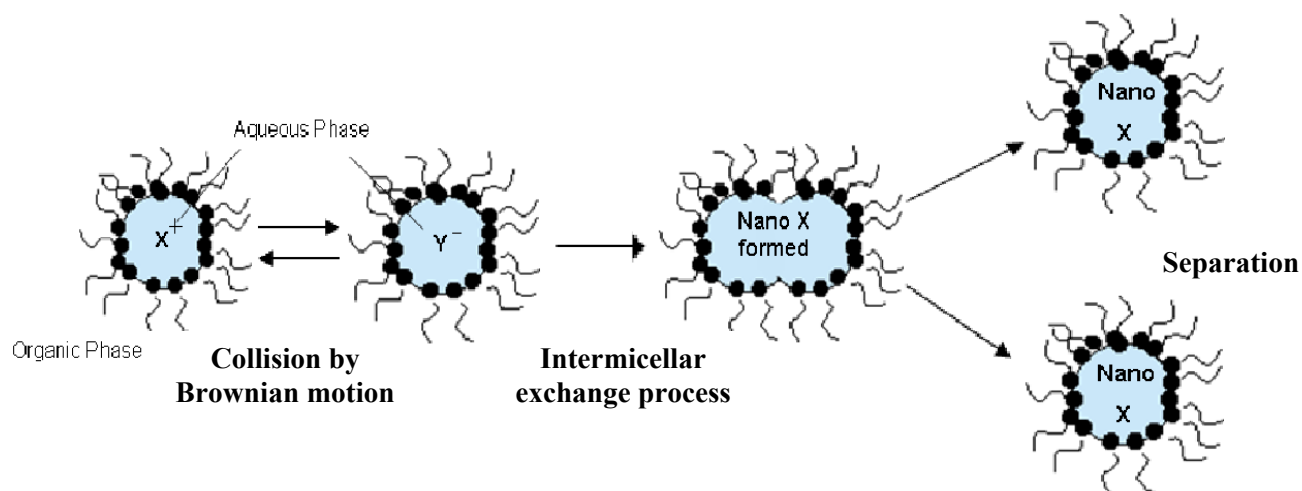


**Figure 2.1.3** Illustration of the mechanism for the synthesis of metal nanoparticles in reverse micelles.

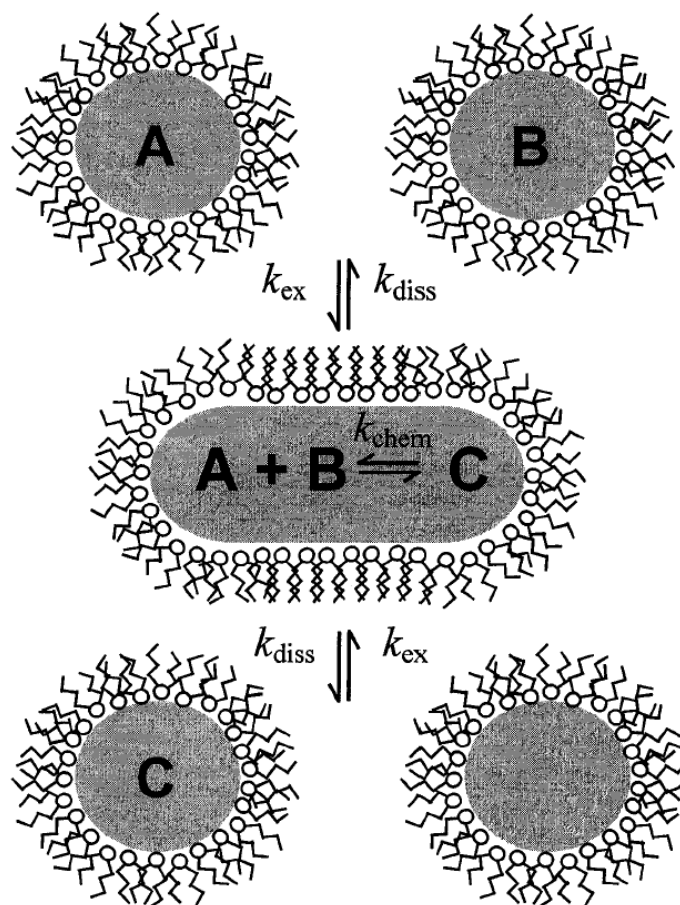


**Figure 2.1.4** Mechanism for intermicellar exchange of the water cores of the reverse micelles that were formed by AOT surfactant molecules (Kitchens 2004).

In synthesis reactions in which reverse micelles act as microreactors, a significant control on the size and shape of produced nanoparticles can be achieved (Salzemann et al. 2004). This control requires a better understanding of the reaction mechanism and kinetics and the controlling thermodynamic and physical properties (Kitchens 2004). Employing the reverse micellar system for fabricating nanomaterials has been studied since the early 1990s. Different types of materials, including purely metallic nanoparticles (Cu, Ag, Co, Al), metal sulfides (CdS, ZnS), oxides (TiO<sub>2</sub>, SiO<sub>2</sub>), and various nanocomposite materials, have been produced by colloidal synthesis methods (Bagwe and Khilar 2000; Cason et al. 2001; Hirai et al. 1995; Hirai et al. 1994; Sato et al. 1995; Towey et al. 1990). Among these works, we focus primarily on two prominent approaches for synthesizing metal nanoparticles: one by Pileni and co-workers that demonstrates the production of copper nanoparticles using the water/AOT/liquid alkane

reverse micelle system (Lisiecki and Pileni 1993; Lisiecki and Pileni 1995; Pileni and Lisiecki 1993; Pileni et al. 1999), and another work by Leff and co-workers that describes the synthesis of alkylamine-capped gold nanoparticles in the water/alkylamine/toluene reverse micelle system (Leff et al. 1996).

## **2.2 Synthesis of copper nanoparticles in reverse micelles with controlled water content ( $w$ )**

The control of copper nanocrystal size was first accomplished by Lisiecki and Pileni (1993). In this pioneering work, they applied sodium di-2-ethylhexylsulfosuccinate or Aerosol OT (AOT) as the surfactant and copper dioctyl sulfosuccinate,  $\text{Cu}(\text{AOT})_2$ , as the source of copper cations. Metal ions can be introduced into the reverse micellar system in two ways: either as a metal salt dissolved in the aqueous core of reverse micelles or by addition of AOT-derivatised metal ions that have been generated by replacing the sodium counter ion with the desired metal ion (Pileni, Motte and Petit 1992). The benefit of following the second method is the absence of salt anions in the core of the reverse micelles. The presence of anions inside reverse micelles has been shown to change the physical properties of the water content and surfactant layer and therefore vary the size and shape of the reverse micelles and fabricated metal nanoparticles (Filankembo and Pileni 2000b; Hassan et al. 2002; Lisiecki et al. 2000; Pileni et al. 1998). We discuss in Chapter 4 that the presence of anions can cause the formation of an insoluble monolayer on the surface of synthesized copper nanoparticles, and subsequently, modify the surface properties of the produced nanoparticles.

AOT has been widely employed in the formation of reverse micellar systems since its inverted cone geometry, shown in Figure 2.2.1, facilitates the formation of uniformly dispersed, thermodynamically stable, and spherical reverse micelles (Hiemenz and Rajagopalan 1997). The formation of a water/oil (w/o)-microemulsion (AOT/isooctane/water) is described in early studies by Eicke and Rehak (1976), in which the procedure for preparing AOT reverse micelles with controlled water content ( $w$ ) is explained. Bidistilled water was used as solubilize within the reverse micelle core. The solubilize was added to the mixture of nonpolar organic solvent and the surfactant with a microsyringe. This solution was treated in an ultrasonic bath so that the solubilize was entirely taken up by the micelles. Following this procedure, the concentration ratio of water and AOT, which is equal to the water content ( $w$ ) of the reverse micelles, could be calculated. Pileni and co-workers benefited from using AOT as the surfactant in their studies since the water content of the reverse micelles was easily controlled by changing the amount of solvent in the microemulsion system, as described by Eicke and Rehak (1976). Considerable research has been carried out on the AOT reverse micellar system to clarify any unrevealed detail of this

synthesis method. The structure of the reverse micelle core as the reaction site in the colloidal synthesis of nanoparticles has also been carefully studied, and as already shown in Figure 2.1.2, two water environments were recognized for the aqueous core of AOT reverse micelles. The first 6-8 molecules of water close to the AOT head groups are called bound water due to the restricted mobility of water molecules under the influence of the ionic environment. Free water, which has properties similar to those of bulk water, is in the centre of the core (Fendler 1976). The reverse micelle's water pool plays an important role in the colloidal synthesis of metal nanoparticles, and we discuss its affects in this process later.

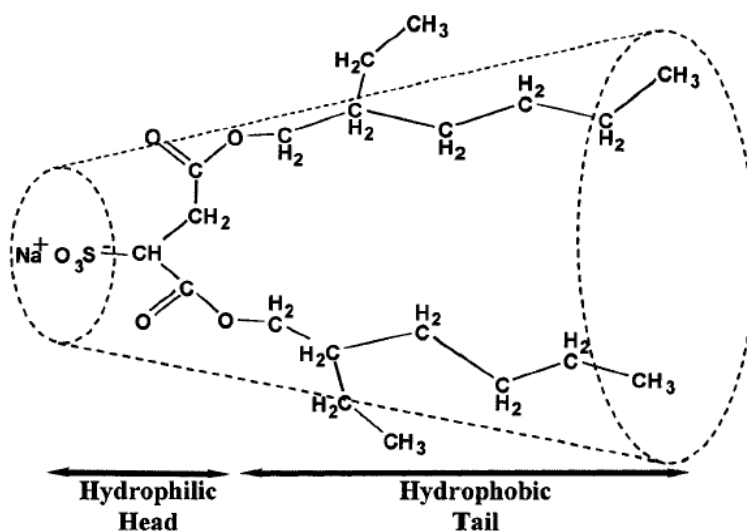


**Figure 2.2.1** Molecular structure of Aerosol OT (= AOT = Sodium di-2-ethylhexylsulfosuccinate), used as the surfactant (Pileni and Lisiecki 1993; Pileni and Tanori 1995a; Pileni and Tanori 1995b). The dotted lines show the inverted cone geometry of this surfactant (Kitchens 2004).

Synthesis of copper nanoparticles within AOT reverse micelles is a two-step procedure that starts with the reduction of metal ions in the core of reverse micelles to generate ground state metal atoms, followed by particle growth that is facilitated by intermicellar exchange of the reverse micelles' cores (Kitchens 2004). The schematic for this synthesis can be seen in Figure 2.2.2. Typical reducing agents used in the work by Lisiecki and Pileni (1993) were sodium borohydride ( $\text{NaBH}_4$ ) and hydrazine ( $\text{N}_2\text{H}_4$ ). Upon the addition of a reducing agent such as hydrazine or sodium borohydride to the reverse micellar solution of copper cations, a sudden color change can be observed; however, no precipitation occurs due to the presence of the AOT reverse micelles that keep the synthesized copper nanoparticles colloidally

dispersed in nonpolar organic solvent (Lisiecki and Pileni 1993). To avoid metal oxidation, the entire synthesis procedure was done in a glove box with a nitrogen flow.

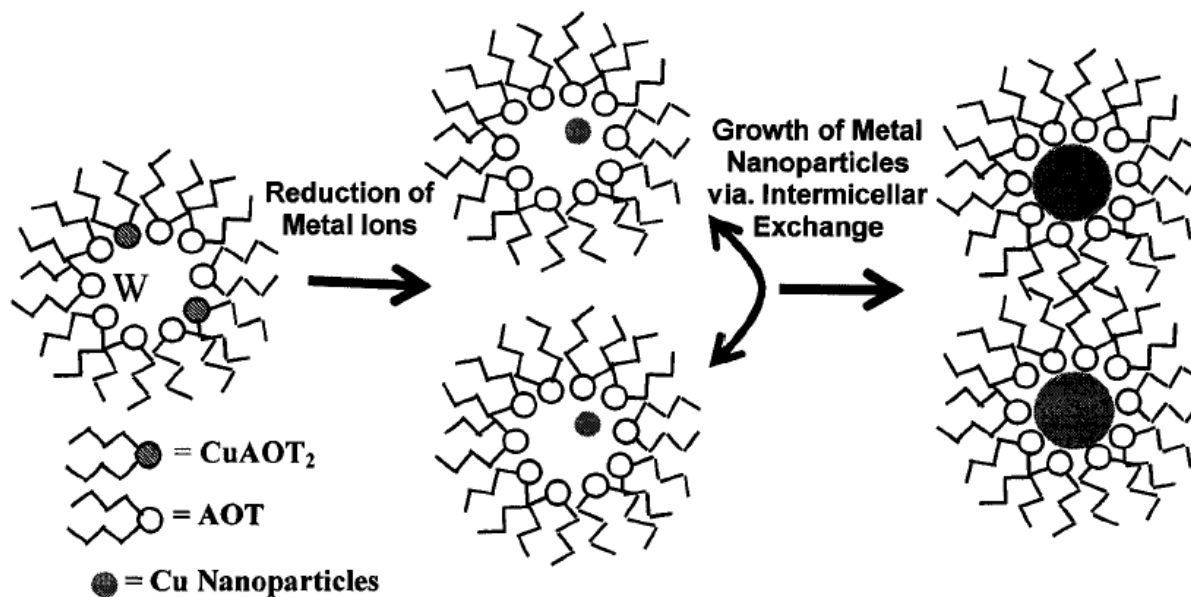


**Figure 2.2.2** Reaction mechanism for the synthesis of copper nanoparticles upon chemical reduction of AOT-derivatised copper ions followed by particle growth as a result of the dynamic intermicellar exchange of the contents of reverse micelles' cores (Kitchens 2004).

Lisiecki and Pileni (1993, 1995) reported that the size of the metallic nanoparticles produced by this method increases with the water content. Moreover, they demonstrated that other experimental parameters, such as the intermicellar interaction and the number of copper ions and reducing agent per micelle influence the final particle size. Increasing the water content in the range of 1.5 to 15, Salzemann *et al.* (2004) produced copper nanoparticles with diameters varying from 3 to 13 nm. The characteristic radius of the reverse micelle was found to be linearly proportional to the water content ( $r_w = 1.5 \times w$ ) (Pileni, *et al.* 1985). The diameter of the water pool was believed to control the ultimate nanoparticle size (Cassin *et al.* 1995; Kotlarchyk 1985). The results of Salzemann *et al.*'s static studies (2004), which were TEM images and UV-visible absorption spectra of produced copper particles at a certain reaction time, are in a good agreement with this assumption; that is, an increase in  $w$  or the size of the reverse micelle results in an increased diameter of copper nanoparticle. Since water content was found to affect the

particle size and production yield (Pileni and Chevalier 1983; Pileni et al. 1982), they justified the low yield production of small nanoparticles at low  $w$  values by claiming that the reactants were poorly hydrated. In contrast, at higher values of  $w$ , increase in the reactant hydration led to an increase in the reaction yield, and eventually, the number of nuclei increased (Salzemann et al. 2004). However, strong nanocrystal – surfactant interactions are also recognized as an influential parameter on the final nanoparticle size produced by this method. Salzemann *et al.* (2004) realized these interactions' important impact when the copper nanocrystal growth was considerably reduced from  $w = 5$  and then stopped at  $w = 10$ .

Another study by Cason *et al.* (2001) revealed that the average particle sizes for reverse micellar systems with different water content (in the range of 3 to 15) were the same after the synthesis reaction had adequately progressed. They performed in-situ time-resolved absorbance measurements to study the reaction kinetics of the formation of copper nanoparticles. These time- resolved results prove that the water content,  $w$ , does not affect final particle size in the reverse micellar synthesis technique, but does facilitate nanoparticle growth. Thus, interestingly enough, this investigation illustrates the imprecise nature of the description of reverse micelles as templates for particle synthesis (Filankembo and Pileni 2000a; Pileni 1997; Pileni et al. 1999), in which the final size and shape of produced nanoparticles are dependent on the size and shape of the reverse micelles. For instance, the studies on the formation of copper nanoparticles in the reverse micellar system showed that the final copper nanoparticle sizes were sometimes two times larger than those of the host micelles (Salzemann et al. 2004). Though this case has not been observed for all nanomaterials produced by this method, it is reliable evidence that the average particle size of copper nanoparticles fabricated by this technique is not influenced by the micelle templating (Kitchens 2004).

An alternative explanation for the control of the final size of nanoparticles synthesized inside AOT reverse micelles is the steric stabilization of the metal nanoparticles by the AOT surfactant. In other words, the surfactant hydrophilic head is capped to the surface of metal nanoparticles, and its hydrophobic tails protect the particle in the solution by interacting with the solvent in the bulk fluid; hence, the surfactant plays the role of stabilizing ligand (Kitchens 2004). In the following section, we discuss further the role of conventional stabilizing capping agents, such as thiols and amines, in the synthesis of metal nanoparticles by microemulsion methods. More investigation is required to clarify the role of steric stabilization and templating effects in the synthesis of copper nanoparticles within AOT reverse micelles.

In addition to the water content, the bulk solvent type, surfactant concentration, reactant concentration, anion presence, pH, and temperature have all been found to influence the reaction kinetics and the size

and shape of the nanoparticles fabricated by reverse micellar synthesis methods. Several researchers have investigated their roles; however, the facts about these complicated systems still remain a mystery (Adair and Suvaci 2000; Dixit et al. 1998; Hirai et al. 1995; Hirai et al. 1994; Kitchens 2004; Sato et al. 1995; Wu and Chen 2004; Wu et al. 2001).

### **2.3 Colloidal Synthesis of metal nanoparticles in a two-phase liquid-liquid system**

Colloidal metals in a two-phase system were first prepared by Faraday (1857), who introduced a synthesis method in which an aqueous gold salt was reduced with phosphorus in carbon disulfide and a ruby colored aqueous solution of dispersed gold particles was obtained. Brust *et al.* (1994) combined this two-phase approach with more elaborate ion extraction techniques and self-assembly with alkane thiols and established a method for synthesizing an extraordinary new metallic material of thiol-derivatised gold nanoparticles. While Pileni and co-workers (Lisiecki and Pileni 1993) used AOT-derivatised metal ions ( $\text{Cu}(\text{AOT})_2$ ) as the source of metal cations, Brust *et al.* (1994) initiated the synthesis with hydrogen tetrachloroaurate trihydrate ( $\text{HAuCl}_4 \cdot 3\text{H}_2\text{O}$ ). Therefore, at the beginning of their method, metal cations exist in the aqueous solution, and are later entrapped in the aqueous core of the reverse micelles.

This synthesis technique consists of two steps, as illustrated in Figure 2.3.1. A surfactant is added to a vigorously stirring two-phase system with metal cations in the aqueous layer, thus starting the first step, the stirring step. In this step, upon stirring two immiscible phases in the presence of the surfactant, dodecanethiol, reverse micelles are formed. In Brust *et al.*'s colloidal approach (1994), the interface between two phases provides the reverse micellar system with an unlimited source of solubilizate, in contrast to the method by Lisiecki and Pileni (1993) discussed previously. Therefore, in this synthesis technique, metal nanoparticles are produced in reverse micelles with no control on their water content.

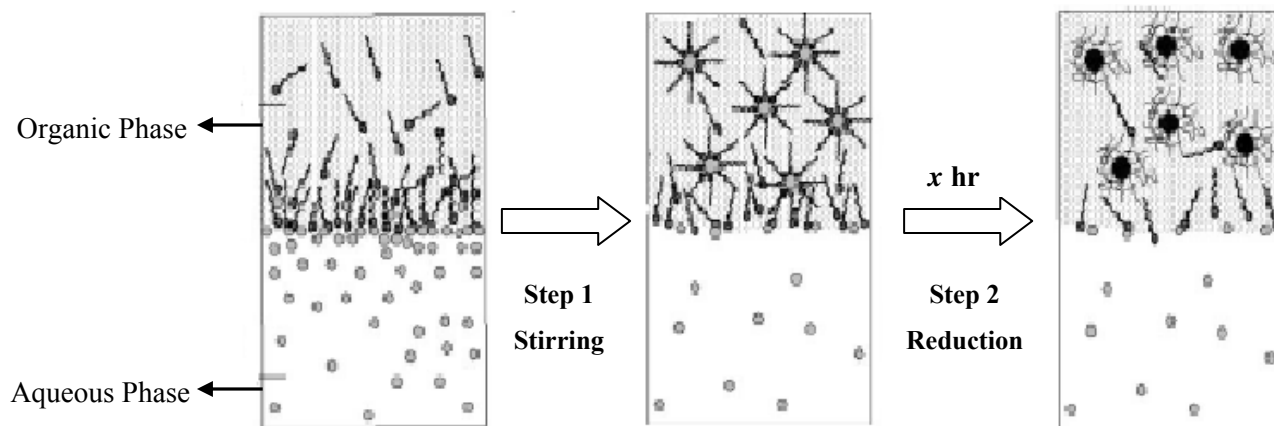
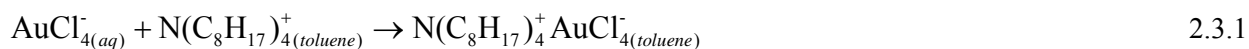


**Figure 2.3.1** Two steps of the colloidal synthesis technique, first established for synthesizing thiol-stabilised gold nanoparticles in a two-phase liquid/liquid system (modified image of Swami *et al.* (2004) work).

In the recipe suggested by Brust and co-workers (1994) for synthesis of gold nanoparticles, a phase transfer reagent, tetraoctylammonium bromide, was applied to increase the stirring step's efficiency in transferring gold cations to the organic phase. The organic solution of the phase transfer reagent was added to the aqueous solution of  $\text{AuCl}_4^-$  to form the two-phase system, which was later provided with dodecanethiol as the surfactant. The cationic part of the phase transfer reagent reacts with the anionic complex of  $\text{Au}^{3+}$ , as in equation 2.3.1, and an organic-soluble compound forms. Thus, in this method, the phase transfer reagent along with the surfactant plays the transferring role for metal cations. The first step is finished as soon as the aqueous phase becomes clear, meaning that  $\text{AuCl}_4^-$  is quantitatively removed from this phase.



The second step of this technique is the reduction of metal cations within reverse micelles by adding sodium borohydride,  $\text{NaBH}_4$ . The source of electron,  $\text{BH}_4^-$ , is also captured by free surfactant molecules that are floating at the interface. Similar to the mechanism that was discussed earlier for the synthesis technique by Pileni *et al.*, the reduction of metal cations starts at the reaction sites, which are the aqueous cores of reverse micelles, as a result of thermal Brownian motion. Usually, this step takes several hours to ensure that the reduction reaction is complete. This second step is summarized in equation 2.3.2:



Applying this colloidal recipe, Brust and co-workers synthesized 1-3 nm gold nanocrystals, which were functionalized with covalently bound alkanethiols. These thiol-derivatised gold nanoparticles, which act like simple chemical compounds, are hydrophobic, meaning that they are extremely soluble and resolvable in organic solvents such as toluene and hexane (Brust et al. 1994; Leff et al. 1996).

Moreover, these nanoparticles show a tendency to spontaneously form highly ordered superlattices by allowing the slow evaporation of the organic solvent on a suitable substrate (Brust and Kiely 2002). The self-assembly of synthesized gold nanoparticles occurs as a result of van der Waals interactions between long alkyl chains of the capping thiol ligands (Hao et al. 2006). Brust and Kiely (2002) reported that the self-assembly phenomenon observed for thiol-stabilised gold nanoparticles may not be significantly dependent on the type of stabilising ligand if a certain balance between attractive and repulsive interactions is held. The nature of the substrate and the wetting characteristics of the solvent are believed to affect on this phenomenon, but have not been studied yet. The assembly of two- and three-dimensional structures, in which synthesized nanoparticles are closely packed without any agglomeration, is now of intrinsic interest as it is a new class of fabricating nanostructures, called the *bottom-up* approach (Brust and Kiely 2002). Although the self-assembly route seems to have many advantages for the fabrication of nanostructures – including experimental simplicity down to the atomic size and the potential for inexpensive mass fabrication – our understanding of the mechanism by which ordered or complex structures take shape spontaneously by self-assembly should be developed in order to control this process in such a way that a self-assembled nanostructure with a pre-determined geometry can be produced. Moreover, as one important requirement for this fabrication approach, synthesized nanoparticles are required to be sufficiently stable so that they can be applied as building blocks for self-organisation processes. Interestingly enough, Brust *et al.* (1994) improved their method to produce very stable ligand-derivatised metal nanoparticles (i.e., gold and silver) that are later self-assembled into well-ordered nanostructures. Thus, an outstanding amount of research has been carried out on this synthesis technique as a straightforward way of producing self-assembled metal nanoparticles.

This preparative method has been refined repeatedly for different metals and stabilizing ligands. For instance, silver nanoparticles have been successfully synthesized by the application of refined versions of the technique by Brust *et al.* (Heath et al. 1997; Korgel et al. 1998). Alkylamines have also substituted for alkanethiols to confirm the flexibility of this method for various kinds of surfactants (Heath et al. 1997; Leff et al. 1996).

In contrast, few studies have been done on synthesizing copper nanoparticles by refining Brust *et al.*'s colloidal method. In a study by Chen and Sommers (2001) on synthesizing copper nanoparticles with an alkanethiolate protecting monolayer in one phase system, they briefly referred to another work in which they produced copper nanoparticles with an average particle size of less than 2 nm using a two-phase system like the one established by Brust *et al.* (1994). However, they did not provide further information about these copper nanoparticles.

Among the refined versions of Brust *et al.*'s synthesis recipe, the one by Leff *et al.* (1996) is of most interest for our work. In this synthesis method, which is detailed in the next chapter, alkylamines are employed to synthesize gold nanoparticles functionalized with amines. Two preparative schemes proposed by them are different in using the phase transfer reagent,  $N(C_8H_{17})_4Br$ , only in Scheme 1 and ignoring it in Scheme 2. In our studies, in which Scheme 1 of Leff *et al.*'s work was modified for copper, we tried to investigate the potential of this synthesis technique for producing stable and metallic copper nanoparticles capped with amines.

## Chapter 3: Experimental Methods

### 3.1 Materials

The basis for this work is the recipe reported by Leff *et al.* (1996) originally for producing alkylamine-capped gold nanoparticles. All of the reagents were used as obtained. Copper (II) chloride hydrate, puratronic 99.999% (metal basis) ( $\text{CuCl}_2 \cdot x\text{H}_2\text{O}$ ,  $x \approx 2$ ), was bought from Alfa Aesar. Tetraoctylammonium bromide 98% ( $\text{N}(\text{C}_8\text{H}_{17})_4\text{Br}$ ), oleylamine, tech 70% ( $\text{C}_{18}\text{H}_{35}\text{NH}_2$ ), sodium borohydride, ReagentPlus 99% (sodium tetrahydridoborate,  $\text{NaBH}_4$ ), and dodecane, anhydrous +99% ( $\text{C}_{12}\text{H}_{26}$ ), were all purchased from Sigma-Aldrich. Toluene, high purity solvent 99.98% ( $\text{C}_7\text{H}_8$ ), a product of EMD, was used in our experiments. Hydrochloric acid (HCl), A.C.S. reagent, was purchased from Fisher Scientific. Hexane was obtained from two different companies. First, hexane bought from Caledon Labs was used; however, high levels of impurities were found in this type of hexane after its gas chromatography was taken. Thus, hexane optima (HPLC) was purchased from Fisher Scientific. Anhydrous ethanol used in our work was supplied by Commercial Alcohols Inc.

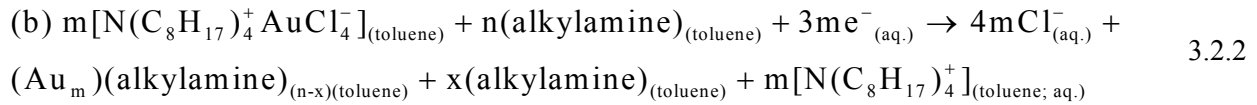
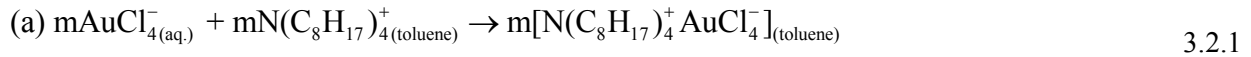
### 3.2 Copper Nanoparticle Synthesis

Although copper nanoparticles have been synthesized by various colloidal procedures, the potential of the two-phase liquid-liquid approach by Brust *et al.* (1994) for fabricating these particles has been rarely investigated. Leff *et al.* (1996) substituted alkylamine for alkanethiol and followed exactly the same steps as those of Brust *et al.*'s method to produce amine-derivatized gold nanoparticles. The following sections first present the original recipe for synthesizing alkylamine-capped gold nanoparticles and then go on to detail of the modifications for making the technique practical for copper.

#### 3.2.1 Original Recipe for Gold Nanoparticles

The four-step preparation scheme for gold nanoparticles by Leff and co-workers starts with dissolving 112 mg (0.284 mmol) of hydrogen tetrachloroaurate trihydrate (chloroauric acid,  $\text{HAuCl}_4 \cdot 3\text{H}_2\text{O}$ ) in 25 mL deionized water to make a yellow solution. Next, 365 mg (0.667 mmol) of tetraoctylammonium bromide ( $\text{N}(\text{C}_8\text{H}_{17})_4\text{Br}$ ) in 25 mL toluene was prepared and added to the vigorously stirring aqueous solution containing the Au salt. At this step,  $\text{AuCl}_4^-$  was quantitatively transferred from the aqueous phase into the organic one by making a complex with the cationic part of the phase transfer reagent,

$N(C_8H_{17})_4Br$ . This two-phase system was kept stirring until the orange-tinted aqueous phase turned clear, confirming successful transfer of  $Au^{3+}$  into the organic phase on top. In the third step, 574 mg (3.1 mmol) of dodecylamine ( $C_{12}H_{25}NH_2$ ) in 25 mL of toluene was added to the rapidly stirring two-phase mixture. Both dodecylamine and oleylamine ( $C_{18}H_{35}NH_2$ ) were used as surfactant and Leff *et al.* (1996) claimed that the variation of the amine capping agent did not affect either the reaction or the average particle size. Finally, a solution of 165 mg (4.36 mmol) of  $NaBH_4$  in 25 mL of deionized water was prepared and added to the system. An instant color change occurred in the organic phase from orange to black/brown and ultimately to dark purple. The appearance of this dark color indicated that the reduction reaction had started. The source of electron for the reaction was  $BH_4^-$ . The mixture was further stirred rapidly for  $\approx 12$  h, while it was open to ambient atmosphere, to allow the reaction to complete. The overall reaction is summarized by equations 3.2.1 and 3.2.2. The possible byproducts of this reaction are  $H_2(g)$ , sodium borate, and  $NaCl$ .



When the reaction was completed, the aqueous phase was decanted and removed, and the volume of the organic phase reduced to  $\sim 5$  mL by rotary evaporation. Synthesized gold nanoparticles, colloiddally dispersed in toluene, were precipitated by adding 350 mL of 95% ethanol and cooling to  $-60^\circ C$  for 12 h. Next, the dark purple sediment was filtered with  $0.65\mu m$  nylon filter paper, washed with excess of ethanol, and dried under vacuum to give  $\approx 60$  mg of dry product. The resultant particles could be re-dispersed in nonpolar organic solvents such as hexane, to be stored or characterized further.

### 3.2.2 Modified Synthesis Procedures

One of the disadvantages of the chemical approach to nanoparticle synthesis, particularly colloidal synthesis techniques, is the number of modifications to the preparation scheme that are required for each material. Since we applied a recipe that was originally proposed for gold, we had to adjust the procedure for copper so that the synthesis of non-agglomerated stable nanoparticles would be practical. In the following subsections, the various modifications that were made to the initial recipe will be reviewed. Results for processes with combinations of these changes are further discussed in Chapter 4.

#### 3.2.2.1 Glove box

The simple preparative method for producing thiol-stabilised gold nanoparticles (Brust et al. 1994) has been subjected to various refinements for synthesizing particles of other inert metals, such as silver (Heath et al. 1997; Korgel et al. 1998). One important modification to the recipe for those metals that are sensitive to air (i.e. copper) is to provide an inert atmosphere during the entire synthesis. In our experiments, we ran the four-step synthesis procedure and post-synthesis treatments (decanting, evaporation, filtering) in an anaerobic glove box under the flow of nitrogen ( $N_2$  (gas)) or argon (Ar). Prepared samples were stored in a liquid nitrogen dewar to avoid possible post-synthesis oxidation of the nanoparticles that were dispersed in the non-polar solvent.

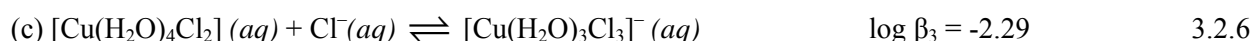
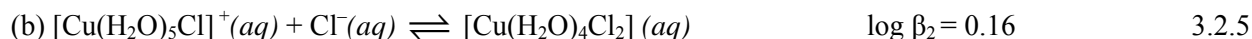
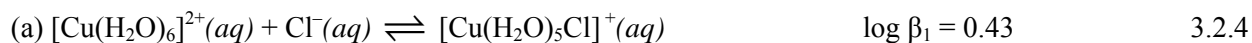
#### 3.2.2.2 Increasing the concentration of $Cl^-$

In the second step of the gold synthesis recipe, the phase transfer reagent was added to enhance the transfer of the gold cation from the aqueous phase to the organic one. As was summarized in Equation 3.2.1,  $AuCl_4^-$ , the source of  $Au^{3+}$ , reacted with the cationic part of  $N(C_8H_{17})_4Br$  and was successfully removed from the aqueous solution.

Dissolving copper (II) chloride hydrate ( $CuCl_2 \cdot xH_2O$ ,  $x \approx 2$ ) in distilled water results in the formation of a cationic complex of copper ( $[Cu(H_2O)_6]^{2+}$ ). This cation is generally believed not to be transferred into the organic phase by typically used cationic phase transfer agents, such as  $[N(C_8H_{17})_4]^+$ . Thus, further refinements are required to make an anionic complex of copper in the aqueous phase. If the concentration of  $Cl^-$  increases, anionic complexes are formed through multi-step equilibrium reactions. The following mechanism was suggested by Andreev (Andreev and Sapozhnikova 1965) for complex formation in the  $CuCl_2$ -HCl- $H_2O$  system:



Stability constants are available for four steps of the above mechanism (Benjamin 2002):



$\beta$  is defined as :  $\text{M} + n\text{L} \rightleftharpoons \text{ML}_n$   $\beta_n = \frac{[\text{ML}_n]}{[\text{M}][\text{L}]^n} = \prod_{i=1}^n K_i$

In our experiments, we started with HCl as the source of  $\text{Cl}^-$ . As  $\text{H}_3\text{O}^+$  can be a competitor for  $\text{Cu}^{2+}$  in the reduction step of this synthesis, KCl was substituted for HCl to avoid foam ( $\text{H}_2(\text{gas})$ ), which was formed after adding the reducing agent to the two-phase mixture including HCl.

### 3.2.2.3 Decanting organic phase (prior to the reduction step)

The main difference between chemical reduction techniques and microemulsion synthesis methods is the reaction site, that is, the bulk phase and the core of the reverse micelles, respectively. Metal cations are reduced during the micellar exchange process, while a layer of surfactant protects the nascent nanoparticles. Hence, agglomeration is less likely to happen in colloidal routes. However, the transfer step has to be efficient enough so that a high percentage of cations are surrounded by surfactant in the organic phase before we start the reduction step.

As mentioned before, we added enough KCl to facilitate transferring copper cations. Nevertheless, the cationic copper complex,  $[\text{Cu}(\text{H}_2\text{O})_6]^{2+}$ , was partially unchanged and remained in the aqueous phase. Consequently, the reaction would occur in both reverse micelles and the bulk phase once we added the reducing agent, meaning that, the synthesis was a combination of chemical reduction and microemulsion techniques.

To avoid having two different sites for the reduction reaction, we decanted the organic phase prior to the reduction step and discarded the aqueous phase in which some copper cations still remained.

#### 3.2.2.4 Post-synthesis heating

As almost all of our results showed, a fraction of synthesized copper nanoparticles was concentrated in the form of large clusters, and sometimes these clusters were surrounded by separated nanoparticles. Based on a study of annealing suspensions of silver nanoparticles synthesized via laser ablation (Henneke 2001), we decided to heat synthesized copper nanoparticles in a nonpolar solvent with high boiling point, such as dodecane. Post-synthesis heating presumably facilitates surfactant capping to the surface of nanoparticles and maximizes the steric barrier. Due to the increased steric barrier, nanoparticles can disperse better in a nonpolar solvent. When a dodecane solution of copper nanoparticles was heated at 150°C, its color changed from light brown to light green after ~ 20 minutes. In Chapter 4, the effect of heating on synthesized copper nanoparticles is further investigated.

### 3.3 Characterization Techniques

We applied various techniques to analyze the chemical and physical properties of synthesized copper nanoparticles. Size, shape, and composition of these particles were of interest. We also tried to gain enough knowledge about any possible bonding at the surface of copper nanoparticles. The oxidation state of copper was studied to investigate whether this synthetic method is better than current techniques for controlling metal oxidation.

#### 3.3.1 High-Resolution Transmission Electron Microscopy

Transmission electron microscopy (TEM) is a unique technique for characterizing the structure of as-synthesized nanoparticles. It is quite straightforward to determine nanoparticle size by electron microscopy. A modern TEM has an illumination system, a specimen stage, an objective lens system, the magnification system, the data recording system(s), and sometimes the chemical analysis system. The main part of the illumination system is the electron gun which typically uses a LaB<sub>6</sub> thermionic emission source or a field emission source (Wang 2000).

TEM is almost similar to an optical microscope, except that the optical lenses are substituted with electromagnetic lenses. It uses transmitted and diffracted electrons to image a sample. To take an image of a nanometric sample, a primary electron beam of high energy (in the range of 100-300 keV) passes through a condenser to make parallel rays. This electron beam is diffracted by the lattices of the crystal, forming the Bragg beams which spread out to different directions. Those electrons which exit without deviation from the illumination direction contain the full structural information on the specimen; however, these waves will be transmitted nonlinearly by the optic system, as can be seen in Figure 3.3.1.

Those diffracted beams will be focused in the back focal plane which is also called the “image plane”, as in Figure 3.3.1. Figure 3.3.2 shows how those waves leaving the specimen in the same direction (angle with the optic axis:  $\theta$ ) are brought together at a point on the back focal plane, forming a diffraction pattern. This diffraction pattern, known as selected-area electron diffraction (SAED) pattern, is a good source of information to determine the crystalline structure of the sample (Wang 2000).

Two different TEMs were used for analyzing samples: a LaB<sub>6</sub> source Philips CM10 at the Biology Department of University of Waterloo and a field emission source electron microscope JEOL JEM.2010F at the Canadian Centre for Electron Microscopy (CCEM) at McMaster University. The LaB<sub>6</sub> gun provides a high illumination current, but the current density and the beam coherence are not as high as those of a field emission source. The field emission source is ideal for performing high coherence lattice imaging, electron holography, and high spatial resolution microanalysis. Electron microscopes have four types of lenses: condenser lenses, the objective lens, intermediate lenses, and projection lenses. The condenser lenses are critically important for making a fine electron probe, while the objective lens determines the limit of image resolution. Intermediate lenses and projection lenses together form the magnification system which gives a magnification up to 1.5 million times (Wang 2000).

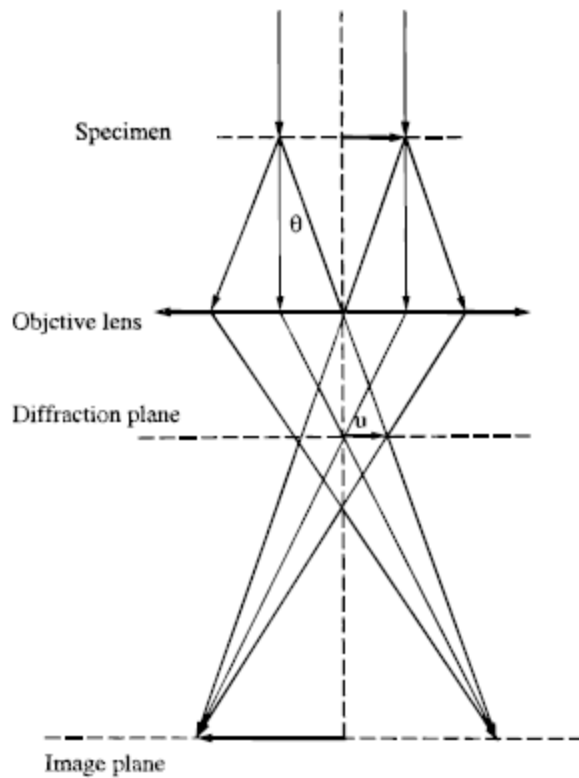


**Figure 3.3.1** Abbe's theory of image formation in a one-lens transmission electron microscope. This theory is for a general optical system in TEM (Wang 2000).

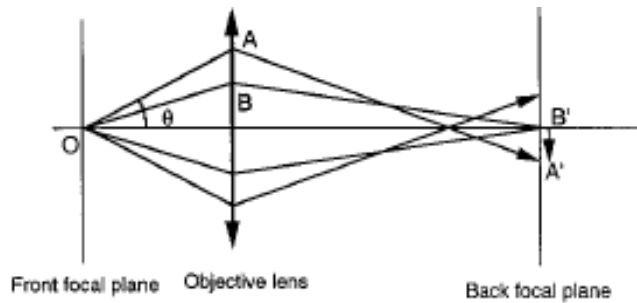


**Figure 3.3.2** Schematic diagrams showing how the waves leaving the specimen in the same direction (or angle  $\theta$  with the optic axis) are brought together by the objective lens at a point on the back focal plane (Wang 2000).

Samples are analyzed by TEM in a vacuum; thus, oxidation is avoided during characterization. We prepared our samples mostly by drying a drop of hexane solution of copper nanoparticles on a Formvar coated gold grid.

### **3.3.2 Energy-Dispersive X-ray Spectroscopy (EDS)**

One of the chemical analysis systems of TEM is energy-dispersive X-ray spectroscopy (EDS) which can be applied to quantify the chemical composition of the specimen. Incident electrons impinge the specimen and excite the electrons bound to the atoms of the sample either to a free electron state or to an unoccupied higher energy level. The quantum transitions due to these excitations will cause many scattering signals, e.g., X-rays and Auger electrons, as can be seen in Figure 3.3.3. These signals are the fingerprints of the elements in the sample, and can be used as a source of quantitative chemical and electrical structural information. In EDS, we are concerned with the counting of the X-rays emitted from the beam-illuminated specimen region as a function of the photon energy. The probe size for the incident electron can be in the range of 2 – 3nm, providing the possibility of taking EDS spectra from every single nanocrystal. EDS is mostly sensitive to heavy elements due to the fluorescence effect that is associated with Auger emission for light elements (Wang 2000).

We acquired EDS data for our samples during HRTEM analysis to investigate the chemical compositions of synthesized copper nanoparticles.

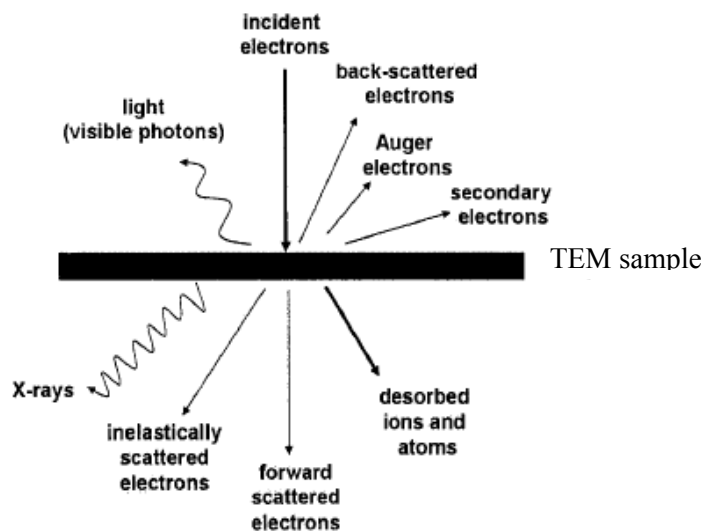


**Figure 3.3.3** Signals generated when high energy electrons interact with a thin specimen. The directions shown for these signals schematically represent the regions at which the signals are relatively stronger and hence detected (Gai and Boyes 2003).

### 3.3.3 Ultra Violet – Visible Spectroscopy (UV-Vis)

Among various spectroscopic methods, Ultra Violet – Visible spectroscopy has been often used for characterizing metal nanoparticles, especially for those plasmon resonances, such as gold, silver, and copper.

In UV-Vis, high energy electromagnetic radiation in the wavelength range of 100-700nm is utilized to promote electrons to higher energy orbitals. Since orbitals have quantized energy, only certain transitions can occur in the UV-Vis energy range. The differences in the incident and transmitted beam give us information about the frequencies which are absorbed by the sample molecules. Based on absorbance data, the sample chemical structure can be analyzed.

UV-Vis analyses in our work were done for either hexane-dissolved or toluene-dissolved samples at room temperature using an Ultrospec 4300 pro UV-visible spectrophotometer. We took 80 $\mu$ L of our solution with micropipettes and poured it into a clean and dry quartz cuvette. All spectra were taken in the range of 210-850nm with 1nm resolution. The spectrum of the background (hexane or toluene) was subtracted from the sample UV-Vis spectrum at each step of characterization.

### 3.3.4 FTIR Spectroscopy

Fourier transform spectroscopy is a technique for collecting spectra and measuring the temporal coherence of its radiation source, applying time-domain measurements of electromagnetic or other types of radiation. It can be utilized to various spectroscopy methods including infrared spectroscopy. Molecular vibrations can be analyzed by infrared spectroscopy (IR spectroscopy), and since for each molecule these vibrations occur at specified frequencies, the spectra can be interpreted by checking the peaks with the IR database to determine the chemical structure of the sample. There are two instrumental variations of IR spectroscopy, the older dispersive one, in which prisms are used to disperse the IR radiation, and the more recent version, that is, Fourier transform infrared spectroscopy (FTIR) that uses the principle of interferometry.

All of the FTIR spectra in this work were taken with a Bruker Tensor 27 FT-IR spectrophotometer. The data were processed by OPUS data collection program. The liquid sample, which was either toluene or hexane solution of the synthesized nanoparticles, was spread between NaCl disks and its infrared spectra were recorded for the wavenumbers in the range of 400-4000  $\text{cm}^{-1}$  with a resolution of 4  $\text{cm}^{-1}$ . These spectra were compared with FTIR spectra of the pure surfactant to indicate whether the surfactant bonds to the surface of the nanoparticles.

## Chapter 4: Results and Discussion

### 4.1 Addition of HCl

The first modification made to the original recipe by Leff *et al.* (1996) was the addition of HCl as a source of  $\text{Cl}^-$ . Based on the reaction mechanism reported for gold, an anionic complex of the metal was required to react with the phase transfer reagent. Tetraoctylammonium bromide ( $\text{N}(\text{C}_8\text{H}_{17})_4\text{Br}$ ) was applied by Leff and his co-workers to improve transfer of the metal cation to the organic phase (the synthesis phase) and therefore increase the production yield. A quantitative transfer of  $[\text{Cu}(\text{H}_2\text{O})_6]^{2+}$  was attempted by making an anionic complex of it by adding an excess of  $\text{Cl}^-$ . Formation of an anionic complex of copper containing chloride was considered since the gold salt used in the recipe was hydrogen tetrachloroaurate ( $\text{HAuCl}_4$ ).

Hydrogen chloride (HCl), a strong Lewis acid, was the first option for providing the aqueous phase with the chloride ion. The changes made to the amount of materials were for  $\text{N}(\text{C}_8\text{H}_{17})_4\text{Br}$  and  $\text{NaBH}_4$ . The moles of the phase transfer reagent were doubled because the charge ratio of  $[\text{Cu}(\text{H}_2\text{O})_2\text{Cl}_4]^{2-}$  to  $\text{N}(\text{C}_8\text{H}_{17})_4^+$  is 2. We also increased the amount of  $\text{NaBH}_4$  to 0.567 g so that we had enough of it for reducing two cations ( $\text{H}_3\text{O}^+$  and  $\text{Cu}^{2+}$ ).

First, 0.048 g of  $\text{CuCl}_2 \cdot 2\text{H}_2\text{O}$  was dissolved in 25 mL of distilled water. Then, 1 mL of 12 M HCl was added to this aqueous solution of copper chloride. The initially prepared blue solution of copper did not experience any color change, even though the mixture was kept stirring for half an hour. The organic solution of the phase transfer reagent was prepared by dissolving 0.73 g of  $\text{N}(\text{C}_8\text{H}_{17})_4\text{Br}$  in 25 mL toluene, and once it was added to the aqueous mixture, a sudden color change was observed in the aqueous phase (light blue to yellow) and the organic phase turned orange/red. After 1 hour of stirring, the aqueous phase became clear, meaning that copper cations were mostly transferred to the upper organic phase. The organic phase color at the end of this step was orange.

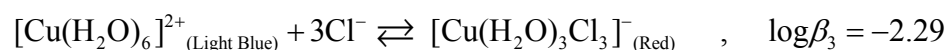
Anytime HCl or other sources of  $\text{Cl}^-$  were applied for the aqueous solution of copper, no color change appeared until the organic solution of the phase transfer reagent was added. In other words, the formation of anionic complex(es) of copper would not be recognized unless we entered the phase transfer reagent to the system. The concentrations of chemical reagent solutions used in this modified synthesis procedure are listed in Table 4-1.

**Table 4-1** Concentration of chemical reagents used for the modified recipe with HCl

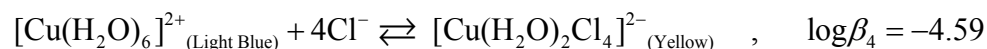
Chemical	Concentration
CuCl <sub>2</sub> ·2H <sub>2</sub> O	0.01136 M (0.284 mmol in 25 mL water)
N(C <sub>8</sub> H <sub>17</sub> ) <sub>4</sub> Br	0.05336 M (1.334 mmol in 25 mL toluene)
HCl	12 M
C <sub>12</sub> H <sub>25</sub> NH <sub>2</sub>	0.124 M (3.10 mmol in 25 mL toluene)
NaBH <sub>4</sub>	0.6 M (15 mmol in 25 mL water)

As can be seen, the concentration of the primary complex of copper, [Cu(H<sub>2</sub>O)<sub>6</sub>]<sup>2+</sup>, was 0.01136 M. Concentrations of anionic complexes of copper were derived from the equilibrium constants listed in Chapter 3:

$$[\text{Cu}(\text{H}_2\text{O})_6]^{2+} = \frac{0.284 \text{ mmol}}{25 \text{ mL}} = 0.0113 \text{ M} \quad , \quad [\text{Cl}^-] = \frac{1 \text{ mL} \times 12 \text{ M}}{(1+25) \text{ mL}} = 0.4615 \text{ M}$$

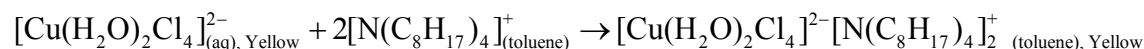
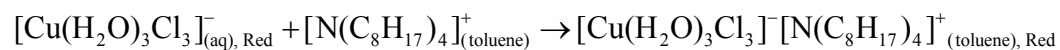


$$\frac{[\text{Cu}(\text{H}_2\text{O})_3\text{Cl}_3]^-}{[\text{Cu}(\text{H}_2\text{O})_6]^{2+} \times [\text{Cl}^-]^3} = 10^{-2.29} \rightarrow \frac{x}{0.0113 \times 0.4615^3} = 10^{-2.29} \rightarrow [\text{Cu}(\text{H}_2\text{O})_3\text{Cl}_3]^- = 5.72 \times 10^{-6} \text{ M}$$



$$\frac{[\text{Cu}(\text{H}_2\text{O})_2\text{Cl}_4]^{2-}}{[\text{Cu}(\text{H}_2\text{O})_6]^{2+} \times [\text{Cl}^-]^4} = 10^{-4.59} \rightarrow \frac{x}{0.0113 \times (0.4615)^4} = 10^{-4.59} \rightarrow [\text{Cu}(\text{H}_2\text{O})_2\text{Cl}_4]^{2-} = 1.32 \times 10^{-8} \text{ M}$$

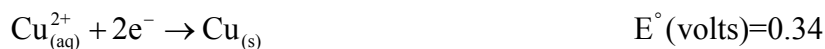
The low concentrations of these complexes cannot make obvious changes in the color of the aqueous phase which was dominated by the light blue cationic complex of copper, [Cu(H<sub>2</sub>O)]<sup>2+</sup>. Upon adding the organic solution of N(C<sub>8</sub>H<sub>17</sub>)<sub>4</sub>Br, an anionic complex of copper and the cationic complex of the phase transfer reagent start to react and the color corresponding to the copper complex appears in the organic phase:



Apparently, at the end of this step, copper cations were mostly transferred to the organic phase and made it colorful. There was probably a mixture of both anionic complexes in the organic phase as its color was orange.

In the next step, a solution of dodecylamine ( $C_{12}H_{25}NH_2$ ) was made by dissolving 0.574 g of it in 25 mL toluene, and this surfactant solution was then added to the system. The two-phase system became milky in the presence of the surfactant, meaning that dodecylamine changed the immiscible two-phase system to the liquid-liquid colloid.

Although the quantitative transfer of copper cations into the organic phase was successfully done, HCl was not the best reagent for this purpose. When the reducing agent solution (0.11 g  $NaBH_4$  in 25 mL distilled water) was added to the colloidal mixture, a lot of foam was formed, the result of  $H_3O^+$  reduction. Thus, there were two cations competing for reduction when we provided the source of electron,  $BH_4^-$ , to the system:  $Cu^{2+}$  and  $H_3O^+$ . As can be seen in the table of standard electrode potentials in aqueous solutions at 25°C,  $Cu^{2+}$  is more likely to be reduced:



However, the formation of foam ( $H_{2(g)}$ ) after adding the reducing agent indicates that  $H_3O^+$  was reduced prior to  $Cu^{2+}$ . Given that these potentials are for aqueous solutions of cations, these electrode potentials are not reliable because one of our cations,  $Cu^{2+}$ , was in the organic phase when we were adding the reducing agent. As described before, in this synthesis technique, copper cations are reduced by collision between two different reverse micelles: one has the metal cation in the core and the other contains the source of electron. Therefore, the reduction for copper cation starts when surfactants start forming numbers of reverse micelles in which the source of electrons are trapped.

When HCl was used as the source of  $Cl^-$ ,  $H_3O^+$  cations were primarily reduced by  $BH_4^-$  in the aqueous phase as almost no copper cations remained in this phase to compete with them. The reduction of copper did not start until an excess of  $NaBH_4$  was added to first reduce all  $H_3O^+$  in the aqueous phase. As soon as the foam stopped rising, the color of the organic phase began to get darker. This was the time that surfactants got the chance to trap  $BH_4^-$  at the interface and form the secondary reverse micelles that later started the reduction reaction. In this vigorously stirring system, Brownian motion played the key role in the collision of reverse micelles and subsequently the intermicellar exchange process. The appearance of dark color in the organic phase illustrated the reduction of copper cations during this process, which resulted in the synthesis of copper nanoparticles.

Foam formation is a challenge when applying HCl because it delays the reduction reaction for copper cations. This problem was resolved by replacing HCl with another chloride provider that has a more stable cation, such as KCl. We discuss the results of this modification in Section 4.3.

## 4.2 Studies of Cu Reduction in a Glove Box

Copper is very sensitive to air, and copper nanoparticles with high specific area are even more likely to become oxidized. Thus, the whole synthesis procedure and the post-preparation steps were done under an inert gas, N<sub>2</sub> or Ar, in a glove box to avoid fabricating metal oxide particles.

When Leff *et al.*'s recipe was followed for copper without using a glove box, the organic phase turned darker and darker upon adding the reducing agent. The blue color of this phase vanished and eventually turned to darker colors such as brown, so that, after ~15 minutes, the top phase was dark purple. However, when this dark purple solution was exposed to air during the reduction step, it started to become brighter after only 5 minutes. In other words, running the reduction reaction for copper without having an inert atmosphere results in an unstable final solution. After 1 hour of stirring with the reducing agent, a yellow organic solution at the top and a clear aqueous phase at the bottom were obtained. After continuous stirring for 15 hours, the aqueous phase became blue, which indicated that copper cations were re-dissolved in the aqueous phase. A probable mechanism for reducing copper cations in the organic phase while the system is exposed to air is schematically shown in Figure 4.2.1.

To check whether oxygen was the reason behind these color changes, we duplicated the whole procedure in the glove box under a nitrogen gas atmosphere. Once the reducing agent was added, the same pattern of color change was observed for the organic phase: the blue color eventually turned to brown and ultimately to dark purple. However, this time, the dark purple organic phase was maintained as long as the nitrogen gas was flowing. The conclusion made by running this trial was that the surfactant used in this method is not protective enough to prevent the oxidation while copper nanoparticles were being synthesized in air. As soon as copper cations are reduced in the temporary dimers shaped by Brownian motion, they are at risk of oxidation since copper oxides are thermodynamically more stable. Therefore, either a stable surfactant coating strongly bonded to the surface of copper nanoparticle should be provided to keep oxygen away from their surfaces or the synthesis procedure would be better run in an environment free of oxygen. According to our observations, alkylamine is not reliable for avoiding oxidation; hence, further modifications were carried out in the glove box. In the following sections, all results are for the modified procedures done in the glove box under the flow of either nitrogen or argon.

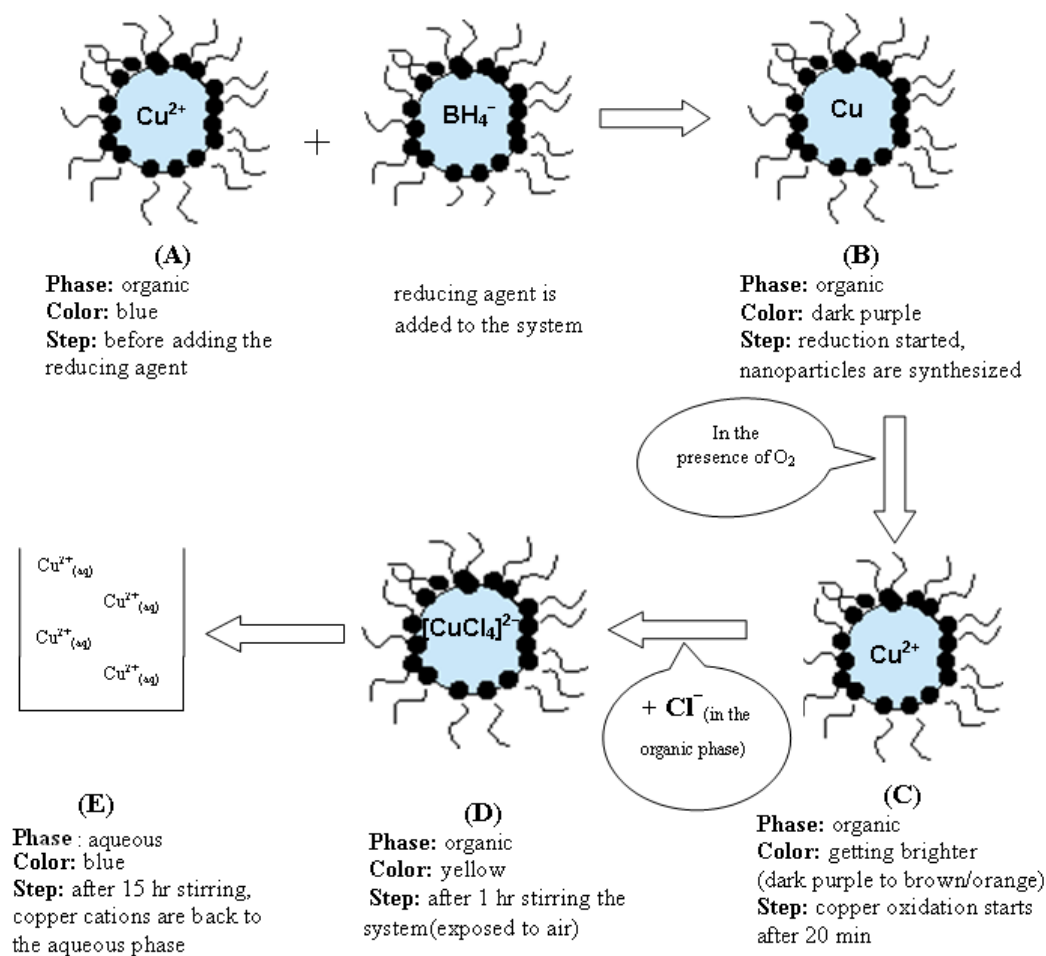


**Figure 4.2.1** Schematic view of the oxidation mechanism during the synthesis of copper nanoparticles when the system was exposed to air during the reduction step.

## 4.3 Substituting KCl for HCl

### 4.3.1 Procedure

To increase the efficiency of the phase transfer reagent, the concentration of chloride was increased by adding HCl to the aqueous phase prior to the transfer step. However, due to the foam formation in the reducing step, a substitute for HCl with a more stable cation was required. KCl was chosen since K<sup>+</sup> has a very negative standard electrode potential, -2.92 volts:



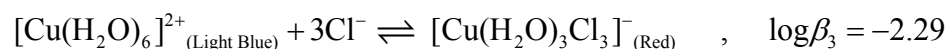
The solubility of KCl is 35.5 g /100 g H<sub>2</sub>O at 25°C (CRC Handbook of Chemistry and Physics 2007-2008); therefore, 8.87 g of KCl is soluble in 25 mL of water. Half of this amount was added to the aqueous phase at this step. In Table 4-2, the concentrations of chemicals used in this modified recipe are listed.

**Table 4-2** Concentrations of the chemical reagents used for the modified recipe with KCl

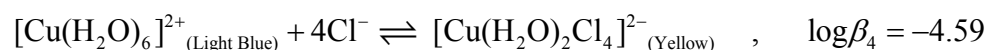
Chemical	Concentration
CuCl <sub>2</sub> ·2H <sub>2</sub> O	0.01136 M (0.284 mmol in 25 mL water)
N(C <sub>8</sub> H <sub>17</sub> ) <sub>4</sub> Br	0.02668 M (0.667 mmol in 25 mL toluene)
KCl	2.146 M (4 g added to 25 mL aqueous phase)
C <sub>18</sub> H <sub>35</sub> NH <sub>2</sub>	0.12157 M (3.03925 mmol in 25 mL toluene)
NaBH <sub>4</sub>	0.11626 M (2.906 mmol in 25 mL water)

The concentrations of two anionic complexes of copper are calculated considering the equilibrium constants:

$$[\text{Cu}(\text{H}_2\text{O})_6]^{2+} = \frac{0.284 \text{ mmol}}{25 \text{ mL}} = 0.0113 \text{ M} \quad , \quad [\text{Cl}^-] = \frac{\frac{4000 \text{ mg}}{74.55 \text{ mg/mmol}}}{25 \text{ mL}} = \frac{53.65 \text{ mmol}}{25 \text{ mL}} = 2.146 \text{ M}$$



$$\frac{[\text{Cu}(\text{H}_2\text{O})_3\text{Cl}_3]^-}{[\text{Cu}(\text{H}_2\text{O})_6]^{2+} \times [\text{Cl}^-]^3} = 10^{-2.29} \rightarrow \frac{x}{0.0113 \times 2.146^3} = 10^{-2.29} \rightarrow [\text{Cu}(\text{H}_2\text{O})_3\text{Cl}_3]^- = 5.73 \times 10^{-4} \text{ M}$$



$$\frac{[\text{Cu}(\text{H}_2\text{O})_2\text{Cl}_4]^{2-}}{[\text{Cu}(\text{H}_2\text{O})_6]^{2+} \times [\text{Cl}^-]^4} = 10^{-4.59} \rightarrow \frac{x}{0.0113 \times (2.146)^4} = 10^{-4.59} \rightarrow [\text{Cu}(\text{H}_2\text{O})_2\text{Cl}_4]^{2-} = 6.16 \times 10^{-6} \text{ M}$$

The synthesis steps (adding the surfactant and the reducing agent) and post-synthesis treatments were done in the glove box under the flow of an inert gas (N<sub>2(gas)</sub> or Ar). First, 0.048 g of CuCl<sub>2</sub>·2H<sub>2</sub>O was dissolved in 25 mL of distilled water. The color of this aqueous solution was light blue. Then, 4 g of KCl was added to the stirring solution of copper chloride. This mixture was stirred for half an hour and no color change was observed. The organic solution of the phase transfer reagent was prepared by dissolving 0.365 g of N(C<sub>8</sub>H<sub>17</sub>)<sub>4</sub>Br in 25 mL of toluene. The molar ratio of the copper salt to the phase transfer reagent in these series of modifications is similar to that of Leff *et al.*'s recipe, a necessity due to

the lack of knowledge about the proportion of each anionic complex in the aqueous phase. Thus, this ratio was left unchanged until a better understanding about the kinetics of both complex forming reactions could be obtained. Upon adding the phase transfer reagent to the solution, the two-phase liquid-liquid mixture was formed with an orange organic phase at the top and a light blue aqueous phase at the bottom. As discussed before for HCl, a color change would not occur until the phase transfer reagent was present in the system. We took this mixture to the glove box and kept it stirring for 2 hours. At that time, the blue color of the aqueous phase lessened, but did not totally vanish. Next, 1 mL of oleylamine ( $C_{18}H_{35}NH_2$ ) was dissolved in 25 mL of toluene and added to the vigorously stirring mixture. Once the surfactant was added, a sudden color change from orange to sharp blue could be observed in the organic phase. The appearance of the whole system was cloudy, meaning that the colloidal solution was formed in response to the presence of the surfactant, oleylamine, in the two-phase water/toluene mixture. The color of the aqueous phase was cloudy blue, but much brighter than the sharp blue organic phase. After an hour of stirring with the surfactant, the aqueous phase turned almost clear with some fluffy structures, which could have been the excess oleylamine. The reduction step started after the reducing agent solution, which was 0.11 g of  $NaBH_4$  in 25 mL distilled water, was added. The color of the organic phase changed from blue to white and gradually to brown. After a couple of minutes, the top phase was brown, and the bottom one was clear. The reduction step was stopped after 2 hours due to the limits in flowing the inert gas for a longer time. Next, the brown organic phase was decanted and heated at  $\sim 70^\circ C$  on a stirrer-hot plate to reduce its volume to  $\approx 5$  mL. By adding 350 mL ethanol to the final concentrated solution, the synthesized particles were precipitated. The samples were placed in a liquid nitrogen dewar to avoid any oxidation during storage. To analyze them by TEM, the brown precipitate was filtered with a  $0.45 \mu m$  membrane filter (polyamid), washed with an excess of ethanol, and dried on a Petri dish under a flow of nitrogen gas inside the glove box. Finally, this dry product was dissolved in 200 mL hexane and made into a dilute solution of particles in a nonpolar organic solvent.

#### **4.3.2 Characterization Results (TEM image and EDS spectra)**

The TEM result for this modified method is shown in Figure 4.3.1. Two different structures can be recognized in this image: a big black cluster and the separated nanoparticles that surround it. The average particle size of separated nanoparticles is about 5 nm.

The EDS result, presented in Figure 4.3.2, confirms that these nanoparticles are copper. Br signals in this spectrum may imply that a portion of the surface of the synthesized particles is capped with  $(octyl)_4N^+Br^-$ , which is similar to the case for gold, reported by Leff *et al.* (1996), and other metal

nanocrystals prepared with this and similar passivants, reported by Bönemann *et al.* (1991). Bönemann's particles were primarily soluble in toluene, but as soon as they precipitate, they could not be re-dissolved in nonpolar organic solvents. However, Leff *et al.*'s particles and our synthesized copper nanoparticles could be re-dissolved in hexane after precipitation.

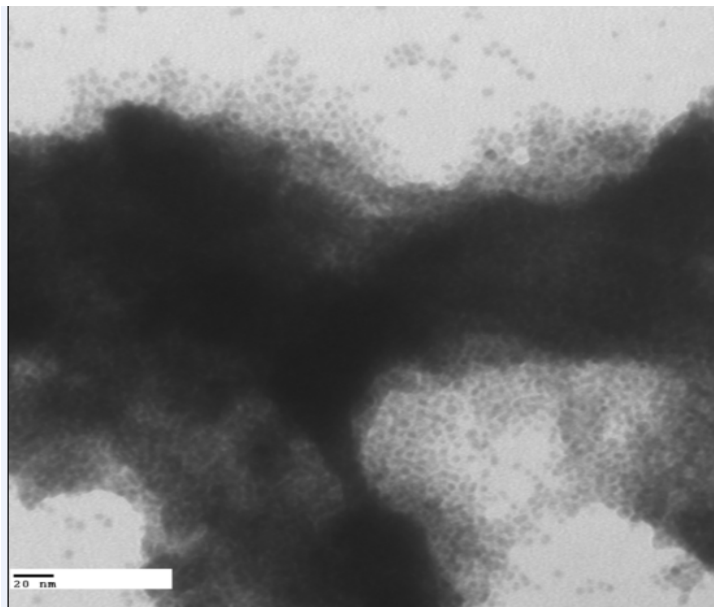


**Figure 4.3.1** TEM results for the modified version of Leff *et al.*'s recipe in which KCl was added to form anionic complexes of copper. Scale bar: 20 nm.

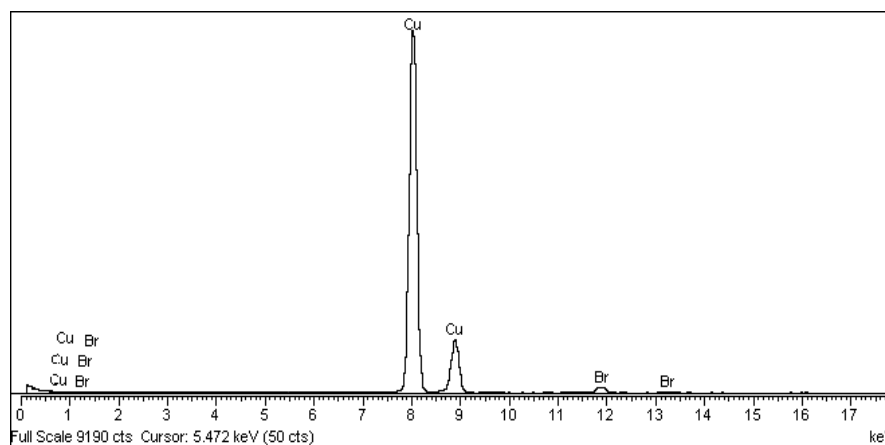


**Figure 4.3.2** EDS data for the synthesized nanoparticles that are apparently copper. Using the phase transfer reagent,  $N(C_8H_{17})_4Br$ , explains the noted Br in this diagram.

Leff and his co-workers (1996) claimed that gold nanoparticles synthesized in the presence of the phase transfer reagent,  $N(C_8H_{17})_4Br$ , have less stability, and they lose their solubility and agglomerate if stored as a powder for a few hours. Conversely, those gold nanoparticles produced without using  $N(C_8H_{17})_4Br$  maintain their solubility characteristics and are non-agglomerated for months regardless of the storage phase (powder or solution). Hence, they believed that the instability of gold nanoparticles is related to the existence of  $(C_8H_{17})_4N^+ Br^-$ . We discuss in Section 4.6 whether the presence of the phase transfer reagent causes instability and aggregation in copper nanoparticles.

Even though copper nanoparticles were re-dissolved in hexane after sedimentation and stored as a solution in liquid nitrogen, some black clusters can still be recognized in the TEM images. It was not clear whether they were formed during the synthesis procedure or were unstable copper nanoparticles aggregated after synthesis in the presence of  $N(C_8H_{17})_4Br$ .

By increasing chloride concentration and starting the equilibrium reaction between the cationic complex of copper and chloride, it was hoped that the phase transfer reagent could efficiently remove copper cations from the aqueous phase. Color change in the organic phase upon adding  $N(C_8H_{17})_4Br$  was justified by claiming that both copper cations were quantitatively transferred to this phase and resulted in its orange color. However, the aqueous phase might include some cationic complex of copper since the reactions by which anionic complexes were produced were not complete. In fact, having such small equilibrium constants, these reactions are not very productive with respect to the formation of anionic complexes. Therefore, a large portion of copper salt would stay unchanged in the aqueous phase unless the surfactant itself could transfer them into the organic layer. To synthesize copper nanoparticles in a colloidal system, copper cations must be reduced inside reverse micelles in the organic phase. If some of them were in the bulk aqueous phase prior to the addition of the water-soluble reducing agent,  $NaBH_4$ , they were reduced in this phase with no protection against agglomeration.

One possibility is that the black clusters in Figure 4.3.1 were aggregated nanoparticles that were synthesized in the wrong phase (the aqueous layer) and eventually diffused into the organic phase at the top. This was observed during a copper synthesis trial duplicating Leff *et al.*'s recipe with another surfactant (dodecanethiol,  $C_{12}H_{25}SH$ ), at which case the black color first appeared in the aqueous phase, meaning that the reduction reaction started in this phase. However, after 2 hours of stirring the two-phase system, the black color moved to the upper layer. The synthesized particles might be more soluble in the organic phase; thus, they diffused into this phase over time. In Figure 4.3.3, a cluster can be seen that was formed as a result of reducing copper cations in the aqueous layer in the absence of protecting surfactants.

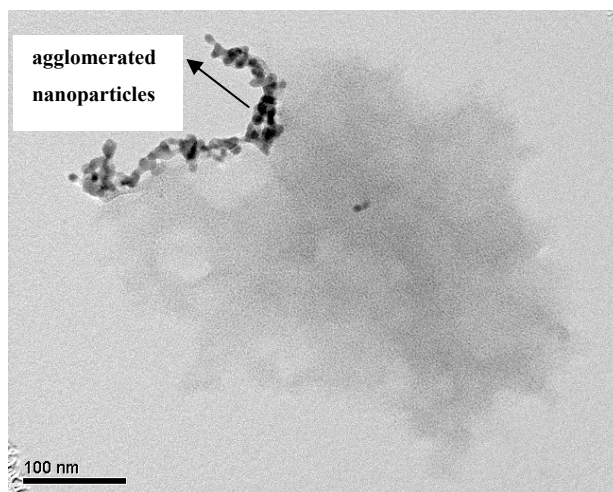


**Figure 4.3.3** A cluster of agglomerated copper nanoparticles formed as the result of inefficient transformation of cations into the organic phase. Leff *et al.*'s recipe was followed using dodecanethiol ( $C_{12}H_{25}SH$ ) as the surfactant. The phase that first turned dark was the aqueous one.

The next decision was to remove the aqueous phase and discard it before adding the reducing agent in order to eliminate completely the presence of any copper cations that remained in this layer. The intention was to limit the reduction site to the core of reverse micelles. The following section discusses the results for decanting the aqueous phase prior to adding  $NaBH_4$ .

## 4.4 Decanting the Aqueous Phase prior to the Reduction Step

### 4.4.1 Procedure

At this step of the modifications, a synthesis procedure similar to the one established for copper in the Section 4.3 was followed, except that the two-phase toluene/water mixture was poured into a separatory funnel before the reduction step was started. After oleylamine was added to the system, the mixture was stirred for an hour. The almost-clear aqueous phase was separated from the sharp blue organic phase and discarded. At the end of the separation, those fluffy structures, which are presumably an excess of surfactant floating in the aqueous phase, were stuck on the wall of the separatory funnel. The reducing agent solution (0.11 g of  $NaBH_4$  in 25 mL of distilled water) was added into the decanted sharp blue organic phase excluding fluffy objects. As soon as the reducing agent was introduced into the single phase system, the color started to change, but the rate of the color change was slower than that of the previous two-phase system. A possible mechanism for this slow color change is discussed later. After 5 minutes, the blue color of the organic phase turned to light brown. When the two-hour reduction time was

finished, the light brown organic phase was decanted from the clear aqueous phase and evaporated on a stirrer-hot plate at  $\sim 75^{\circ}\text{C}$  until its volume reduced to  $\approx 5$  mL. Then, 350 mL of ethanol was added to it and this final light brown liquid was stored in a dewar for a day. After the particle sediment was filtered, washed with an excess of ethanol, and left on a Petri dish for couple of minutes in the glove box to dry, an attempt was made to re-dissolve it in a nonpolar organic solvent such as hexane. Surprisingly, the final dry product was insoluble in hexane, while in the previous trials for the recipe with KCl, the dry product that sat on the filter paper re-dissolved in 200 mL hexane. As mentioned before, the insolubility of nanoparticles synthesized by this technique in nonpolar organic solvents confirms that these particles are unstable and had become agglomerated. Considering nanoparticle solubility characteristics over time, Leff *et al.* (1996) compared the stability of particles synthesized by their two schemes, one with the phase transfer reagent,  $\text{N}(\text{C}_8\text{H}_{17})_4\text{Br}$ , among the chemical reagents and the other without using it. They concluded that the instability of the first type of nanoparticles is related to the presence of  $(\text{C}_8\text{H}_{17})_4\text{N}^+\text{Br}^-$  since these particles are not stable with respect to aggregation and become insoluble in any nonpolar solvent if stored as a powder for few hours. In our case, the reason for synthesizing insoluble particles cannot be the presence of the phase transfer reagent because hexane-soluble copper nanoparticles were produced by adding KCl to Leff *et al.*'s recipe ( $\text{N}(\text{C}_8\text{H}_{17})_4\text{Br}$  was used). The properties of these nanoparticles are discussed in Section 4.3.

## 4.4.2 Characterization Techniques

### 4.4.2.1 TEM analysis

Decanting the organic phase is the new modification made to the synthesis recipe and it ultimately resulted in clusters of nanoparticles that were mostly agglomerated, as can be seen in Figure 4.4.1 and Figure 4.4.2. Separation of the aqueous phase was carried out to remove the copper cations that remained in this phase and to limit the reaction site to the reverse micelles' cores. However, during this separation, some surfactants, which were floating "fluffy" structures in the aqueous phase, were lost. After the reducing agent was added to the organic solution, the color changed slowly from blue to light brown. The formation of secondary reverse micelles, in which the source of electron was trapped, was challenging because the amount of surfactant decreased after decanting. Therefore, the intermicellar exchange process, which is the reduction of the copper cation by  $\text{BH}_4^-$  in a temporary dimer, was delayed. This is the possible mechanism for the slow color change that could not be recognized until 5 minutes elapsed from introducing the reducing agent to the one-phase system.

Moreover, the surfactant loss was the main reason for synthesizing agglomerated nanoparticles that were not soluble in hexane. Since some surfactants were unintentionally discarded while separating two phases, by the end of the synthesis, the number of the surfactant molecules on the surface of the nanoparticles decreased. Thus, some of these improperly protected nanoparticles became agglomerated. As can be observed in Figure 4.4.2, few nanoparticles are unagglomerated. Due to the lack of control in distributing surfactant on the surface of nanoparticles, these isolated particles might be more densely covered with oleylamine molecules than the agglomerated ones.

Studies that had been done on gold particles capped with alkanethiols demonstrated that the surfactant layer on the surface of these particles rendered them soluble in a non-polar organic solvent (Brust and Kiely 2002; Giersig and Mulvaney 1993). Hence, the lack of oleylamine molecules on the surface of particles synthesized by our modified recipe is the main reason for their insolubility in hexane.

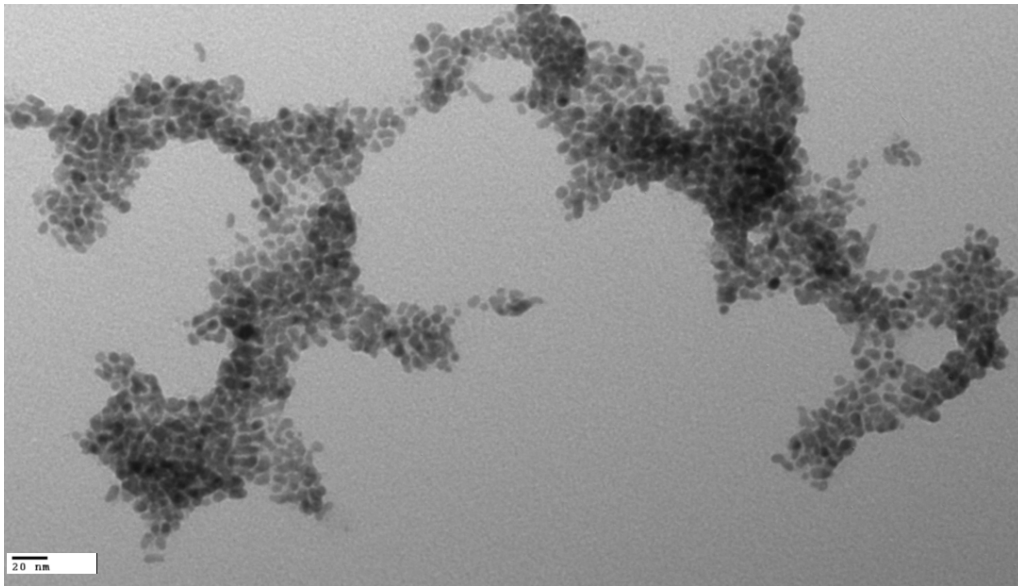


**Figure 4.4.1** Clusters of copper nanoparticles synthesized by reducing the decanted organic phase.

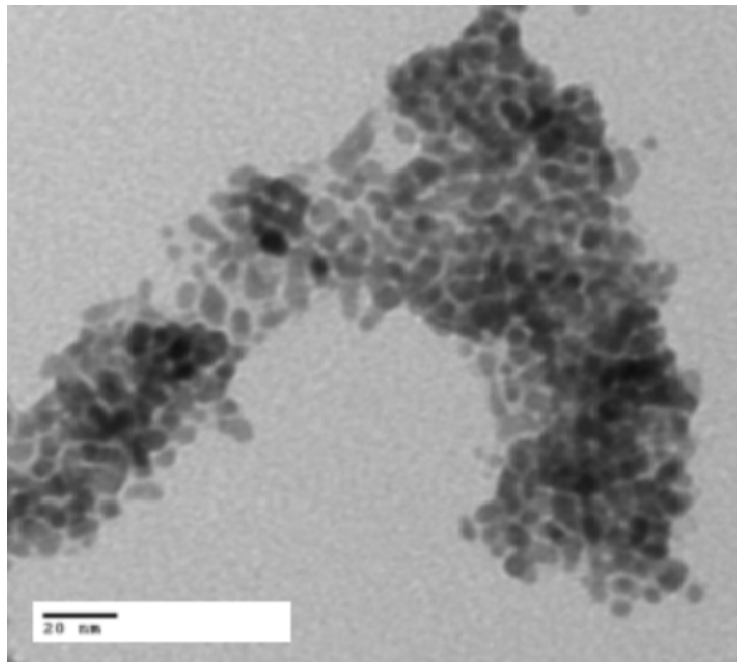


**Figure 4.4.2** A part of a cluster that is mostly made of agglomerated copper nanoparticles. Few nanoparticles, however, are not diffused to the neighboring particles and are isolated.

#### 4.4.2.2 FTIR spectroscopy

Fourier Transform Infrared (FTIR) spectra of neat oleylamine and copper nanoparticles were recorded to examine the previous statement; that is, the particles were not well capped with the alkylamine molecules (Figure 4.4.3).

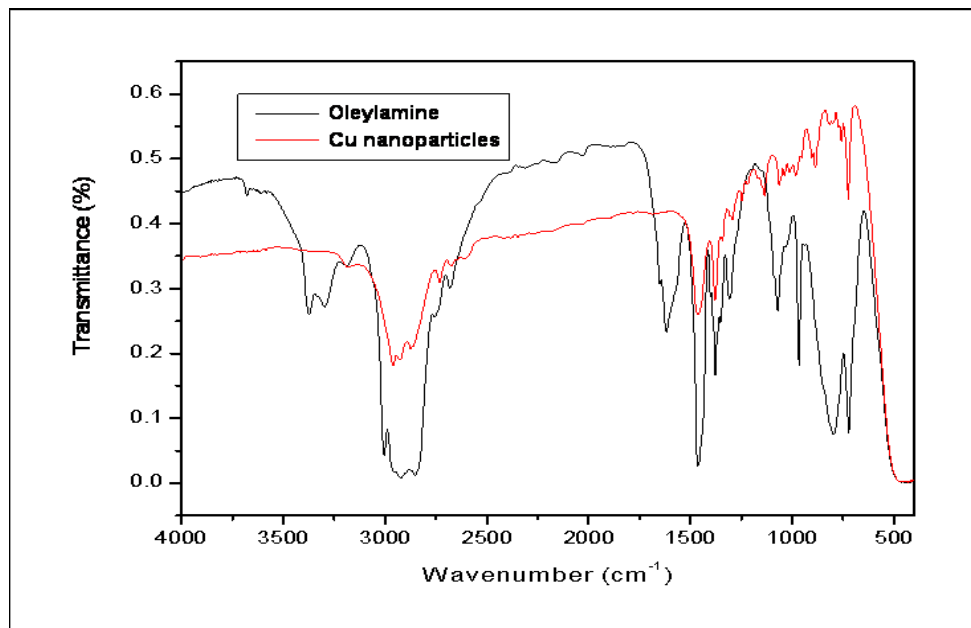


**Figure 4.4.3** FTIR spectra of neat oleylamine and copper nanoparticles synthesized by reducing the decanted organic phase.

Basically, if nanoparticles are functionalized with an alkylamine, IR spectroscopy of these surfactant-capped particles shows the same features as those for the neat amine, except that the bands from  $\approx 3310$  to  $2990 \text{ cm}^{-1}$  (due to the N-H stretch), the band at  $\approx 1600 \text{ cm}^{-1}$  (due to the N-H bend), and the bands in the  $\approx 900\text{-}700 \text{ cm}^{-1}$  region (due to the N-H wag) are all broadened and reduced in intensity, and the band at  $\approx 1100 \text{ cm}^{-1}$  (due to the C-N stretch) is broadened and increased in intensity compared to those same features of the neat amine. These effects predictably appear as the proximity of the metal surface to the bonds involved in these motions (Leff et al. 1996).

In Figure 4.4.3, the FTIR spectrum of copper nanoparticles synthesized by reducing the single phase is compared to the FTIR spectrum of the neat oleylamine. Obviously, few features of the amine can also be recognized among the bands of the copper nanoparticles. Moreover, in the ranges in which N-H bands

(stretch, bend, and wag) are evident for the free amine, no significant peaks for nanoparticles can be observed. Since the surfactant supposedly binds to the surface of the metal nanoparticles from its hydrophilic head (N-H), the lack of these bands proves that the synthesis of alkylamine-capped copper nanoparticles was not achieved. The peaks in the FTIR of the copper nanoparticles are due to the hydrocarbon solvent (toluene) in which nanoparticles were dispersed. The spectra of nanoparticles had been recorded before they were precipitated in ethanol.

Although decanting the organic phase prior to the reduction step caused undesirable agglomeration of copper nanoparticles, it was still possible to avoid agglomeration and also get rid of those cationic complexes of copper in the aqueous phase. A useful direction for future studies might be the calculation of the amount of surfactant lost upon separating the two phases by measuring the concentration of the surfactant in the final separated aqueous phase. Through addition of the same amount of oleylamine to the toluene solution prior to the reduction step, a two-phase liquid-liquid system can be established that has enough surfactant to transfer the source of electron quickly to the organic phase (no delay in color change) and protect synthesized nanoparticles against agglomeration, while the copper cations will be reduced only inside the reverse micelles. It is likely that these particles will be soluble and resolvable in nonpolar organic solvents.

#### 4.4.2.3 Ultra-Violet/Visible spectroscopy

Since the LaB<sub>6</sub> source TEM microscope used for analyzing these samples was not equipped with any chemical analysis system, such as EDS or SAED patterns, UV-visible spectroscopy was applied to determine whether the synthesized particles were metallic copper. Colloidal dispersions of metals show absorption bands or broad regions of absorption in the UV-visible range due to the excitation of plasma resonances or interband transitions, characteristic properties of the metallic nature of the particles (Pileni and Lisiecki 1993). The absorption band for the colloidal solution of metallic copper nanoparticles was studied for different sizes by Pileni and Lisiecki (1993). They reported a broad absorption band with a 570 nm peak which corresponded to the plasmon absorbance band of Cu nanoparticles as reported by Creighton and Eadon (1991). The peak became more significant as the size of nanoparticles increased from 2 to 10 nm. Furthermore, Yanase and Komiyama (1991) revealed that metallic nanoparticles surrounded by an oxide monolayer were characterized by a peak centered at 570 nm, and a residual absorption at 800 nm due to the oxide monolayer was also detected. If nanoparticles start to react with air during UV-visible analysis, this process can be monitored by UV-visible absorption spectroscopy, as was determined in a study by Ng and Fan (2006).

As shown in Figure 4.4.4, the intensity of the weak band that appeared after 30 minutes at  $\sim 700$  nm gradually decreased as copper nanoparticles were oxidizing. The absorption peak at 700 nm was due to the formation of the oxide monolayer, but its intensity decreased over time, indicating that the copper nanoparticles were further oxidized. After 180 minutes, upon the formation of  $\text{Cu}_2\text{O}$  nanoclusters the broad absorption band from 600-800 nm fully disappeared, and simultaneously, another sharp peak appeared at  $\sim 270$  nm.

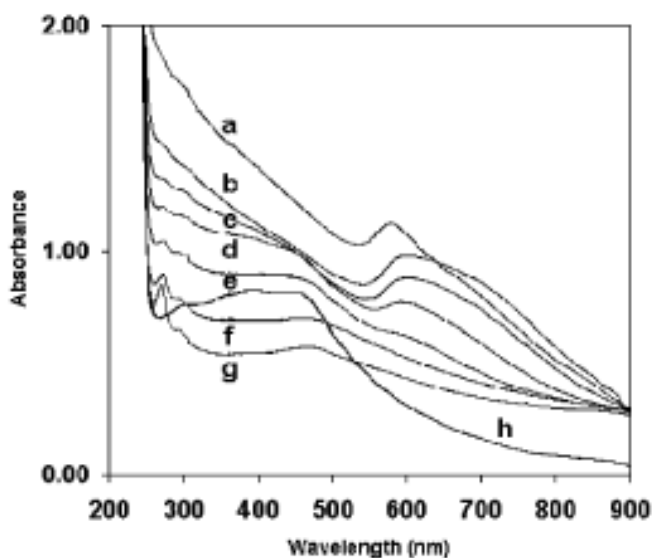


**Figure 4.4.4** UV-visible absorption spectra of reaction mixture at various times of oxidation accompanying a change in particle morphology of the  $\text{Cu}_2\text{O}$  nanocrystals: (a) 30, (b) 60, (c) 90, (d) 120, (e) 150, (f) 180, and (g) 210 min and (h) after aging for 3 days (Ng and Fan 2006).

Half of the final toluene solution of nanoparticles, which were synthesized by adding the reducing agent to the decanted organic phase, was diluted with plenty of toluene ( $\sim 300$  mL). This colloidal dispersion of synthesized nanoparticles was analyzed with UV-visible spectroscopy.

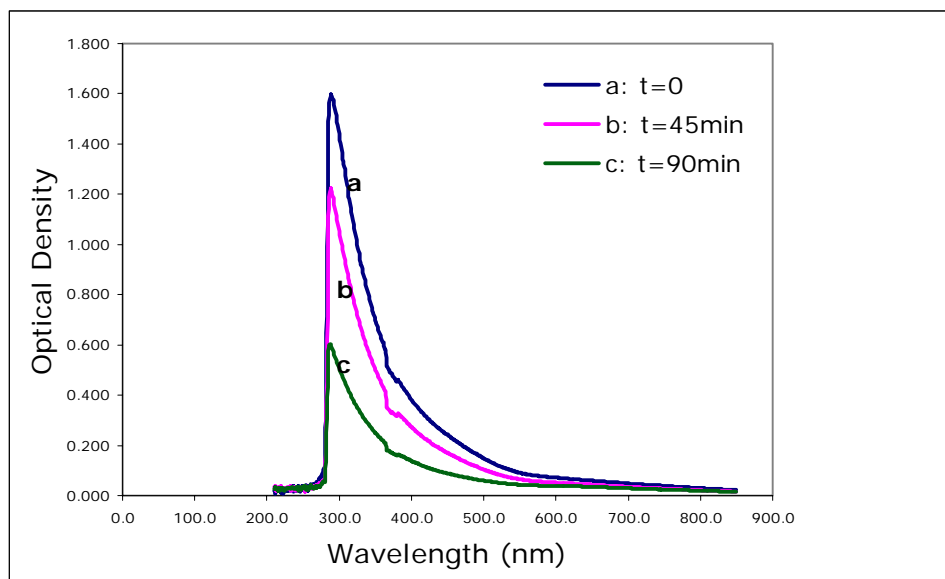


**Figure 4.4.5** UV-visible absorption spectra of the nanoparticles synthesized by reducing the decanted organic layer: (a) just after the toluene solution of the particles was exposed to air, after (b) 45 min, and (c) 90 min of exposure to air.

The UV-visible spectra of nanoparticles over time are shown in Figure 4.4.5. The intensity of the sharp peak that appeared just at the beginning of the analysis at  $\sim 300$  nm decreased over time. Hardly any conclusion about the chemical characteristics of the sample can be made as our findings differ from the UV-visible spectroscopy data given in the literature for Cu and  $\text{Cu}_2\text{O}$ . The 300 nm band may be considered as a 270 nm peak with a red shift, meaning that the size of the  $\text{Cu}_2\text{O}$  crystals in our sample is larger than that of the  $\text{Cu}_2\text{O}$  nanocrystals synthesized by Ng and Fan (2006). However, the size of triangular  $\text{Cu}_2\text{O}$  nanoplates synthesized in their work was 150 nm at the edge, as can be seen in Figure 4.4.6, and the size of those rarely non-agglomerated nanoparticles observed in Figure 4.4.2 is  $\sim 5$  nm. Thus, the peak at 300 nm cannot be interpreted by referring to Ng *et al.*'s UV-visible spectroscopy data.

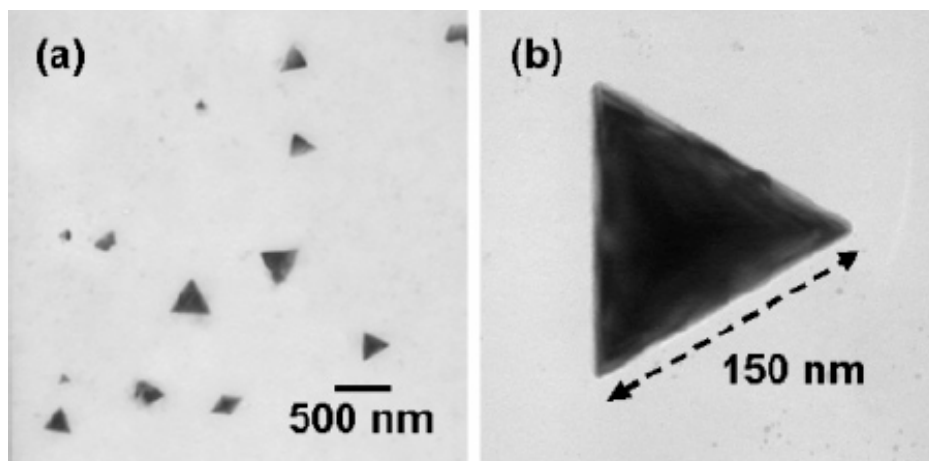


**Figure 4.4.6** (a) TEM image of  $\text{Cu}_2\text{O}$  triangular nanoplates synthesized by Ng *et al.*'s method. Oxidation time = 210 min. (b) Single triangular nanoplates (Ng and Fan 2006).

Some interpretations that can be made confidently by looking at these spectra are as follows:

1) The absorption band usually centered at 570 nm for colloidal dispersions of metallic copper is not observed. This absence indicates that either metallic nanoparticles have not been produced by the end of the synthesis or the plasmon absorption band of copper has been influenced by chemical modification of the surface.

One assumption for not seeing the 570 nm band is incomplete reduction reaction. In other words, copper cations trapped inside the reverse micelle,  $\text{Cu}^{2+}$ , might be reduced to  $\text{Cu}^+$  instead of Cu. Thus, we might synthesize copper (I) salt nanoparticles instead of metallic copper nanoparticles by following this modified version of Leff *et al.*'s recipe. However, no further investigation has been done to see whether this mechanism caused the undesirable clusters at this stage of our modifications since the other mechanism is more likely to be the reason for the lack of a plasmon absorption band.

The second possible mechanism for the disappearance of the 570 nm peak is the chemical modification of the surface. It has been reported for Ag that the plasmon absorption band of metals is very strongly affected by chemical modification of the surface (Henglein 1993). Those anions that readily form complexes with  $\text{Ag}^+$  ions are absorbed on silver particles and result in a decrease in band intensity and broadening of the band. For copper, which is a more reactive metal than silver, the absorbance of these anions is even more feasible. Qi and co-workers (1997) observed the same UV-visible spectra (Figure 4.4.7) as we did for copper nanoparticles they synthesized by reducing  $\text{CuCl}_2$  with  $\text{NaBH}_4$  in nonionic water-in-oil microemulsions. They justified the absence of a plasmon peak by claiming that  $\text{Cl}^-$  anions

that can form CuCl, the insoluble salt, with  $\text{Cu}^+$  might be strongly absorbed on Cu particles and form a CuCl monolayer, leading to significant damping of the plasmon band.

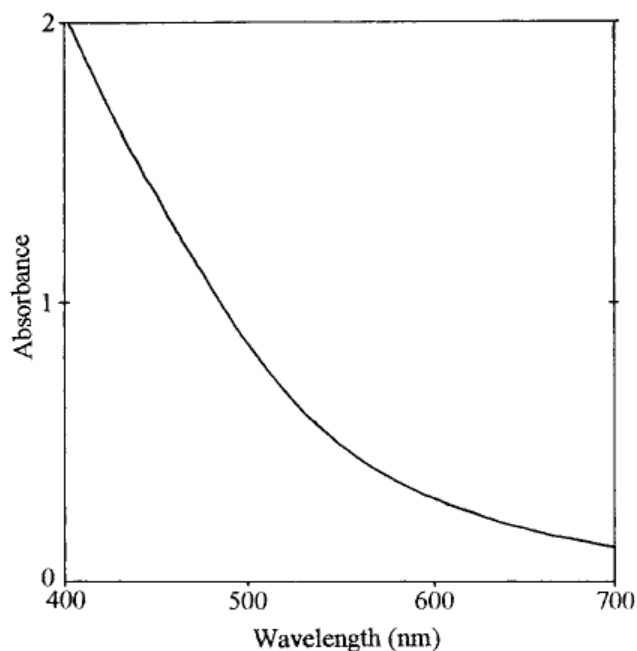


**Figure 4.4.7** Absorption spectrum of copper particles synthesized in nonionic water-in-oil microemulsions by reducing  $\text{CuCl}_2$  with  $\text{NaBH}_4$  (Qi et al. 1997).

Since the copper salt used in all modified recipes in this work is also  $\text{CuCl}_2$ , the mechanism proposed by Qi *et al.* (1997) can be implied to explain the lack of a plasmon band in the UV-visible spectra obtained for the synthesized particles at this step. Moreover, plenty of KCl was added at the beginning of the procedure to produce anionic complexes of copper ( $[\text{CuCl}_3]^-$  and  $[\text{CuCl}_4]^{2-}$ ). Thus, there were lots of  $\text{Cl}^-$  anions in the system that might have ultimately been absorbed on the surface of particles after they were synthesized in microemulsion media. To investigate whether adding KCl was the main reason for the possible formation of a CuCl monolayer at the surface of the particles, some trials were done without adding KCl, and UV-visible spectra of those synthesized particles were obtained. We discuss these results in Section 4.6.

2) The intensity of the sharp peak that first appeared at  $\sim 300$  nm decreased so quickly over time that, after 90 minutes of exposing the toluene solution of the synthesized particles to air, the intensity of the peak reduced to about  $\sim 1/3$  of its original magnitude. This fast reduction in peak intensity demonstrates that the particles are changing most likely due to oxidation. This instability is due to the absence of a protective surfactant layer on the particle surface and also the presence of  $(\text{octyl})_4\text{N}^+\text{Br}^-$ , as discussed previously.

In the next section, a post-synthesis heating procedure that was applied to re-stabilize the poorly-capped nanoparticles synthesized at this step of our modifications is detailed. In later sections, the results obtained for post-synthesis heated particles are compared with those shown in this section to determine whether this method is a successful approach for preventing the formation of black clusters of agglomerated particles.

## 4.5 Post-synthesis Heating

### 4.5.1 Principles and Procedure

Clusters of agglomerated nanoparticles were undesirably synthesized in all the synthesis procedures followed up to this step, especially in the last modified version of Leff *et al.*'s recipe: reducing the decanted organic layer. As discussed before, the lack of a capping agent layer (oleylamine) on the surface of synthesized nanoparticles is the main reason for their instability (agglomeration) and insolubility in organic media such as hexane. These poorly capped copper nanoparticles were colloidally dispersed in toluene before ethanol was added to flocculate them for post-synthesis treatments (i.e., filtering, washing with an excess of ethanol, drying, and re-dissolving in a nonpolar organic solvent). However, after sedimentation, the particles come into contact with each other, and consequently, they became agglomerated in the absence of the strong steric barrier. The formation of nanoparticle clusters could have been avoided if the synthesized nanoparticles had been provided with enough protective surfactant molecules while they were still in the organic solution. Besides adding the amount of oleylamine lost in the separation step to the stirring two-phase system at the reduction step, another approach for increasing the steric barrier is heating nanoparticles after the synthesis. In previous studies on post-synthesis annealing (Henneke 2001), it was suggested that heating nanoparticles after they were collected would ensure that the capping molecules sufficiently covered the surface and maximized the steric barrier. In other words, if there were some surfactant molecules around the nanoparticles surface, which did not cap properly the surface from the hydrophilic side (N-H), post-synthesis heating was found efficient in re-organizing them and facilitating the nanoparticle stabilization process.

Figure 4.5.1 schematically shows the possible mechanism that synthesized copper nanoparticles go through in the post-synthesis heating step to be capped properly by surfactant.

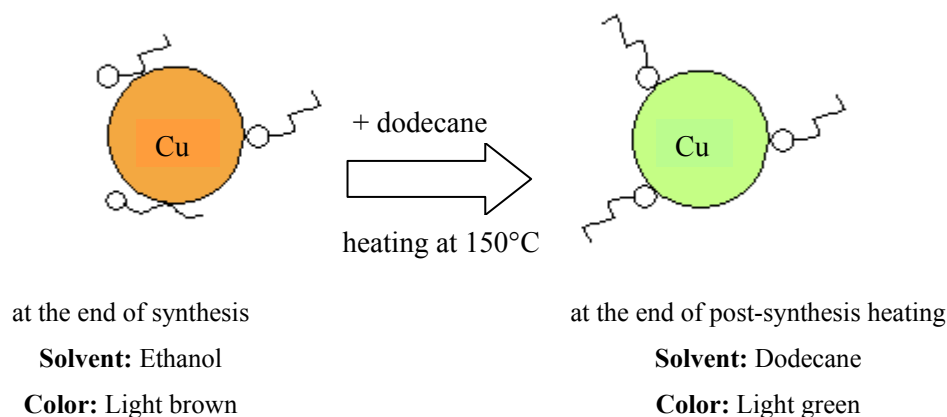


**Figure 4.5.1** Schematic view of the post-synthesis heating step in which the synthesized copper nanoparticles become more stable after uncapped surfactant molecules have had the chance to bind to the nanoparticle surface by their hydrophilic head.

A 20 mL vial of flocculated copper nanoparticles in ethanol was taken to start the process. The color of this liquid was light brown when shaken. An equal volume of dodecane was mixed with it to make a homogenous brown solution of copper nanoparticles. As the temperature for the post-synthesis heating step was 150 °C, a solvent with a suitable boiling point was required. Moreover, the media in which nanoparticles were being heated had to be organic since these particles were still soluble in nonpolar organic solvents. Dodecane (boiling point: 216.2 °C) was chosen for this process in view of these two points. The heating of the copper nanoparticles dissolved in dodecane was started on a hot stir plate while the solution was vigorously stirring. After ~ 20 minutes heating at 150 °C, the solution turned light green. No further color change was observed for this system, even when the whole solution was evaporated and a thin light green residue was left on the bottom of the beaker. After the color change, the solution was maintained at 150 °C for ~ 15 minutes to reduce its volume to  $\approx$  10 mL. Next, this light green solution was dissolved in 150 mL of hexane. Although we tried to be consistent in our treatment of the synthesized nanoparticles after reducing the volume of the organic layer, the same procedure could not be followed for dodecane-dissolved nanoparticles at the end of the post-synthesis heating step. Based on Leff *et al.*'s recipe, the organic solution that remained after the evaporation step should be mixed with enough ethanol so that nanoparticles became flocculated and precipitated at the bottom. After cooling this solution, the precipitate was then filtered, washed with an excess of ethanol, and dried. Finally, an

attempt was made to re-dissolve the precipitate in a nonpolar organic solvent to reform a colloidal solution of synthesized particles for later analyses. However, this time, synthesized copper nanoparticles that had been heated for almost half an hour at 150 °C did not precipitate after 300 mL of ethanol was added. To find an explanation for this phenomenon, the flocculation process should be first considered. Upon the addition of a polar solvent to a colloidal suspension of nanoparticles, the Gibbs free energy of the suspension changes. As a result, the dispersed particles become more attracted to each other. Being proportional to the particle size, the attraction force is stronger for larger particles. Hence, for flocculating smaller nanoparticles, more polar solvent is required. While the average particle size did not change during the post-synthesis heating step, as supported by the TEM results that are presented later, a reasonable assumption for this unsuccessful precipitation is that the attraction forces were not strong enough to bring nanoparticles close to each other. Therefore, post-synthesis heating might enhance the repulsion force– the steric barrier due to the presence of long alkyl chains surrounding nanoparticles– so significantly that the attraction force caused by the introduction of a polar solvent such as ethanol could not overcome it.

## **4.5.2 Characterization Techniques**

### **4.5.2.1 TEM analysis and EDS spectroscopy**

For further analysis of the copper nanoparticles after the post-synthesis heating step, 150 mL of hexane was added to the final 10 mL light green organic phase. A homogenous light green colloidal suspension of nanoparticles was obtained and then placed in the liquid nitrogen dewar to be protected against oxidation.

For TEM analysis, a drop of the hexane solution of nanoparticles (light green) was dried on a Formvar coated gold grid. First, the sample was analyzed with the LaB<sub>6</sub> source Philips CM10, and the results shown in Figure 4.5.2 were obtained. As can be seen, the nanoparticles are separately oriented without having any black clusters consisting of agglomerated particles. Since these nanoparticles were colloiddally dispersed in hexane, they were pushed to the edges of the drop while it was drying on the TEM grid. That is how the arrays of nanoparticles, shown in Figure 4.5.2 (a), were shaped. At higher magnifications, these nanoparticles were recognized as spherical particles with an average size of about 5 nm.

Next, the sample was taken to the field emission source JEOL JEM.2010F to determine its crystalline structure and oxidation state. Two methods can be used for examining these properties when using HRTEM microscopes: Selected-Area Electron Diffraction (SAED) patterns and HRTEM images of a

nanocrystal, in which the  $d$  spacing can be measured. Both of these data were collected for the sample during the HRTEM analysis.

As discussed before, the green organic phase was dissolved in hexane without any post-synthesis treatments. Our purpose in washing the filtered sediment with an excess of ethanol in previous trials was to remove any spare hydrocarbons from the sample. The presence of any heavy hydrocarbon with a high boiling point on the surface of the specimen results in charge build up under HRTEM analysis. As the hydrocarbon layer is a lower emitter of electrons than metal nanoparticles, this contamination shows up in TEM images as a dark area.

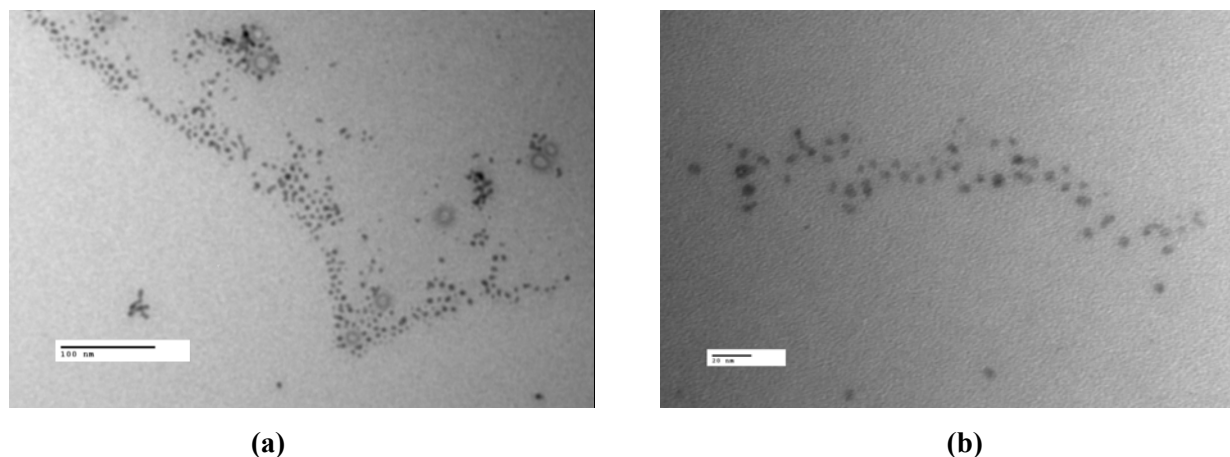


**Figure 4.5.2** (a) TEM images of copper nanoparticles after half an hour post-synthesis heating at 150 °C showing how arrays of separated nanoparticles were formed, (b) The particles were almost spherical, with an average size  $\sim$  5 nm.

It is worthwhile recalling that 150 mL of hexane was added to 10 mL of light green dodecane-dispersed nanoparticles at the end of the post-synthesis step. Obviously, dodecane was not discarded from the system prior to the HRTEM analysis and remained on the surface of the TEM grid. Moreover, gas chromatography of hexane, given in Figure 4.5.3, showed multiple peaks, meaning that there were possibly some impurities in hexane that might have caused the charge build-up on the TEM images (Figure 4.5.5 (a)), but less remarkably than that for dodecane.

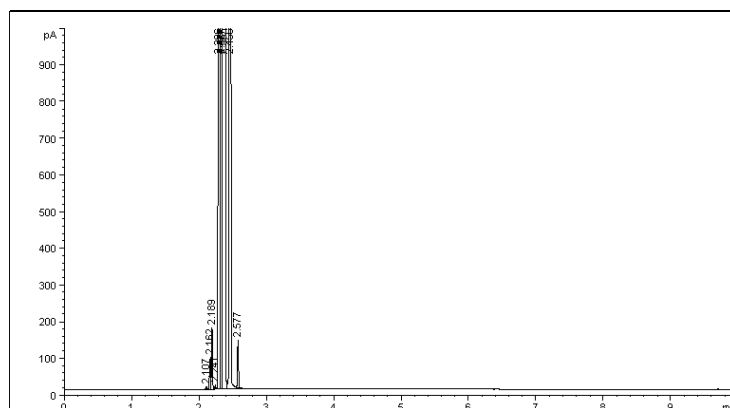
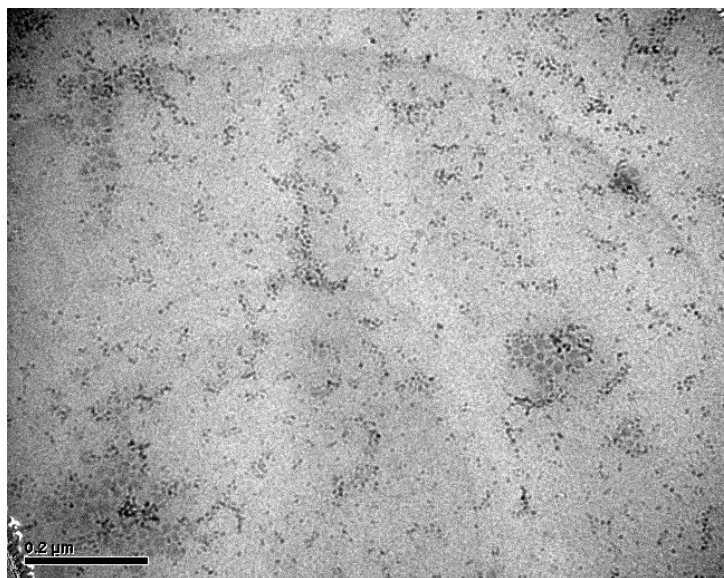
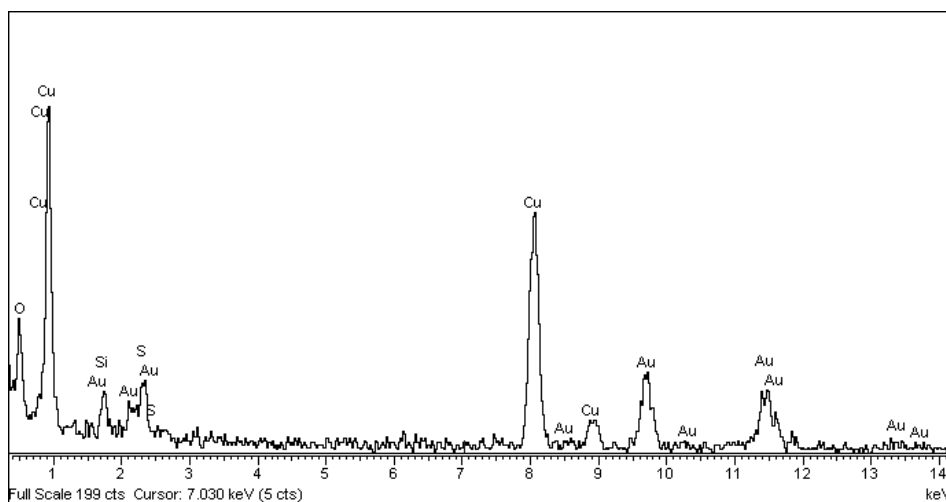


**Figure 4.5.3** The result of gas chromatography (GC) for hexane used as the solvent for the post-synthesis heated nanoparticles.

If the EDS spectrum in Figure 4.5.4 (b), which was taken before the charge cloud formation, is compared to the spectrum of the sample after the black area appeared on the specimen in Figure 4.5.5 (b), one can determine their differences in many ways. Upon the black cloud formation, copper peaks dropped off, while the oxygen peak significantly increased. Bromine (Br) traces appeared only in the second EDS, where they took the place of sulfur (S) peaks, which were unexpectedly detected for the sample before the charge build-up. Although there is no certain explanation for these differences, an assertion is made that the presence of the hydrocarbon impurities (dodecane) does affect the characterization results. The charge build-up was not observed while the LaB<sub>6</sub> source TEM microscope was used possibly due to the lower beam current when compared to the field emission HRTEM microscope.

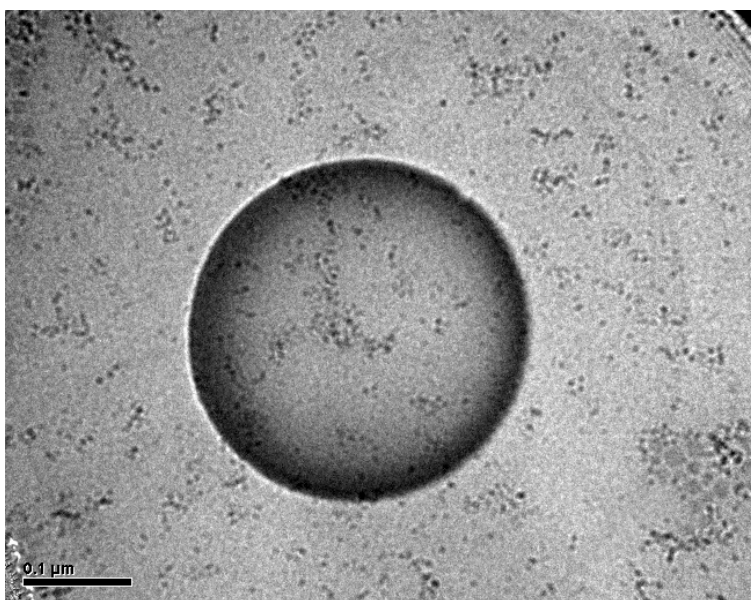


(a)

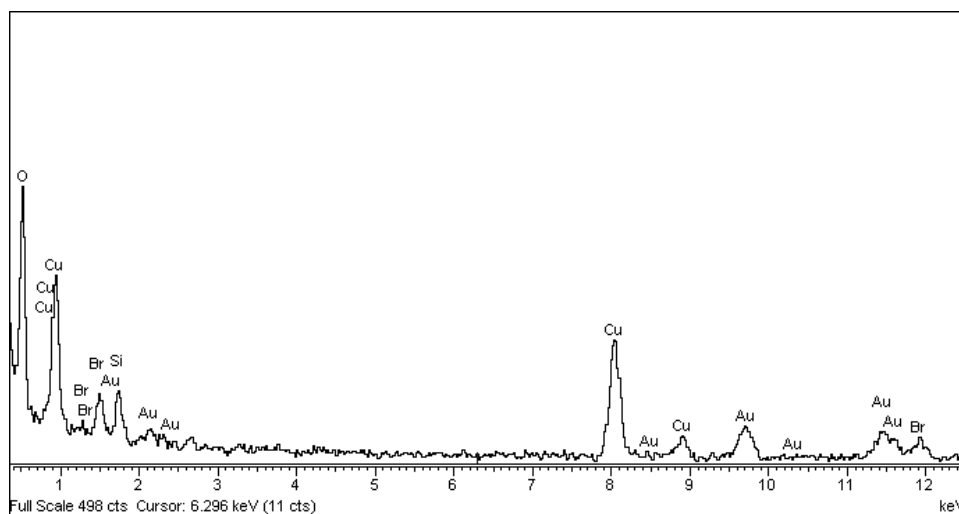


(b)

**Figure 4.5.4** (a) The overall TEM image of the post-synthesis heated sample taken by HRTEM microscope and (b) the EDS spectrum of nanoparticles prior to the charge build-up.



(a)



(b)

**Figure 4.5.5** (a) TEM image taken by HRTEM microscope of the post-synthesis heated nanoparticles after the formation of the charge cloud and (b) EDS spectrum of the black area (charge build-up) caused by the hydrocarbon impurities (dodecane) on the surface of the specimen.

#### 4.5.2.2 HRTEM analysis and SAED diffraction patterns

HRTEM images picturing lattice-fringes are a reliable source for measuring  $d$  spacings of nanocrystals. By matching these data with the tables of Miller indices and interplanar spacings of different materials, the phase(s) of the specimen can be determined.

For instance, in Table 4-3, interplanar spacings of face-centred cubic copper are listed.

**Table 4-3** Miller indices and interplanar spacings of face-centred cubic copper (Andrews et al. 1971)

<b>Cu(fcc), Lattice parameter <math>a_0 = 3.6150\text{\AA}</math></b>	
<b>hkl</b>	<b>d-spacing (<math>\text{\AA}</math>)</b>
111	2.087
002	1.808
022	1.278
113	1.090
222	1.044
004	0.904
133	0.829
024	0.808
224	0.738

Cubic copper oxide (cuprite),  $\text{Cu}_2\text{O}$ , has the same set of data, presented in Table 4-4:

**Table 4-4** Miller indices and interplanar spacings of cubic copper (I) oxide (Cu<sub>2</sub>O) (Chiang et al. 2000)

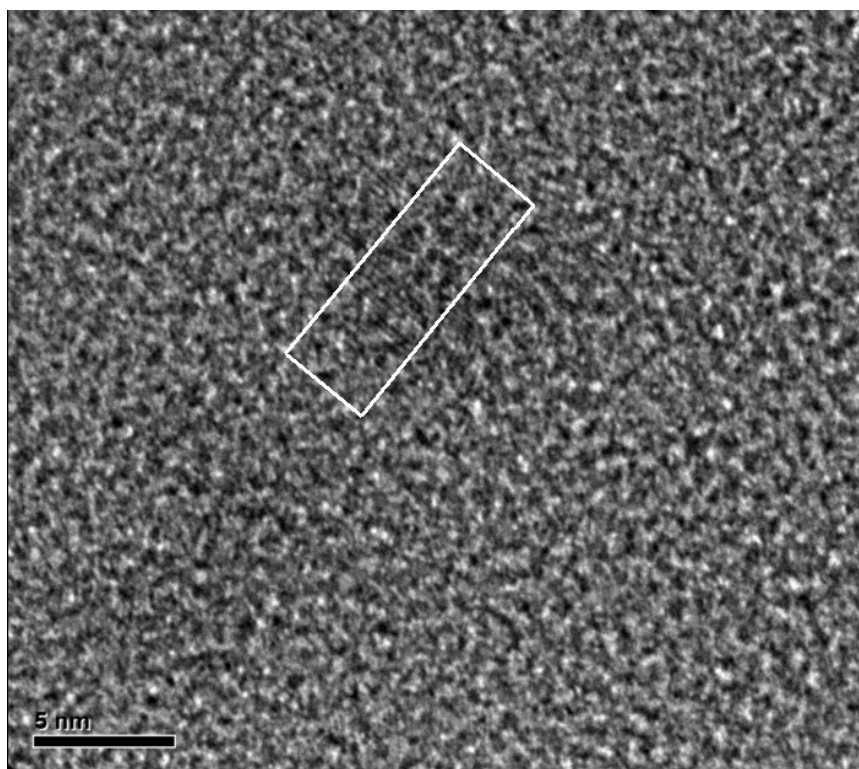
<b>Cu<sub>2</sub>O (cubic)</b>	
<b>hkl</b>	<b>d-spacing (Å)</b>
110	3.02
111	2.47
200	2.14
220	1.51
311	1.29

Figure 4.5.6 (a) shows the HRTEM image taken of a single copper nanocrystal that underwent post-synthesis heating. The histogram, which can be seen in Figure 4.5.6 (b), is the result of the software analysis on the white box area illustrated in Figure 4.5.6 (a). It is the profile of those parallel lines, which are representatives of the lattice fringes, and the distance between two subsequent peaks provides us with the  $d$  spacing that corresponds to the crystalline structure of this single particle. Usually, these histograms are symmetric, unless the surface of the nanocrystal is covered with impurities that bias the signals. Since in this case, the excess of hydrocarbons on the specimen created difficulties in analyzing them with different techniques, i.e., TEM and EDS, the asymmetric histogram can also be justified by the presence of the hydrocarbon impurities that blurred the HRTEM image and made it challenging to determine the crystalline area. The  $d$  spacing derived from the diagram is 0.269 nm, which is close neither to  $d$  spacings of Cu nor to those of  $\text{Cu}_2\text{O}$ .

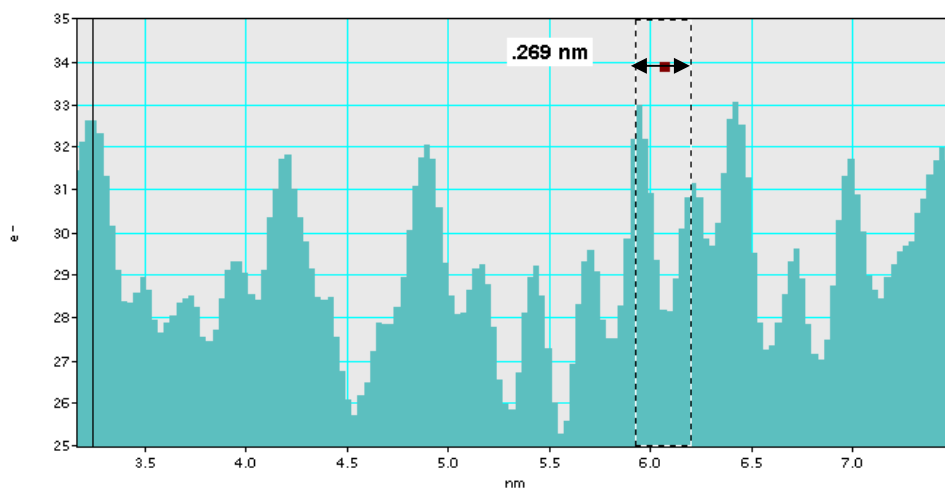
We tried to find a less impure area in which to redo HRTEM analysis. In Figure 4.5.7, another HRTEM image and its resultant histogram can be seen. As the histogram is still asymmetric, the measured  $d$  spacing, 0.219 nm, is still unreliable, even though it is close to 0.214 nm, which corresponds to the {200} plane of cubic  $\text{Cu}_2\text{O}$ .

The SAED of the sample could also clarify its phases; however, due to the impurities, no points or rings were observed in the diffraction pattern, as can be seen in Figure 4.5.8, meaning that no crystalline structure was detected.

The post-synthesis procedure is efficient in stabilizing poorly protected nanoparticles by providing the opportunity to the improperly capped surfactant molecules to re-organize and bind to the surface of copper nanoparticles. Dodecane, the solvent used in the heating step because of its high boiling point, contributed to the hydrocarbon impurity and biased the characterization results. The excess of heavy hydrocarbons could not be washed away from the sample by following post-synthesis treatment since the resulted nanoparticles did not flocculate upon the addition of ethanol. The challenge in characterizing post-synthesis heated nanoparticles might be resolved by developing appropriate purification techniques.

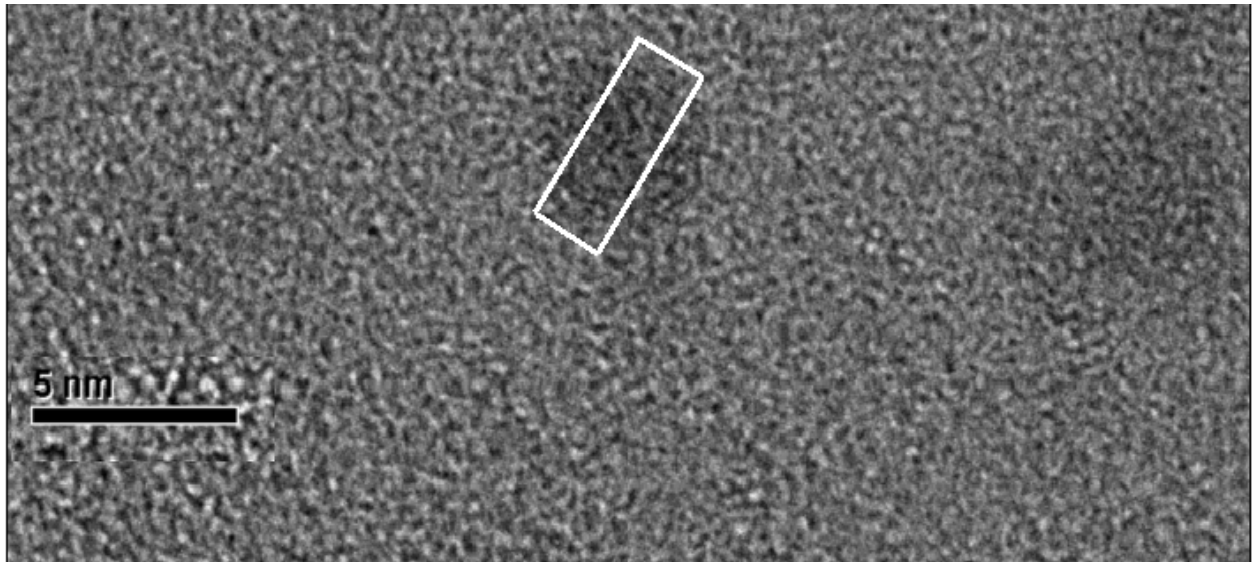


(a)

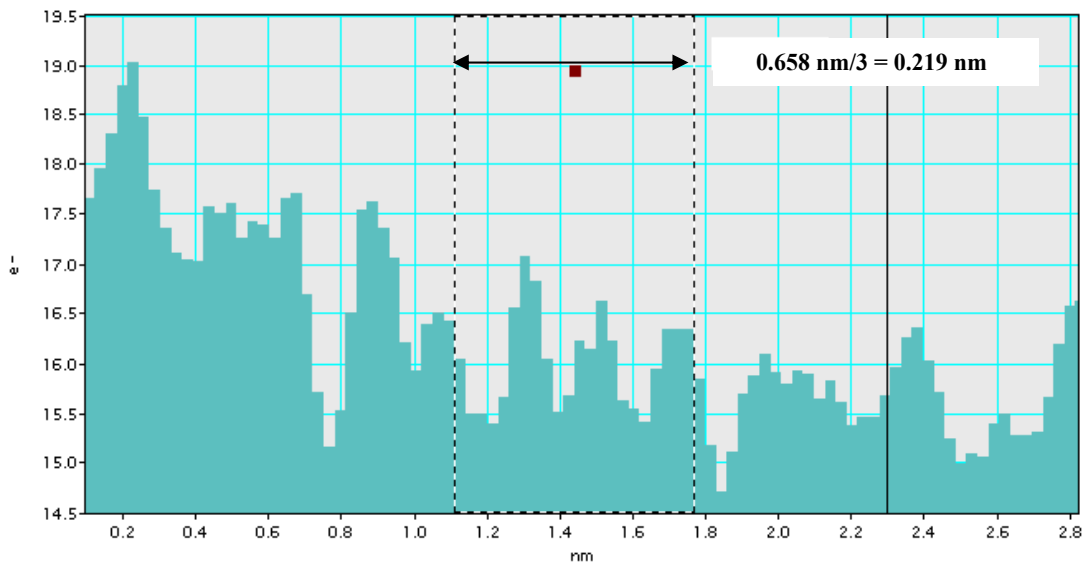


(b)

**Figure 4.5.6** (a) HRTEM image of a single copper nanocrystal that was heated after the synthesis in dodecane at 150 °C for half an hour and (b) the histogram that facilitates the measurement of the  $d$  spacing corresponding to the particle crystalline structure.



(a)



(b)

**Figure 4.5.7** (a) HRTEM image of a single copper nanocrystal and (b) the corresponding histogram of the white box area shown in (a).

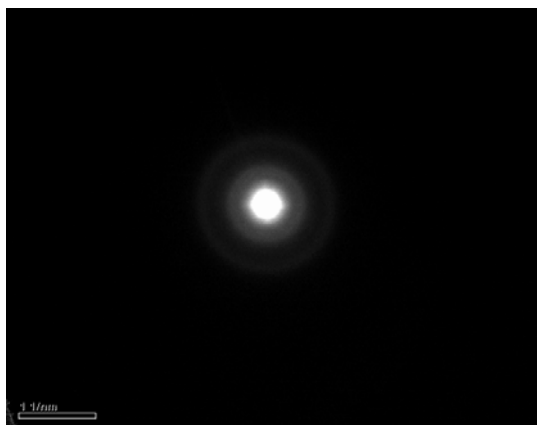


**Figure 4.5.8** SAED pattern obtained for the sample of the post-synthesis heating procedure with no obvious ring or point.

#### 4.5.2.3 FTIR spectroscopy

The FTIR spectra of the post-synthesis heated nanoparticles were collected for comparison with those of oleylamine. Since TEM images show that the result from the post-synthesis heating step is separated nanoparticles without any case of black agglomerated clusters, these two spectra are expected to show the same peaks. In fact, these particles were thought to become well capped by the end of the heating procedure and consequently stabilized. However, the FTIR spectra of these nanoparticles, shown in Figure 4.5.9, are almost the same as those of non-heated nanoparticles, as shown in Figure 4.4.3.

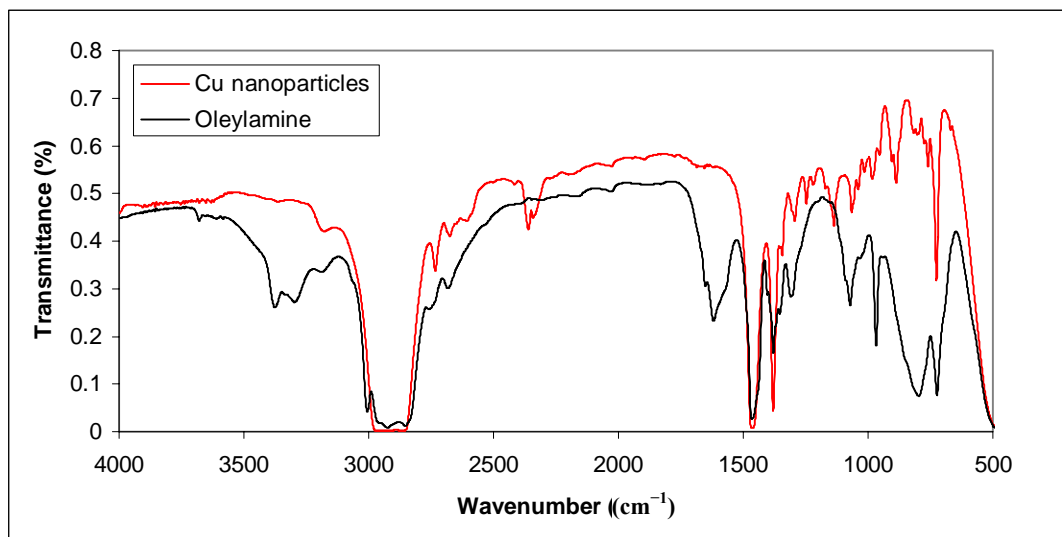


**Figure 4.5.9** FTIR spectra of oleylamine and copper nanoparticles that were heated after synthesis in dodecane at 150°C for half an hour.

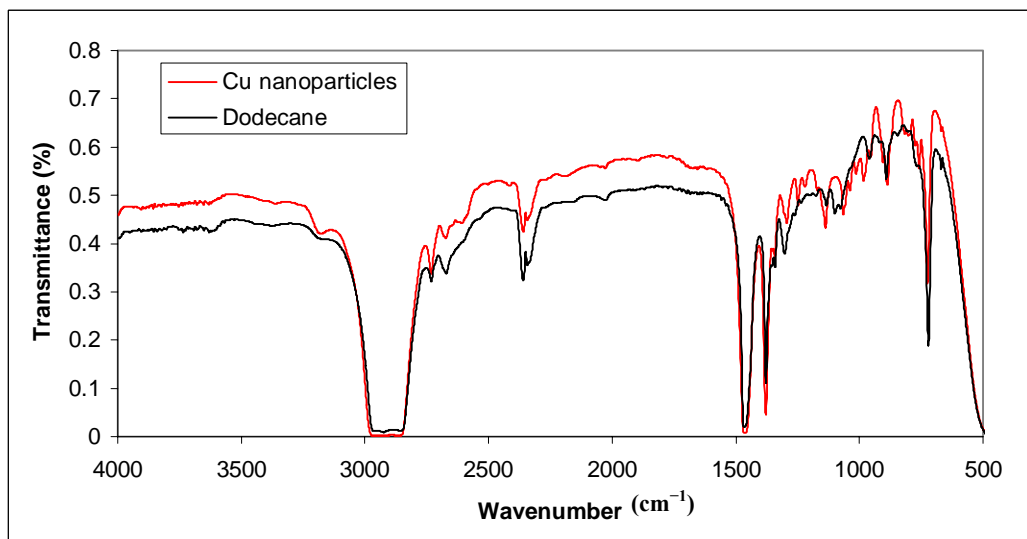


**Figure 4.5.10** FTIR spectra of dodecane and nanoparticles that were dissolved in dodecane and heated after synthesis.

As can be seen in Figure 4.5.9, the FTIR spectra of the post-synthesis heated nanoparticles do not show the bands corresponding to the N-H stretch ( $\approx 3310$  to  $2990$   $\text{cm}^{-1}$ ), the N-H bend ( $\approx 1600$   $\text{cm}^{-1}$ ), and the N-H wag ( $\approx 900$  to  $700$   $\text{cm}^{-1}$ ). Due to some uncertainties about the peaks in the range of  $1000$ - $700$   $\text{cm}^{-1}$ , the FTIR spectra of nanoparticles was compared with the FTIR spectra of neat dodecane, in which the

synthesized nanoparticles were heated at 150°C for half an hour. Since excess dodecane was not discarded after the post-synthesis step, much of it was in the hexane solution of the nanoparticles while the FTIR spectra were recorded. Comparison of two spectra in Figure 4.5.10 shows that they are almost identical. Therefore, the peaks in the range of 1000-700  $\text{cm}^{-1}$  are likely due to the presence of dodecane in the sample.

Regarding the results of FTIR spectroscopy, one may conclude that there is no significant bonding between the hydrophilic head of the surfactant (N-H) and the surface of nanoparticles. However, based on TEM results and our observation during the post-synthesis procedure -unsuccessful precipitation after adding the usual amount of ethanol in this recipe and color change from light brown to light green- it is believed that the nanoparticles that experienced the post-synthesis heating step were well-protected against aggregation. The only clear reason for this protection is the steric barrier provided by amphiphilic molecules of oleylamine. The low concentration of the surfactant in this system (due to the surfactant loss at the pre-reduction separating step) might also have caused the N-H bands not to appear in the FTIR spectra of the nanoparticles. Nevertheless, the mechanism of nanoparticle stabilization during post-synthesis heating should be investigated further to see whether the surfactant reorganization on the surface of nanoparticles is the main reason for the production of non-agglomerated nanoparticles.

#### 4.5.2.4 Ultra-Violet/Visible spectroscopy

The hexane solution of the post-synthesis heated nanoparticles was used for UV-visible spectroscopy. Absorption spectra of the sample were collected over a period of 100 minutes. These spectra, shown in Figure 4.5.11, have almost the same features as those for non-heated nanoparticles (Figure 4.4.5) with a shift towards higher energy that has been shown in previous work to be due to a decrease in the size of produced particles. Since the separated nanoparticles fabricated by the end of the post-synthesis heating step are much smaller (with an average particle size of  $\sim 5$  nm) than the black clusters of agglomerated nanoparticles synthesized by reducing the decanted organic phase, this blue shift is not surprising.

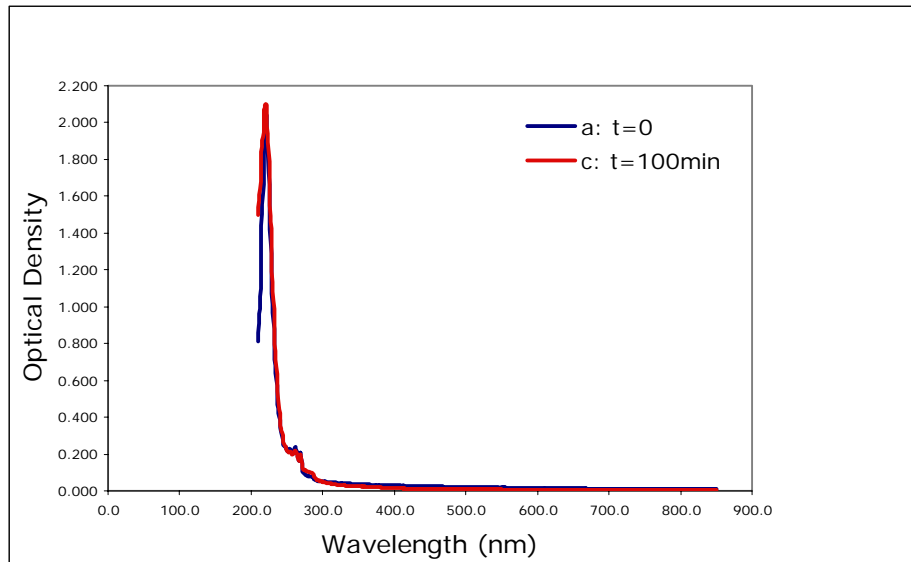


**Figure 4.5.11** (a) UV-visible absorption spectra of post-synthesis heated nanoparticles just after the hexane solution of nanoparticles was exposed to air and (b) after 100 min of exposure to air.

The plasmon peak at 570 nm is not observed for the post-synthesis heated nanoparticles. As KCl and  $\text{CuCl}_2$  were both among the materials used for synthesizing these nanoparticles, the previous statement about the formation of the insoluble monolayer of CuCl on the nanoparticle surface significantly damping the plasmon band is still valid. To a lesser extent, the small average particle size ( $\sim 5$  nm) could also lead to a strong broadening of the plasmon band, based on the studies by Lisiecki and Pileni (1993; 1995).

The main difference between the UV-visible spectra of post-synthesis heated nanoparticles (Figure 4.5.11) and those of non-heated particles shown in Figure 4.4.5 is the unchanged peaks over time. Unlike the spectra of particles synthesized by reducing the decanted organic phase, the features of the UV-visible spectra of heated nanoparticles are almost identical at different times of exposure to air. As can be seen in Figure 4.5.11, even after 100 minutes of exposing the hexane sample of post-synthesis heated nanoparticles to air, the UV-visible spectra are the same as the initial absorption spectra. Thus, the result of the post-synthesis heating procedure is much more stable than those of the previous modified versions of Leff *et al.*'s recipe for synthesizing copper nanoparticles that have been discussed so far. However, as mentioned before, further purification techniques are required after the post-synthesis heating step to avoid the presence of any hydrocarbon impurities during the nanoparticle characterization.

## 4.6 Duplicating the Colloidal Recipe by Leff and co-workers for Copper

### 4.6.1 Procedure

In the last section of this chapter, the result of a synthesis recipe that is a duplicate of Leff *et al.*'s method is discussed, except that KCl was not added and the organic phase was not decanted. The questions we hoped to address in running this series of experiments are listed below

- 1- Would the plasmon peak at 570 nm for the colloidal solution of copper be seen without adding KCl? In other words, the main source of  $\text{Cl}^-$  for the formation of the CuCl monolayer on the surface of nanoparticles was investigated. The possible mechanism for the damping of the plasmon band had been suggested by Qi *et al.*(1997)).
- 2- Could the phase transfer reagent itself remove enough  $\text{Cu}^{2+}$  from the aqueous phase for the next steps?
- 3- Do any N-H bands appear in the FTIR spectra of the final products if the two phases are not separated prior to the reduction step?

In Section 4.1, the first modification made to the synthesis method was introduced: adding HCl to the aqueous solution of copper chloride ( $\text{CuCl}_2 \cdot 2\text{H}_2\text{O}$ ). The concentration of  $\text{Cl}^-$  was increased to generate anionic complexes of copper that could be transferred to the organic phase by reacting with the cationic part of the phase transfer reagent ( $\text{N}(\text{C}_8\text{H}_{17})_4\text{Br}$ ). Later, UV-visible spectra of nanoparticles synthesized by the modified recipes, in which KCl (instead of HCl) was among the reactants, did not show the plasmon peak at 570 nm. One possible mechanism suggested by Qi *et al.*(1997) was the formation of an insoluble monolayer of CuCl on the surface of the copper nanoparticles as a result of the presence of  $\text{Cl}^-$  anions in the organic phase.

This proposed mechanism provided a possible explanation for the lack of the plasmon band in our UV-visible data, but there were still uncertainties about the main source of  $\text{Cl}^-$  anions in the organic phase. Therefore, Leff *et al.*'s recipe (1996) was duplicated without adding KCl to verify its role in providing  $\text{Cl}^-$  for the organic phase. Furthermore, the reduction step was started without decanting the organic phase so that surfactant molecules would not be lost upon separating the two phases. The nanoparticles fabricated by this recipe were not heated after synthesis in order to be able to characterize them and demonstrate their oxidation state. If the current approach for the post-synthesis heating had been

followed, the characterization results would have been unreliable due to the hydrocarbon impurities. All of the synthesis and post-preparation steps were done in an inert atmosphere (N<sub>2</sub> or Ar). The materials used in this set of experiments and their concentrations are listed in Table 4-5.

**Table 4-5** Concentrations of the chemical reagents used in duplicating Leff *et al.*'s recipe.

Reactant	Concentration
CuCl <sub>2</sub> ·2H <sub>2</sub> O	0.01136 M (0.284 mmol in 25 mL water)
N(C <sub>8</sub> H <sub>17</sub> ) <sub>4</sub> Br	0.02668 M (0.667 mmol in 25 mL toluene)
C <sub>18</sub> H <sub>35</sub> NH <sub>2</sub>	0.12157 M (3.03925 mmol in 25 mL toluene)
NaBH <sub>4</sub>	0.11626 M (2.906 mmol in 25 mL water)

As in previous trials, the synthesis started with dissolving 0.048 g of CuCl<sub>2</sub>·2H<sub>2</sub>O in 25 mL of distilled water. Next, the organic solution of the phase transfer reagent was prepared by adding 0.365 g of N(C<sub>8</sub>H<sub>17</sub>)<sub>4</sub>Br in 25 mL of toluene. Adding the phase transfer reagent to the light blue solution of copper chloride while it was vigorously stirring produced no color change. After half an hour stirring this two-phase system, the aqueous phase at the bottom was still light blue and the organic phase was clear. Later, a discussion is presented describing how the copper cations were possibly transferred into the organic phase in this process without being modified to the anionic complexes by adding a source of Cl<sup>-</sup>.

In the third step of the duplication of Leff *et al.*'s synthesis recipe, 1 mL of oleylamine was dissolved in 25 mL of toluene. Adding the surfactant solution to the stirring mixture resulted in an obvious color change in both phases. The clear organic phase turned sharp blue, the appearance of the aqueous phase became cloudy, and the blue color in this phase did not vanish even after stirring for 1 hour of the colloidal mixture in the presence of the surfactant.

Finally, the reducing agent solution (0.11 gr of NaBH<sub>4</sub> in 25 mL of distilled water) was added to the stirring mixture to start the reduction reaction that leads to the synthesis of copper nanoparticles. The color of the organic phase gradually changed from sharp blue to dark brown, and after 2 hours, to dark purple. The aqueous phase had an opaque appearance a couple of minutes after the reduction step began, but at the end of this step (after 2 hours stirring), it turned clear. The final dark purple organic layer was separated and evaporated until its volume was reduced to ≈ 5 mL. The dispersed nanoparticles were

precipitated by adding 350 mL ethanol. The ethanol-based samples were stored in liquid nitrogen overnight for later analyses.

Earlier, the necessity of increasing the concentration of  $\text{Cl}^-$  to produce anionic complexes of copper ( $[\text{CuCl}_3]^-$  and  $[\text{CuCl}_4]^{2-}$ ) was discussed so that the cationic part of the phase transfer reagent could react with them and transfer them into the synthesis phase (the organic layer). However, in 2002, Brust and Kiely (2002) mentioned one of the uncertainties in preparing silver nanoparticles when following the two-phase liquid-liquid synthesis technique pioneered by Brust *et al.* (1994) that is similar to the method by which the copper nanoparticles were synthesized. They demonstrated that "...the mechanism of the phase transfer step in the silver preparation is, however, unclear, since silver is presumably present in the aqueous phase as a cation and therefore should not be transferred to the organic phase by the typically used cationic (quaternary ammonium halogenides) phase transfer agents. This step requires further attention and research..." (Brust and Kiely 2002). In other words, the cationic phase transfer agent, in this case  $\text{N}(\text{C}_8\text{H}_{17})_4\text{Br}$ , successfully removed silver cations from the aqueous phase, though the mechanism is not clear. Thus, one cannot definitely claim that applying the phase transfer agent without generating the proper complex of copper (anionic) is not effective since it was used for another cation ( $\text{Ag}^+$ ) despite the lack of knowledge about the mechanism for this transfer. Moreover, because of its amphiphilic nature, the surfactant itself is capable of transferring these cations to the organic phase as it did in Scheme 2 of Leff *et al.*'s recipe, in which gold nanoparticles were synthesized without the use of the phase transfer reagent,  $\text{N}(\text{C}_8\text{H}_{17})_4\text{Br}$ ; however, as mentioned before, without the phase transfer agent, the yield decreases. Upon adding the surfactant, a sudden color change was observed in the organic phase from clear to sharp blue, meaning that those cations were transferred successfully to the top layer with the help of either the surfactant molecules or both the phase transfer and capping agents.

More investigations are needed, as already pointed out by Brust and Kiely, to clarify the role of the phase transfer agent in removing cations from the aqueous phase, especially in the cases of those metals such as silver and copper that are dissolved in the aqueous phase in the form of cationic complexes, which are believed not to react with cationic phase transfer agents.

## 4.6.2 Characterization Techniques

### 4.6.2.1 TEM analysis and EDS spectroscopy

The precipitate of synthesized nanoparticles was filtered with 0.45  $\mu\text{m}$  membrane filter (polyamid), washed with an excess of ethanol, and dried on a Petri dish under a flow of nitrogen gas inside the glove

box. This dry product was then re-dissolved in 200 mL of hexane and a light brown colloidal dispersion of nanoparticles was generated. Unlike the filtered sediment obtained upon reducing the decanted organic layer, this time, the precipitated nanoparticles on the filter paper were resolvable in the nonpolar organic solvent (hexane). TEM samples were prepared by evaporating a drop of the hexane solution of nanoparticles on a Formvar - coated gold TEM grid.

In Figure 4.6.1, a TEM image of nanoparticles synthesized by duplicating Leff *et al.*'s recipe is shown. The result is a mixture of assembled layers of separated nanoparticles and aggregated clusters of unstable nanoparticles. This result is quite similar to the one attained for the synthesis recipe in which KCl was added to the reactants (see Figure 4.3.1), except that this time, the separated nanoparticles are more oriented. In fact, the nanoparticles with a narrow size distribution synthesized by this method formed layers of self-assembled particles, and a film of ordered nanoparticles was frequently observed in the specimen, as can be seen in Figure 4.6.2 (a). These separated nanoparticles, shown in Figure 4.6.2 (b), are mostly spherical, and their average size is  $\sim 5$  nm.

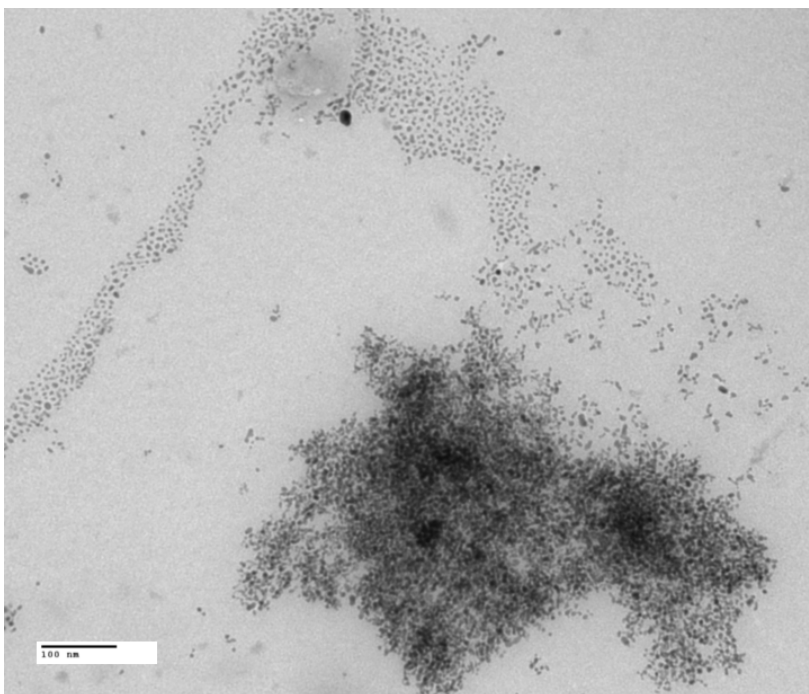
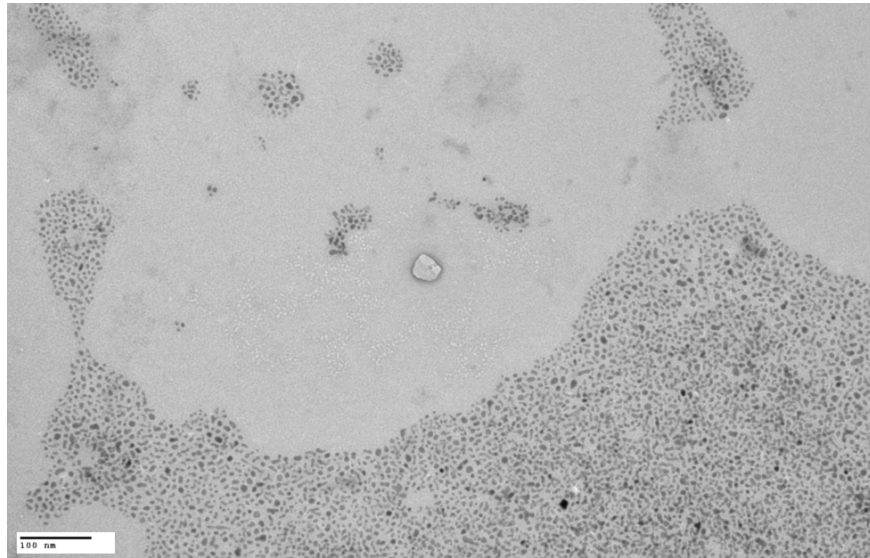
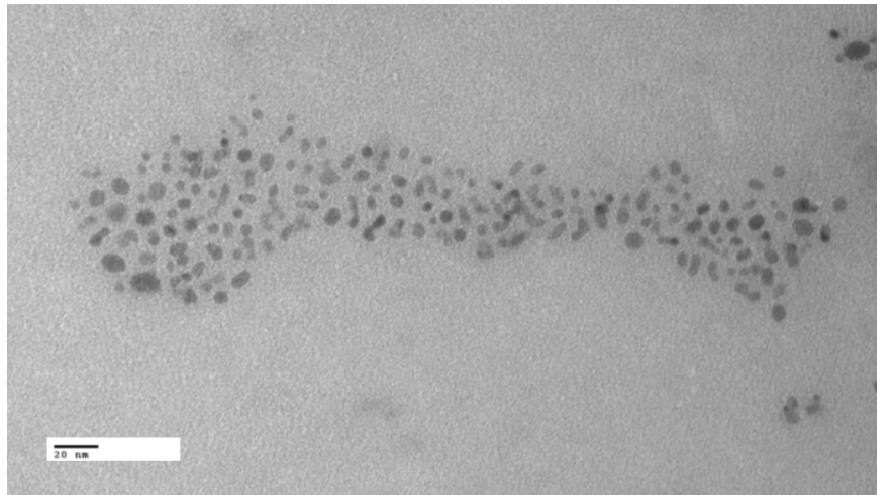


**Figure 4.6.1** TEM image of copper nanoparticles synthesized by duplicating Leff *et al.*'s recipe in an inert atmosphere ( $N_2$  or Ar), Scale bar: 100 nm.



(a)



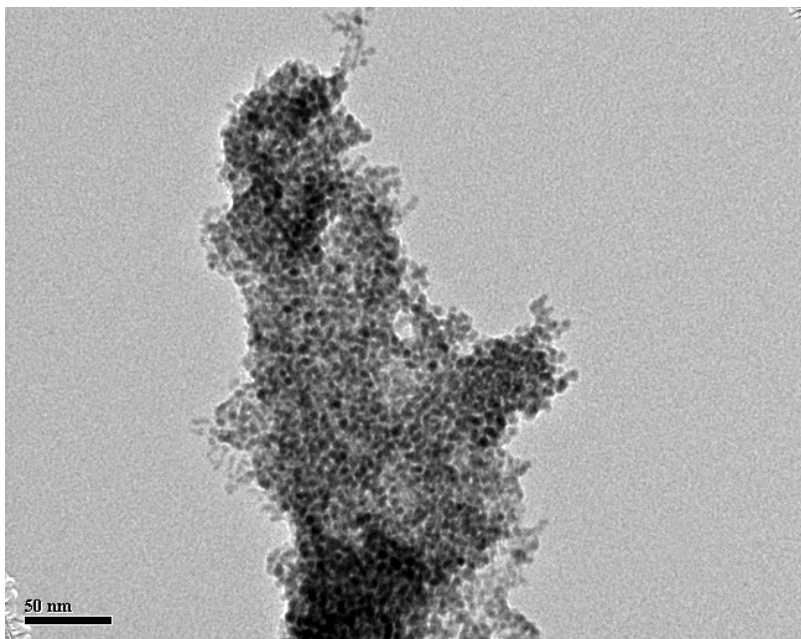
(b)

**Figure 4.6.2** (a) A self-assembled layer of fairly separated copper nanoparticles, Scale bar: 100 nm. (b) A closer view of these particles shows that the result was nanoparticles with an average particle size of  $\sim 5$  nm, Scale bar: 20 nm.

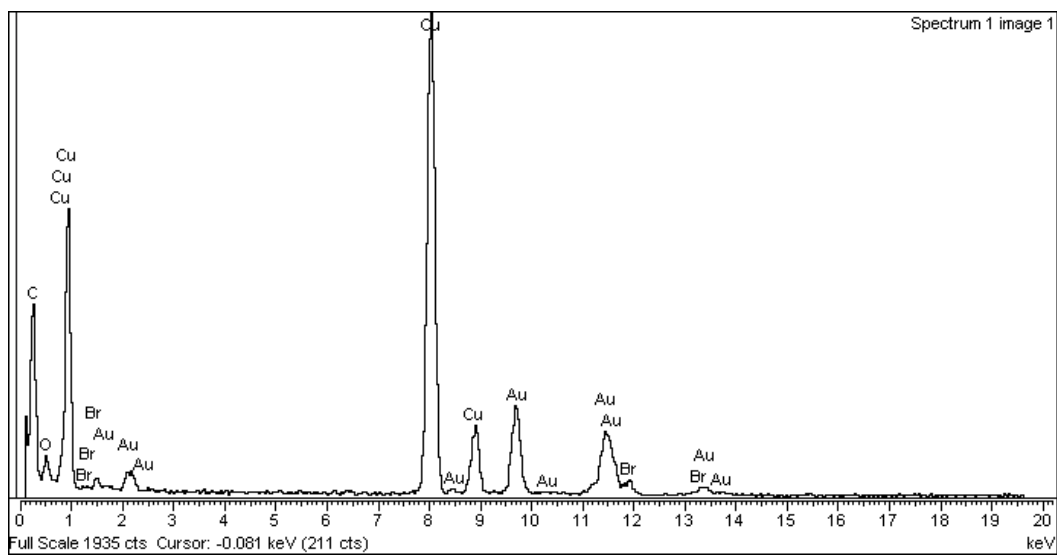
Using the EDS spectroscopy data, a better understanding of the chemical compositions of these two different structures was achieved. In Figure 4.6.3 (a) an overall TEM image of a cluster of aggregated nanoparticles is given, and Figure 4.6.3 (b) shows the corresponding EDS spectra for the same area. The trace of Br in the spectra proves that  $(\text{octyl})_4\text{N}^+\text{Br}^-$  is capped to a fraction of the particles' surface. Gold (Au) was detected as the TEM grid used for analyzing synthesized copper nanoparticles was a Formvar coated gold grid. Moreover, oxygen (O) was detected, meaning that some of these aggregated nanoparticles in the cluster were oxidized, probably during the TEM preparation.

On the other hand, EDS spectra of a couple of separated nanoparticles (Figure 4.6.4 (a) shows their HRTEM image) in Figure 4.6.4 (b) show no Br peak. In addition to that, no oxygen was detected either. Hence, a possible conclusion is that in the absence of any trace of Br, synthesized copper nanoparticles remained stable (with no aggregation) and also free of oxides. As mentioned before, Leff and his co-workers explained that gold nanoparticles synthesized by using tetraoctylammonium bromide ( $\text{N}(\text{C}_8\text{H}_{17})_4\text{Br}$ ) as the phase transfer reagent lose their solubility in nonpolar organic solvents and agglomerate if stored as a powder for a few hours (Leff et al. 1996). In the case of copper nanoparticles synthesized by the same recipe, the presence of  $(\text{octyl})_4\text{N}^+\text{Br}^-$  leads to aggregation and oxidation in the fabricated nanoparticles as well. Since the synthesized copper nanoparticles were not stored as a powder in these experiments, those nanoparticles that were unstable due to the  $\text{Br}^-$  capping had a chance to aggregate either when they were precipitated in ethanol or when they were filtered and kept drying in the glove box.

Tetraoctylammonium bromide ( $\text{N}(\text{C}_8\text{H}_{17})_4\text{Br}$ ) is assumed to be the reason for the partial production of aggregated clusters in the synthesis of copper nanoparticles when using Leff *et al.*'s recipe.  $\text{Br}^-$  was obviously traced in the areas of agglomerated nanoparticles, while for isolated copper nanoparticles, it was not detected. Therefore, there is a possibility that the phase transfer reagent affects the stability of produced copper nanoparticles as it does that for gold nanoparticles synthesized by Scheme 1 of Leff *et al.*'s work. Furthermore, oxidation is more likely to happen for those of the copper nanoparticles with the  $\text{N}(\text{C}_8\text{H}_{17})_4\text{Br}$  capping, as the oxygen peak was also observed for the aggregated clusters of nanoparticles in Figure 4.6.3 (b). The amount of oxidation of synthesized nanoparticles can be further assessed by using X-ray photoelectron spectroscopy (XPS).

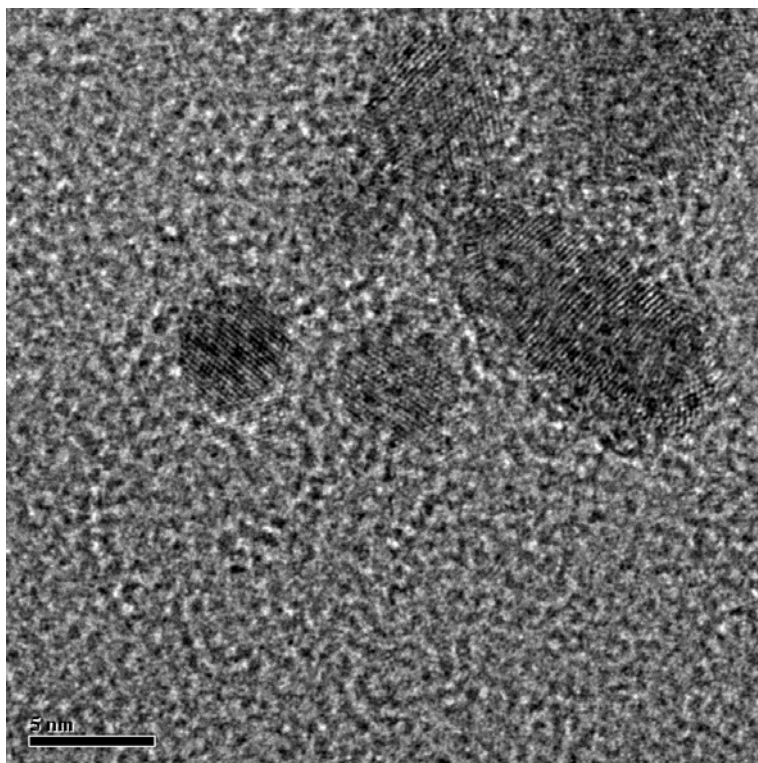


(a)

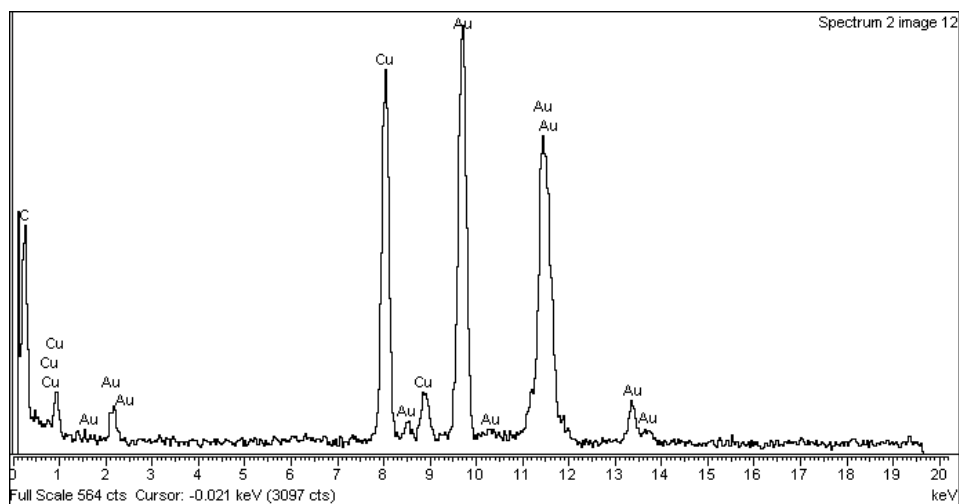


(b)

**Figure 4.6.3** (a) TEM image of agglomerated copper nanoparticles after being stored for two weeks in the liquid nitrogen dewar. (b) EDS spectroscopy of the cluster of aggregated nanoparticles.



(a)



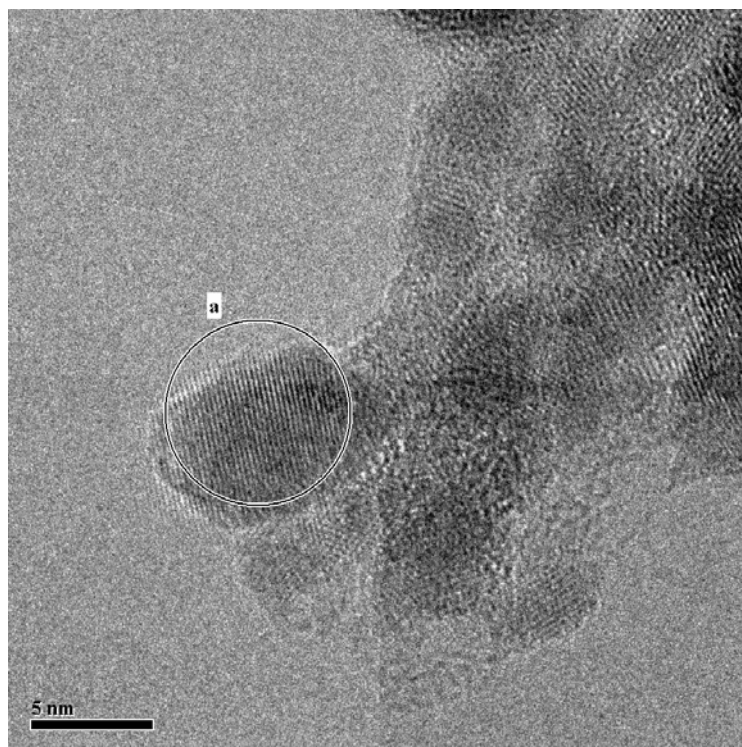
(b)

**Figure 4.6.4** (a) HRTEM image of one of few separated copper nanoparticles with no case of agglomeration after two weeks of storage in the liquid nitrogen dewar, Scale bar: 5 nm. (b) EDS spectroscopy of the same area.

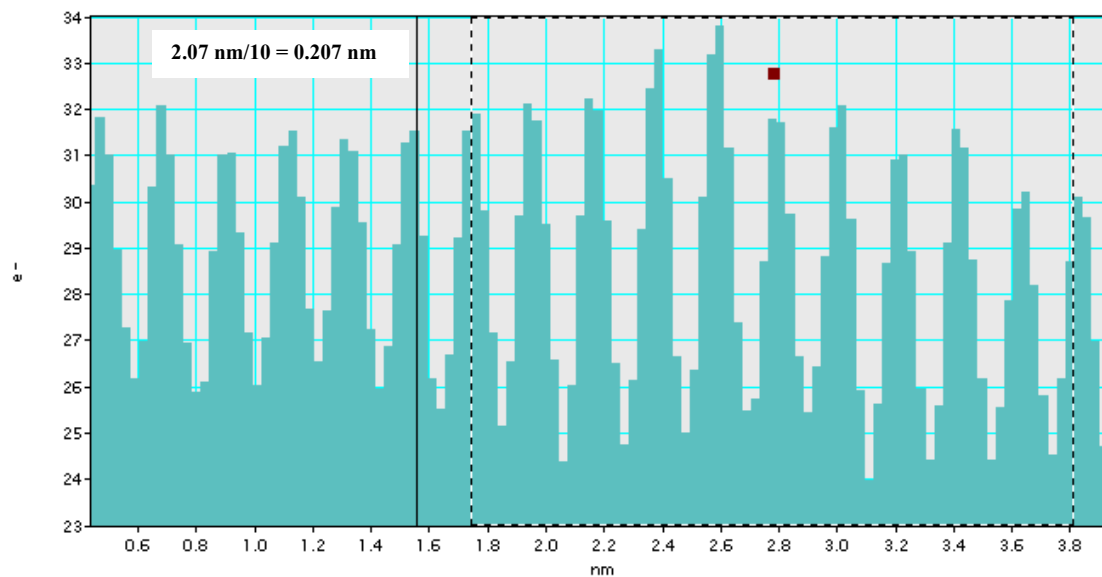
#### 4.6.2.2 HRTEM analysis

HRTEM images of both the separated nanoparticles and a cluster of aggregated nanoparticles are in good agreement with the statements made for these two structures based on the EDS spectroscopy data. In Figure 4.6.5 (a), a HRTEM image of a 10 nm isolated nanocrystal is given, and the corresponding histogram in Figure 4.6.5 (b) provides the  $d$  spacing of this nanostructure. As can be seen, the histogram is quite symmetrical this time, and the measured distance for the two following peaks is 0.207 nm, which is due to the  $\{111\}$  plane of face-centered cubic (fcc) copper. Hence, pure copper nanocrystals were partially synthesized by duplicating the synthesis recipe by Leff and co-workers under the flow of an inert gas in the glove box. However, as discussed before, aggregated nanoparticles in the form of clusters were also generated. The HRTEM image of the agglomerated nanoparticles is shown in Figure 4.6.6 (a), and the  $d$  spacing of the particular area (A) is measured by the histogram in Figure 4.6.6 (b). The  $d$  spacing is 0.246 nm, corresponding to the  $\{111\}$  plane of cubic  $\text{Cu}_2\text{O}$ . Thus, this agglomerated nanoparticle is crystalline copper (I) oxide. As in the EDS spectroscopy data, copper oxides were detected where those unstable nanoparticles (due to the presence of the phase transfer reagent ( $(\text{octyl})_4\text{N}^+\text{Br}^-$ ) on their surface) formed aggregated clusters.

Based on the characterization data that have been presented so far for the results of the duplication of Leff *et al.*'s recipe for copper, we can claim that the copper nanocrystals were successfully fabricated in the mixture of assembled layers of separated nanoparticles and clusters of agglomerated ones. The separated nanoparticles were mostly pure copper nanocrystals, while the aggregated clusters consisted of cubic  $\text{Cu}_2\text{O}$  nanoparticles. Moreover, the possible mechanism for this division is believed to be the presence of the phase transfer reagent ( $\text{N}(\text{C}_8\text{H}_{17})_4\text{Br}$ ) capped to the surface of a portion of the synthesized nanoparticles, leading to the metastability of these particles. This metastability also affected the oxidation state of the nanoparticles so that the aggregated nanoparticles were more likely to be oxidized. The rate of aggregation for these nanoparticles has not been studied yet, but the first results showed that after just a couple of days, the oriented layers of nanoparticles were almost impossible to find. In Section 4.6.2.3, the FTIR spectra of the nanoparticles synthesized by this method are discussed to investigate whether the surfactant (oleylamine) is capped to the surface of copper nanoparticles.

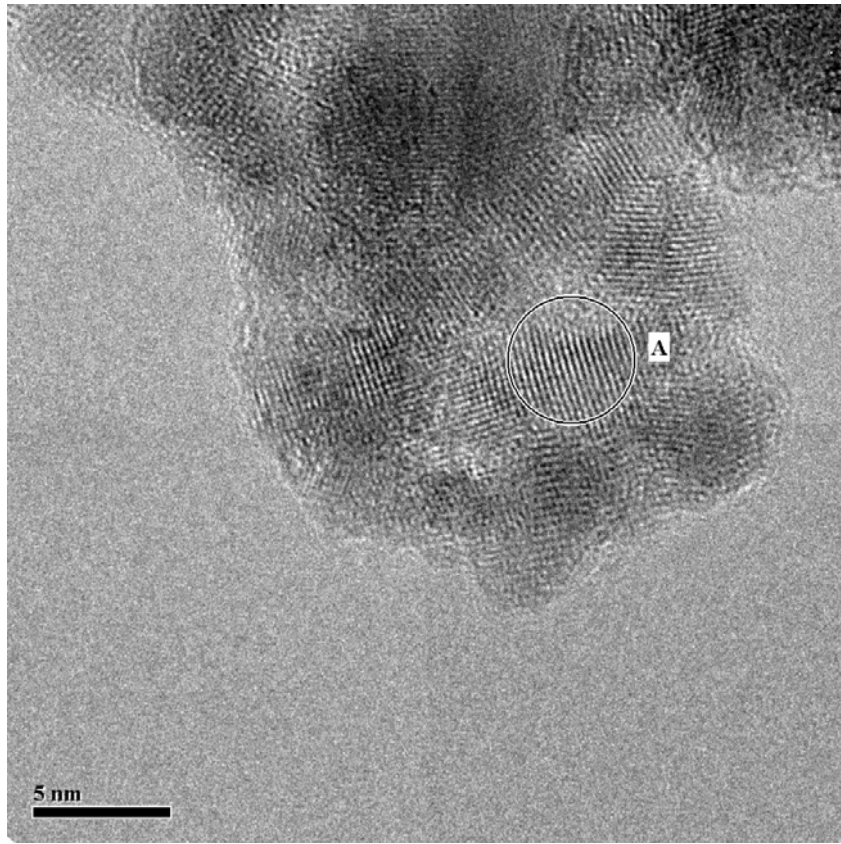


(a)



(b)

**Figure 4.6.5** (a) HRTEM image of a separated copper nanoparticle. The nanocrystal is shown with a circle. (b) Histogram of the area “a” shown in the HRTEM image.



(a)

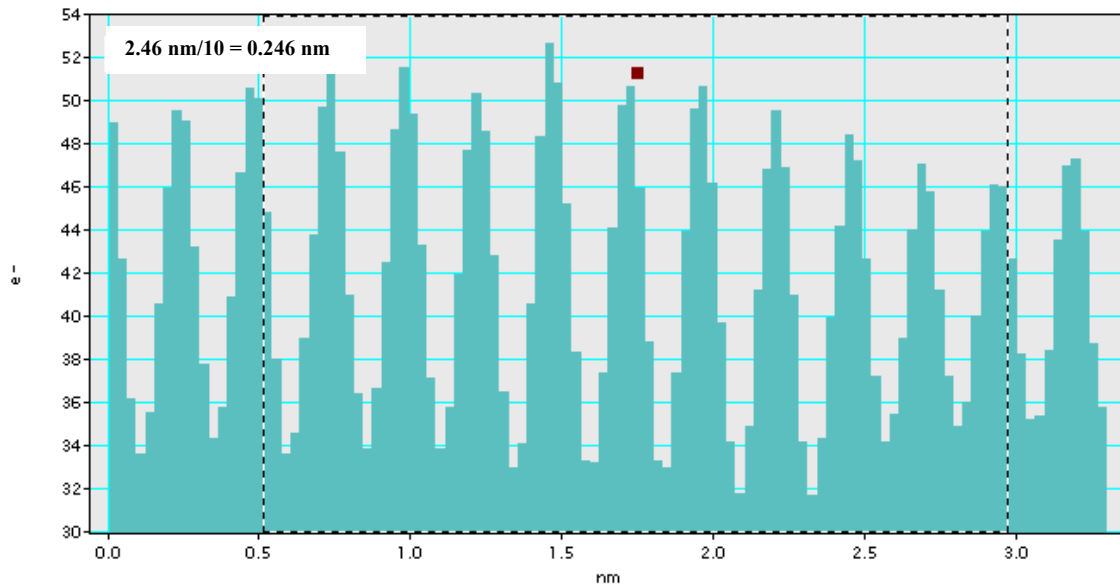


**Figure 4.6.6** (a) HRTEM image of a cluster of aggregated nanocrystals. (b) Histogram of the area “A” shown with a circle in the HRTEM image.

#### 4.6.2.3 FTIR spectroscopy

The FTIR spectra of copper nanoparticles synthesized by duplicating Leff et al.'s recipe in an inert atmosphere in Figure 4.6.7 show two broad peaks, one in the range of  $\approx 3700\text{-}3300\text{ cm}^{-1}$  with a shoulder at  $3200\text{ cm}^{-1}$ , whereas the other is a small peak at  $\approx 1600\text{ cm}^{-1}$ . In the FTIR spectra of pure oleylamine, the band due to the N-H stretch is at  $3300\text{ cm}^{-1}$ , and the peak corresponding to the N-H bend is at  $1593\text{ cm}^{-1}$ , as shown in Figure 4.6.8 (Shukla et al. 2003). Both of the broadened peaks of synthesized nanoparticles are in the same range as the N-H peaks in the FTIR spectra of the primary amine. Furthermore, the intensity of the broadened peak is reduced compared to the same features of the neat amine. The appearance of these broadened peaks, which did not occur in the previous results, may be referred to as evidence for amine surface passivation since Leff and his co-workers also reported the broadened N-H stretch and N-H bend for gold nanoparticles (Leff et al. 1996). However, due to excessive noise, a proper analysis of the N-H wagging modes in the region of  $\approx 900\text{-}700\text{ cm}^{-1}$  of the copper nanoparticle FTIR spectra is not possible. Thus, for more definite statements about bonding on the surface of synthesized nanoparticles, other spectroscopy analyses, such as NMR and Raman spectroscopy are recommended. It should also be noted that only a portion of the final product was separated nanoparticles that were likely to be capped with the surfactant molecules. This small portion might affect the significance of the N-H bonds in the FTIR spectra of the synthesized copper nanoparticles.

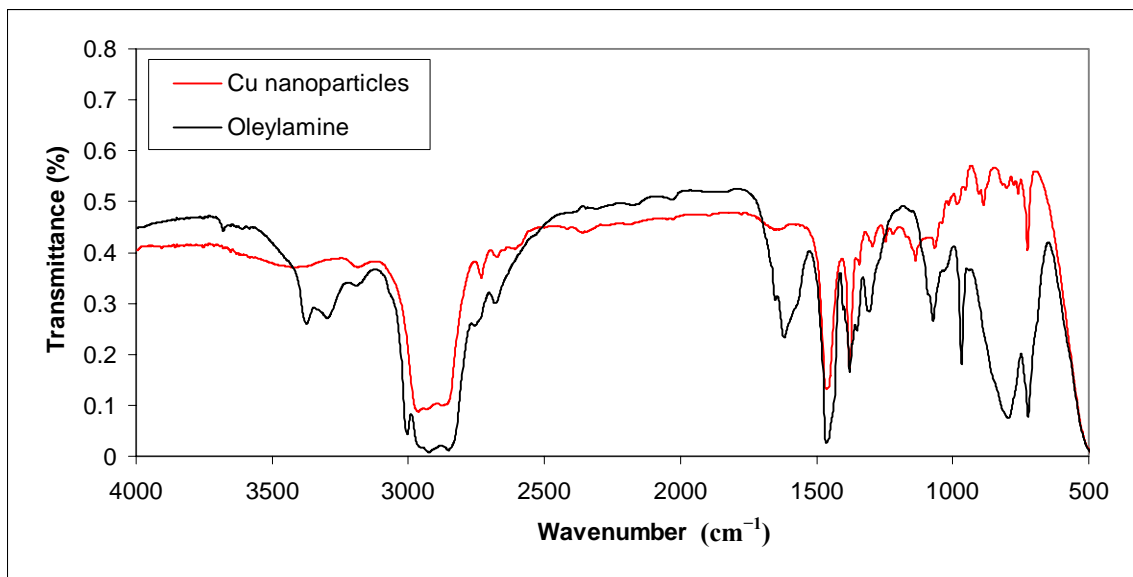


**Figure 4.6.7** FTIR spectra of copper nanoparticles synthesized by duplicating Leff et al.'s recipe in an inert atmosphere.

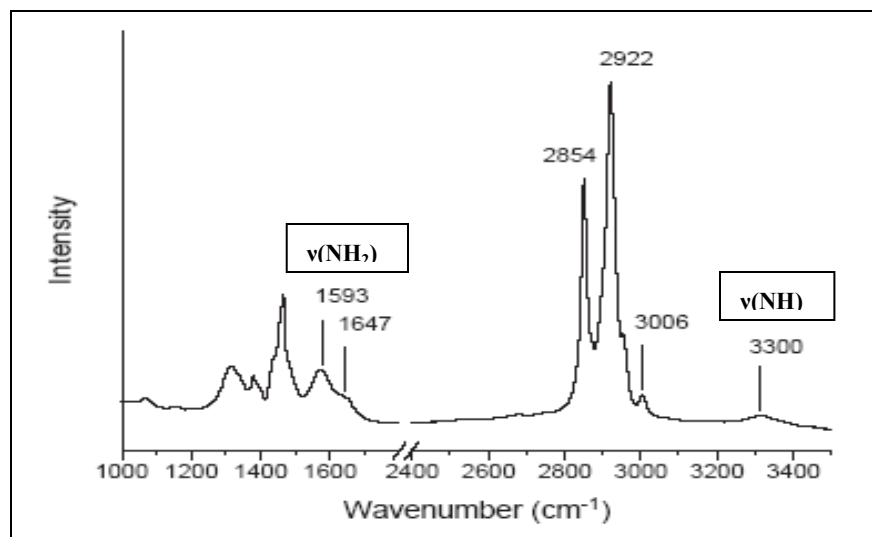


**Figure 4.6.8** FTIR spectra of pure oleylamine in 1000-3500  $\text{cm}^{-1}$  region (Shukla et al. 2003). The bands corresponding to N-H are marked.

Section 4.6.2.4 discusses the UV-visible spectroscopy of these nanoparticles. As mentioned at the beginning of Section 4.6, KCl was not added to the aqueous solution of copper chloride to examine whether it is the main source for  $\text{Cl}^-$  anions in the organic phase. These ions are believed to form an insoluble monolayer of  $\text{CuCl}$  on the surface of the nanoparticles that leads to the damping of the plasmon peak in the UV-visible spectra of the product.

#### 4.6.2.4 UV-visible spectroscopy

UV-visible spectroscopy was run for the hexane solution of the synthesized nanoparticles while the sample was exposed to air. In Figure 4.6.9, a sharp peak at  $\sim 280$  nm is observed in the spectra at the initial step of the analysis. After 45 minutes of exposure to air, the intensity of this peak is dramatically reduced, indicating the instability of the nanoparticles. In a study by Ng and Fan (2006) on the oxidation of Cu nanoparticles to  $\text{Cu}_2\text{O}$  nanostructures that was monitored by UV-visible absorption spectroscopy (Section 4.4.2.3), the 280 nm peak can be considered as a sign for the formation of copper (I) oxide ( $\text{Cu}_2\text{O}$ ) nanostructures. However, based on the HRTEM data, it was expected to see the plasmon peak at 570 nm, at least for the initial step of analysis, since metallic copper nanoparticles were partially produced. As discussed before, the possible mechanism for the disappearance of the absorption band of Cu nanoparticles is the presence of a monolayer of CuCl on the surface of Cu nanoparticles leading to the strong damping of the plasmon peak at 570 nm (Qi et al. 1997). In fact, if this is the main reason for not seeing the plasmon band, then omitting KCl from the chemicals of this synthesis recipe was not effective enough to stop providing  $\text{Cl}^-$  to the organic phase. As Qi *et al.* reported (1997), using copper chloride as the copper salt for the colloidal synthesis method resulted in similar UV-visible spectra with no feature at 570 nm. Therefore, the damping of the plasmon peak, when a portion of our sample was pure copper nanoparticles colloiddally dispersed in hexane, may be due to  $\text{Cl}^-$  anions in the organic phase as a result of starting this synthesis with the copper chloride solution. The mechanism for the transfer of  $\text{Cl}^-$  into the organic phase should be fairly similar to that for the copper cations: due to both the phase transfer reagent and the amphiphilic molecules of the surfactant. If the reaction between  $\text{AuCl}_4^-$  and  $\text{N}(\text{C}_8\text{H}_{17})_4^+$  suggested by Brust *et al.* (1994), given as equation 4.6.1, also implies the two-phase system of the aqueous phase of copper chloride and the organic phase of the phase transfer reagent, then  $\text{Cl}^-$  anions that were initially in the aqueous phase can be transferred to the organic phase by following the same reaction, summarized in equation 4.6.2.



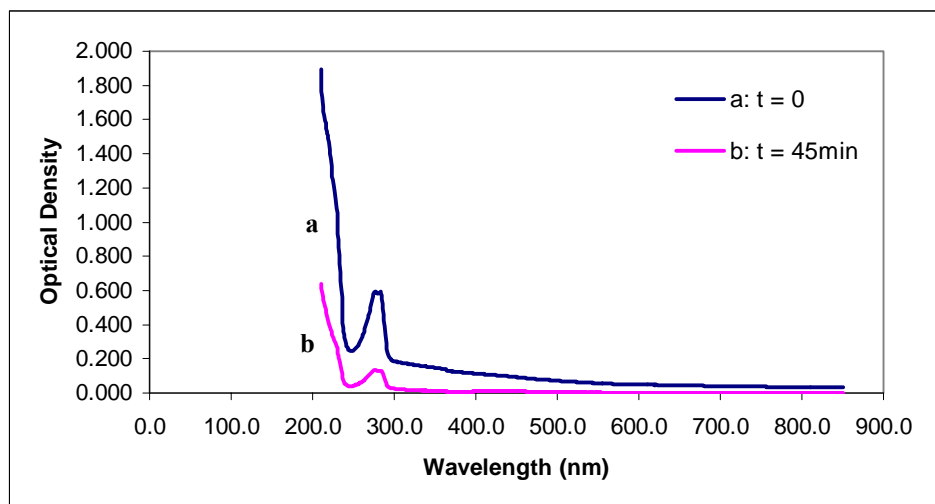


**Figure 4.6.9** UV-visible spectra of the copper nanoparticles synthesized by duplicating Leff *et al.*'s method in an inert atmosphere: (a) just after the hexane solution of the nanoparticles exposed to air and (b) after 45 min exposure to air.

However, as also pointed out by Qi *et al.*, a detailed investigation is required to prove that the formation of the insoluble monolayer of CuCl on the particle surface actually occurs and is the main reason for the lack of the plasmon absorption peak in the UV-visible spectra of the synthesized nanoparticles.

The spectra also show that the nanoparticles produced by this technique are not stable when exposed to air. Since the N-H peaks in the FTIR spectroscopy were not significant either, it may be concluded that even for those separated metallic copper nanoparticles that were detected by HRTEM analysis, the bonding between the hydrophilic head of the surfactant (N-H) and the nanoparticle surface is not strong enough in nature to avoid the oxidation. Nevertheless, some post-synthesis treatment such as heating may be effective to bring more stability to these nanoparticles as this procedure affected the stability of the aggregated nanoparticles synthesized by reducing the decanted organic phase (UV-visible spectra of the post-synthesis heated nanoparticles are shown in Figure 4.5.11).

## Chapter 5: Conclusions and Recommendations

### 5.1 Conclusions

The colloidal synthesis of metal nanoparticles in a two-phase liquid/liquid system that was first introduced by Brust *et al.* (1994) for gold (Au) was studied to fabricate stable pure copper nanoparticles. A modified version of Brust *et al.*'s recipe, which was suggested by Leff and co-workers (1996) to synthesize alkylamine-derivatised gold nanoparticles, was considered as a starting point in this work. To avoid the formation of copper oxides, which are thermodynamically more stable, the whole synthesis procedure was done in an inert atmosphere. The next modification to the synthesis recipe was increasing the concentration of  $\text{Cl}^-$  to make anionic complexes of copper ( $[\text{CuCl}_3]^-$ ,  $[\text{CuCl}_4]^{2-}$ ). These anionic complexes react with the cationic phase transfer reagent,  $\text{N}(\text{C}_8\text{H}_{17})_4^+$  and get transferred to the organic layer. However, once no plasmon absorbance band was observed at 570 nm for colloidal dispersion of the synthesized copper nanoparticles, we stopped adding KCl. It was reported in the literature that  $\text{Cl}^-$  anions can modify the surface of the produced nanoparticles (by forming an insoluble monolayer of CuCl), and subsequently, cause the plasmon peak to disappear. However, the result of duplicating Leff *et al.*'s recipe in the glove box without adding KCl revealed that  $\text{Cl}^-$  can also be provided by  $\text{CuCl}_2$ , the copper salt used in our work.

Based on the results presented in this work, the copper cations in the aqueous solution were found to be transferrable to the synthesis phase (organic phase) by the cationic part of the phase transfer reagent ( $\text{N}(\text{C}_8\text{H}_{17})_4^+$ ) with an unknown mechanism. A similar phenomenon was reported for silver cations ( $\text{Ag}^+$ ) that were also successfully transferred into the organic phase by using the same phase transfer agent, without pursuing further refinements for the metal complex.

The next set of modifications done to the synthesis recipe involved separating two phases by separatory funnel prior to the reduction step and discarding the aqueous phase to get rid of any copper cation left in this phase. This imprecise separation led to losing the excess surfactant that collected at the interface. The result was big clusters of agglomerated nanoparticles formed due to the surfactant loss upon decanting the organic phase. The absence of N-H peaks in the FTIR spectra of these nanoparticles also showed that they were not well capped with the surfactant molecules to be protected against agglomeration. Thus, separating the organic phase was not efficient enough to eliminate the black clouds observed after adding KCl to the chemicals of the synthesis recipe. These clouds were believed to be those copper nanoparticles synthesized in the aqueous phase since some cationic complexes of copper ( $[\text{Cu}(\text{H}_2\text{O})_6]^{2+}$ ) remained unchanged in reacting with KCl. According to the positive charge of these complexes, their transfer to

the organic phase employing the cationic phase transfer reagent was supposed to be impossible. The aqueous phase including these cationic complexes of copper was discarded to limit the reduction reaction site to the cores of reverse micelles so that no copper nanoparticles would be synthesized in the bulk aqueous phase and later diffused into the organic phase. Nevertheless, it was reported in the literature that these cationic phase transfer reagents are capable of transferring the cations ( $[\text{Cu}(\text{H}_2\text{O})_6]^{2+}$ ) as well of anions ( $\text{AuCl}_4^-$ ), but their efficiency for each of these complexes has not yet been studied. While a few separated nanoparticles surrounded the aggregated nanoparticles in the case of no phase separation, aggregated clusters of nanoparticles were the only structure obtained by decanting the organic phase.

The chemical structure of two particulates synthesized by duplicating Leff *et al.*'s recipe, assembled separated nanoparticles and clusters of agglomerated nanoparticles, were analyzed by different characterization techniques. The assembled layers consisted of separated copper nanoparticles, whereas the agglomerated copper oxides shaped large dark clusters. Br was traced only for these clusters, meaning that the synthesized particles at these areas were partially capped with the phase transfer reagent ( $\text{N}(\text{C}_8\text{H}_{17})_4\text{Br}$ ), resulting in metastability for these particles. Leff and his co-workers previously explained that those gold nanoparticles synthesized by using this phase transfer reagent were stable only for a couple of days. For copper nanoparticles synthesized by the same method, this metastability was also observed by studying UV-visible spectra of these particles over time. Although the rate of aggregation for these particles has not been investigated yet, the rough estimate is that they were only stable for less than an hour, and eventually those assembled layers could hardly be found. In addition to the presence of the phase transfer agent on the surface of some particles, the other reason for instability of the synthesized particles was the weak bonding between the hydrophilic head of the surfactant and the surface of the copper nanoparticles. Even though separated copper nanoparticles were partially produced by the end of the synthesis, the capping surfactants were not strongly enough bonded to the surface of the nanoparticles so that they could be protected against oxidation and aggregation.

The post-synthesis treatment for the unstable nanoparticles discussed in this work was annealing synthesized nanoparticles. The suggested mechanism for this procedure that leads to the formation of more stable nanoparticles is re-orientation of weakly capped surfactant molecules so that the steric barrier increases upon heating of the particles. The color change from light brown to green and preliminary TEM images showed that this technique is very helpful to re-disperse the aggregated nanoparticles. However, during the characterization analyses, the heavy hydrocarbon (dodecane) that was used as the solvent for heating the nanoparticles acted as an impurity and biased the analytical data. Thus, an examination of the chemical structure of the post-synthesis heated nanoparticles that were clearly separated in the form of

assembled layers could not be made. Further purification is required after this process if stable nanoparticles are to be fabricated and those treated nanoparticles are to be characterized.

## 5.2 Recommendations for Future Work

Based on the results obtained for copper after making several refinements to the original recipe, developed by Leff and his co-workers for synthesizing alkylamine capped gold nanoparticles, there are some suggestions for future studies on synthesizing copper nanoparticles applying this straightforward method:

- The copper salt used in our work was copper (II) chloride,  $\text{CuCl}_2 \cdot 2\text{H}_2\text{O}$ . Since  $\text{Cl}^-$  can cause the formation of the insoluble monolayer of  $\text{CuCl}$  on the surface of the synthesized copper nanoparticles and result in the disappearance of the plasmon peak, for more precise characterization results, another copper salt, such as copper (II) acetylacetonate ( $\text{Cu}(\text{acac})_2$ ), copper sulfate ( $\text{CuSO}_4$ ), and copper nitrate ( $\text{Cu}(\text{NO}_3)_2$ ), may be better employed in this synthesis.
- Although the phase transfer reagent,  $\text{N}(\text{C}_8\text{H}_{17})_4\text{Br}$ , increases the production yield, those copper nanoparticles that are capped by  $(\text{C}_8\text{H}_{17})_4\text{N}^+\text{Br}^-$  are metastable and eventually become agglomerated and oxidized. The source of instability of these particles is believed to be the presence of  $\text{Br}^-$ . By applying another phase transfer reagent (e.g., orthophosphoric acid, depromedroxyprogesterone acetate (DMPA), and ferrocene derivatives), an enhancement of yield and elimination of the source of metastability for synthesized nanoparticles is expected. Choosing more appropriate phase transfer reagent for copper as has been done for silver (Ag) (Zhou et al. 1999) would be an appealing subject for further investigation.
- The post-synthesis heating procedure seems to be helpful in re-dispersing aggregated unstable nanoparticles. However, the hydrocarbon impurities that resulted from the presence of a solvent with a high boiling point, here dodecane, should be removed prior to the characterization analyses. Thus, purification steps need to be developed after annealing the particles so that the post-synthesis heating process can be applied for stabilizing fabricated nanoparticles.
- The oxidation state of different synthesized nanoparticles can be further studied by using precise characterization methods such as X-ray photoelectron spectroscopy (XPS). XPS has been widely used for analyzing the surface chemical properties of various metal nanoparticles, including gold and copper.

- For colloidal synthesis techniques, there have been few investigations examining the effects and interactions of several processing parameters on the properties of the fabricated nanoparticles' properties, such as average particle size. Running a screening design of experiments is recommended to determine the effective factors on the average particle size during the colloidal synthesis of nanoparticles. There are several parameters that seem to affect the growth and nucleation of these particles, such as reduction time, reduction temperature, and the concentration ratio of the copper salt to the surfactant ( $C_{18}H_{35}NH_2$ ) and the reducing agent ( $NaBH_4$ ). As an example, the average particle size in this synthesis method may be altered if we increase the reduction period from 2 hours to 12 hours. The same type of study could also be done for the post-synthesis heating procedure. The annealing temperature and the period of heating may affect the average size of the heated nanoparticles and their size distribution.

## References

- Adair, James H., and Ender Suvaci. "Morphological Control of Particles." Current Opinion in Colloids and Interface Science 5.1-2: 160-7, (2000).
- Andreev, S. N., and O. V. Sapozhnikova. "Composition and Structure of Cu(II) Chlorides." Zhurnal Neorganicheskoi Khimii 10.11: 2538-2543, (1965).
- Andrews, K. W., D. J. Dyson, and S. R. Keown, eds. Interpretation of Electron Diffraction Patterns. Second Edition ed. London: Adam Hilger LTD, 1971.
- Atik, S. S., and J. K. Thomas. "Transport of Photoproduced Ions in Water in Oil Micro-Emulsions - Movement of Ions from One Water Pool to another." Journal of the American Chemical Society 103.12: 3543-50,(1981).
- Bagwe, Rahul P., and Kartic C. Khilar. "Effects of Intermicellar Exchange Rate on the Formation of Silver Nanoparticles in Reverse Microemulsions of AOT." Langmuir 16.3: 905-10,(2000).
- Barrabés, N., J. Just, A. Dafinov, F. Medina, J. L. G. Fierro, J. E. Sueiras, P. Salagre, and Y. Cesteros. "Catalytic Reduction of Nitrate on Pt-Cu and Pd-Cu on Active Carbon using Continuous Reactor: The Effect of Copper Nanoparticles." Applied Catalysis B: Environmental, 62.1-2: 77-85, (2006).
- Benjamin, Mark M., ed. Water Chemistry. 1st ed. New York: McGraw-Hill, 2002.

- Blitz, J. P., J. L. Fulton, and R. D. Smith. "Dynamic Light-Scattering Measurements of Reverse Micelle Phases in Liquid and Supercritical Ethane." Journal of Physical Chemistry 92.10: 2707-10, (1988).
- Bönnemann, H., W. Brijoux, R. Brinkmann, E. Dinjus, T. Joußen, and B. Korall. "Erzeugung Von Kolloiden Übergangsmetallen in Organischer Phase Und Ihre Anwendung in Der Katalyse." Angewandte Chemie 103.10: 1344-6, (1991).
- Brust, M., and Christopher J. Kiely. "Some Recent Advances in Nanostructure Preparation from Gold and Silver Particles: A Short Topical Review." Colloids and Surfaces A: Physicochemical and Engineering Aspects 202.2-3: 175-86, (2002).
- Brust, M., M. Walker, D. Bethell, D. J. Schiffrin, and R. Whyman. "Synthesis of Thiol-Derivatised Gold Nanoparticles in a Two-Phase Liquid–Liquid System." Journal of the Chemical Society, Chemical Communications 1994.7: 801-2, (1994).
- Cason, J. P., M. E. Miller, J. B. Thompson, and C. B. Roberts. "Solvent Effects on Copper Nanoparticle Growth Behavior in AOT Reverse Micelle Systems." The Journal of Physical Chemistry B 105.12: 2297-302,(2001).
- Cassin, G., J. P. Badiali, and M. P. Pileni. "AOT Reverse Micelles: Depletion Model." The Journal of physical chemistry 99: 12941-6, (1995).

Chakravorty, D., and A. K. Giri. Chemistry of Advanced Materials. Ed. Rao, C. N. R. Boca Raton, FL: Blackwell Scientific Publication, 1993.

Charlton, Ian D., and Andrew P. Doherty. "Simultaneous Observation of Attractive Interaction, Depletion Forces, and "Sticky" Encounters between AOT Reverse Micelles in Isooctane using Microelectrode Voltammetry." Journal of Physical Chemistry B 104.33: 8061-7,(2000).

Chen, S., and J. M. Sommers. "Alkanethiolate-Protected Copper Nanoparticles: Spectroscopy, Electrochemistry, and Solid-State Morphological Evolution." Journal of Physical Chemistry B 105.37: 8816-20, (2001).

Chen, S., Z. Fan, and D. L. Carroll. "Silver Nanodisks: Synthesis, Characterization, and Self-Assembly." The Journal of Physical Chemistry B 106.42: 10777-81, (2002).

Chiang, F. K., S. H. Tsai, F. S. Shieu, and H. C. Shih. "In-Situ Cu<sub>2</sub>O Formation on Amorphous Carbon Nanotubes Induced by Electron Beam." Journal of Materials Science Letters 19.8: 671-3, (2000).

Choi, U. S. Development and Applications of Non-Newtonian Flows. Ed. D. A. Siginer and H. P. Wang. Vol. 231/MD-Vol. 66. New York: The ASME, 1995.

Chokshi, A. H., A. Rosen, J. Karch, and H. Gleiter. "On the Validity of the Hall-Petch Relationship in Nanocrystalline Materials." Scripta Metallurgica 23.10: 1679-83, (1989).

CRC Handbook of Chemistry and Physics. 88th ed., 2007-2008.

Creighton, J. A., and D. G. Eadon. "Ultraviolet-Visible Absorption Spectra of the Colloidal Metallic Elements." Journal of the Chemical Society Faraday Transactions 87.24: 3881-91,(1991).

Dixit, S. G., A. R. Mahadeshwar, and S. K. Haram. "Some Aspects of the Role of Surfactants in the Formation of Nanoparticles." Colloids and Surfaces A: Physicochemical and Engineering Aspects 133.1-2: 69-75,(1998).

Eastman, J. A., S. U. S. Choi, S. Li, W. Yu, and L. J. Thompson. "Anomalously Increased Effective Thermal Conductivities of Ethylene Glycol-Based Nanofluids Containing Copper Nanoparticles." Applied Physics Letters 78.6: 718-20, (2001).

Eicke, Hans-friedrich , John C. W. Shepherd, and Adrian Steinemann. "Exchange of Solubilized Water and Aqueous Electrolyte Solutions between Micelles in Apolar Media." Journal of colloid and interface science 56.1: 168-76,(1976).

Eicke, Hans-Friedrich, and Juraj Rehak. "On the Formation of Water/Oil-Microemulsions." Helvetica chimica acta 59.8: 2883-91, (1976).

Faraday, Michael. "The Bakerian Lecture: Experimental Relations of Gold (and Other Metals) to Light." Philosophical Transactions of the Royal Society of London (1776-1886) 147.-1: 145-81, (1857).

Feldheim, D. L., and Foss Jr., C. A. Metal Nanoparticles; Synthesis, Characterization, and Applications. New York: Marcel Dekker, 2002.

Fendler, Janos H. "Interactions and Reactions in Reversed Micellar Systems." Accounts of Chemical Research 9.4: 153-61,(1976).

Filankembo, A., and M. P. Pileni. "Is the Template of Self-Colloidal Assemblies the Only Factor that Controls Nanocrystal Shapes?" The Journal of Physical Chemistry B 104.25: 5865-8,(2000a).

---. "Shape Control of Copper Nanocrystals." Applied Surface Science 164.1-4: 260-7 (2000b).

Fletcher, P., A. Howe, and B. Robinson. "The Kinetics of Solubilizate Exchange between Water Droplets of a Water in Oil Microemulsions." J. Chem. Soc. Faraday Trans. I 83.4: 985-1006, (1987).

Gai, P. L., and E. D. Boyes. Electron Microscopy in Heterogeneous Catalysis. Philadelphia: Institute of Physical Series in Microscopy in Materials Science, 2003.

García-Santibañez, F., A. Barragán-Vidal, A. Gutiérrez, M. Mendoza, J. A. Ascencio. "Experimental and Simulated Analysis of Cu Nanoparticles Produced by Cooled Sample Irradiation." Applied Physics A Materials Science & Processing 71.2: 219, (2000).

Giersig, Michael, and Paul Mulvaney. "Preparation of Ordered Colloid Monolayers by Electrophoretic Deposition." Langmuir 9.12: 3408-13, (1993).

Haberland, H. (ed). Clusters of Atoms and Molecules. New York: Springer-Verlag, 1994.

Hao, Z., E. W. Edwards, W. Dayang, and H. Mohwald. "Directing the Self-Assembly of Nanocrystals Beyond Colloidal Crystallization." Physical Chemistry Chemical Physics 8.28: 3288-99, (2006).

Hassan, P. A., S. R. Raghavan, and E. W. Kaler. "Microstructural Changes in SDS Micelles Induced by Hydrotropic Salt." Langmuir 18.7: 2543-8, (2002).

Hayat, M. A. (ed.). Colloidal Gold: Principles, Methods, and Applications. Vol. 1. New York: Academic Press, 1989.

Heath, James R., Charles M. Knobler, and Daniel V. Leff. "Pressure/temperature Phase Diagrams and Superlattices of Organically Functionalized Metal Nanocrystal Monolayers: The Influence of Particle Size, Size Distribution, and Surface Passivant." Journal of Physical Chemistry B 101.2: 189-97,(1997).

Henglein, Arnim. "Physicochemical Properties of Small Metal Particles in Solution: "Microelectrode" Reactions, Chemisorption, Composite Metal Particles, and the Atom-to-Metal Transition." The Journal of physical chemistry 97: 5457-71,(1993).

Henneke, D. E. Nanoparticles Produced Via Laser Ablation of Microparticles. University of Texas at Austin, 2001 Austin, Texas.

Hiemenz, P. C., and R. Rajagopalan. Principles of Colloid and Surface Chemistry. 3rd, rev. and expanded/ ed. ed. New York: Marcel Dekker, 1997.

Hirai, T., H. Sato, and I. Komasaawa. "Mechanism of Formation of CdS and ZnS Ultrafine Particles in Reverse Micelles." Science Citation Index Expanded™ (1900-1981) (1994).

HIRAI, T., Y. Tsubaki, H. Sato, and I. Komasaawa. "Mechanism of Formation of Lead Sulfide Ultrafine Particles in Reverse Micellar Systems." Science Citation Index Expanded™ (1900-1981) (1995).

Hoover, N. N., B. J. Auten, and B. D. Chandler. "Tuning Supported Catalyst Reactivity with Dendrimer-Templated Pt-Cu Nanoparticles." Journal of Physical Chemistry B 110.17: 8606-12, (2006).

Howe, A. M., J. A. McDonald, and B. H. Robinson. "Fluorescence Quenching as a Probe of Size Domains and Critical Fluctuations in Water-in-Oil Microemulsions." J. Chem. Soc. Faraday Trans. I 83.4: 1007-1027, (1987).

Ichinose, N., Y. Ozaki, and S. Kashu. Superfine Particle Technology. New York: Springer-Verlag, 1988.

Jana, Nikhil R., Latha Gearheart, and Catherine J. Murphy. "Wet Chemical Synthesis of Silver Nanorods and Nanowires of Controllable Aspect Ratio." Chemical Communications.7: 617-8, (2001).

- Jeong, S., K. Woo, D. Kim, S. Lim, J. S. Kim, H. Shin, Y. Xia, and J. Moon. "Controlling the Thickness of the Surface Oxide Layer on Cu Nanoparticles for the Fabrication of Conductive Structures by Ink-Jet Printing." Advanced Functional Materials 18.5: 679-86, (2008).
- Joshi, S. S., S. F. Patil, V. Iyer, and S. Mahumuni. "Radiation Induced Synthesis and Characterization of Copper Nanoparticles." Nanostructured Materials 10.7: 1135-44, (1998).
- Karch, J., R. Birringer, and H. Gleiter. "Ceramics Ductile at Low Temperature." Nature 330.6148: 556-8, (1987).
- Khanna, P. K., S. Gaikwad, P. V. Adhyapak, N. Singh, and R. Marimuthu. "Synthesis and Characterization of Copper Nanoparticles." Materials Letters 61.25: 4711-4, (2007).
- Kitchens, Christopher L. Metallic Nanoparticle Synthesis within Reverse Micellar Microemulsion Systems. Auburn University, 2004 Auburn, Alabama.
- Korgel, B. A., S. Fullam, S. Connolly, and D. Fitzmaurice. "Assembly and Self-Organization of Silver Nanocrystal Superlattices: Ordered "Soft Spheres"." Journal of Physical Chemistry B 102.43: 8379(1)-8380, (1998).
- Kotlarchyk, M., J. S. Huang, and S. H. Chen. "Structure of Aot-Reversed Micelles Determined by Small-Angle Neutron-Scattering." Science Citation Index Expanded™ (1900-1981) (1985).

Kreibig, U., and M. Vollmer. Optical Properties of Metal Clusters. Berlin: Springer-Verlag, 1996.

Kumar, R. V., Y. Mastai, Y. Diamant, and A. Gedanken. "Sonochemical Synthesis of Amorphous Cu and Nanocrystalline Cu Sub 2 O Embedded in a Polyaniline Matrix." Journal of Materials Chemistry 11.4: 1209-13, CSA Materials Research Database with METADEX (2001).

Leff, Daniel V., Lutz Brandt, and James R. Heath. "Synthesis and Characterization of Hydrophobic, Organically-Soluble Gold Nanocrystals Functionalized with Primary Amines." Langmuir 12.20: 4723-30, (1996).

Lisiecki, I., A. Filankembo, H. Sack-Kongehl, K. Weiss, M. P. Pileni, and J. Urban. "Structural Investigations of Copper Nanorods by High-Resolution TEM." Physical Review B (Condensed Matter) 61.7: 4968-74, (2000).

Lisiecki, I., and M. P. Pileni. "Copper Metallic Particles Synthesized "in Situ" in Reverse Micelles: Influence of various Parameters on the Size of the Particles." Journal of Physical Chemistry 99.14: 5077-82, 2002-05-01 (1995).

---. "Synthesis of Copper Metallic Clusters using Reverse Micelles as Microreactors." Journal of the American Chemical Society 115.10: 3887-96, 2002-05-01 (1993).

Liu, Z., and Y. Bando. "A Novel Method for Preparing Copper Nanorods and Nanowires." Advanced Materials 15.4: 303-5, (2003).

Liu, Zongwen, Yihua Gao, and Yoshio Bando. "Highly Effective Metal Vapor Absorbents Based on Carbon Nanotubes." Applied Physics Letters 81.25: 4844-6, (2002).

Liz-Marzán, Luis M. "Nanometals: Formation and Color." Materials Today, 7.2: 26-31, (2004).

Lu, L., M. L. Sui, and K. Lu. "Superplastic Extensibility of Nanocrystalline Copper at Room Temperature." Science 287.5457: 1463-6, (2000).

Maxwell, J. C. A Treatise on Electricity and Magnetism. 2nd ed. ed. Cambridge: Oxford University Press, 1904.

Molares, M. E. T., V. Buschmann, D. Dobrev, R. Neumann, R. Scholz, I. U. Schuchert, and J. Vetter. "Single-Crystalline Copper Nanowires Produced by Electrochemical Deposition in Polymeric Ion Track Membranes." Advanced Materials (FRG) (Germany) 13.1: 62-5, (2001a).

Molares, M. E. T., J. Brotz, V. Buschmann, D. Dobrev, R. Scholz, I. U. Schuchert, C. Trautmann, and J. Vetter. "Etched Heavy Ion Tracks in Polycarbonate as Template for Copper Nanowires." Nuclear Instruments and Methods in Physics Research, Section B: Beam Interactions with Materials and Atoms (Netherlands) 185.1-4: 192-7, (2001b).

Mott, D., J. Galkowski, L. Wang, J. Luo, and C. J. Zhong. "Synthesis of Size-Controlled and Shaped Copper Nanoparticles." Langmuir 23.10: 5740-5, (2007).

Mulvaney, P. "Surface Plasmon Spectroscopy of Nanosized Metal Particles." Langmuir 12.3: 788-800, (1996).

Naka, K., H. Itoh, and Y. Chujo. "Self-Organization of Spherical Aggregates of Palladium Nanoparticles with a Cubic Silsesquioxane." Nano Letters 2.11: 1183-6, (2002).

Ng, C. H. B., and W. Y. Fan. "Shape Evolution of Cu<sub>2</sub>O Nanostructures Via Kinetic and Thermodynamic Controlled Growth." Journal of Physical Chemistry B 110.42: 20801-7, (2006).

Niu, Y., and R. M. Crooks. "Preparation of Dendrimer-Encapsulated Metal Nanoparticles using Organic Solvents." Chemistry of Materials 15.18: 3463-7, (2003).

Petit, C., A. Taleb, and M. P. Pileni. "Cobalt Nanosized Particles Organized in a 2D Superlattice: Synthesis, Characterization, and Magnetic Properties." Journal of Physical Chemistry B 103.11: 1805-10, (1999).

Pileni, M. P., T. Gulik-Krzywicki, J. Tanori, A. Filankembo, and J. C. Dedieu. "Template Design of Microreactors with Colloidal Assemblies: Control the Growth of Copper Metal Rods." Langmuir 14.26: 7359-63, (1998).

Pileni, M. P., and J. Tanori. "Change in the Shape of Copper Nanoparticles in Ordered Phases." Advanced Materials 7.10: 862-4, (1995a).

---. "Change in the Shape of Copper Nanoparticles in Ordered Phases." Advanced Materials 7.10: 862-4, (1995b).

Pileni, M. P. "Colloidal Assemblies used as Templates to Control the Size, Shape and Self Organization of Nanoparticles." Berichte Der Bunsen-Gesellschaft - Physical Chemistry, Chemical Physics, 101.11: 1578-87 (1997).

Pileni, M. P., and S. Chevalier. "Comparison of the Photochemical Processes of Magnesium Tetraphenylporphyrin in Micellar and in Microemulsion Solution." Journal of Colloid and Interface Science 92.2: 326-31, (1983).

Pileni, M. P., B. Hickel, C. Ferradini, and J. Pucheault. "Hydrated Electron in Reverse Micelles." Chemical Physics Letters 92.3: 308-12, (1982).

Pileni, M. P., and I. Lisiecki. "Nanometer Metallic Copper Particle Synthesis in Reverse Micelles." Colloids and Surfaces A: Physicochemical and Engineering Aspects 80.1: 63-8, (1993).

Pileni, M. P., L. Motte, and C. Petit. "Synthesis of Cadmium Sulfide in Situ in Reverse Micelles: Influence of the Preparation Modes on Size, Polydispersity, and Photochemical Reactions." Chemistry of Materials 4.2: 338-45, 2002-05-01 (1992).

Pileni, M. P., B. W. Ninham, T. Gulik-krzywicki, J. Tanori, I. Lisiecki, and A. Filankembo.

"Direct Relationship between Shape and Size of Template and Synthesis of Copper Metal Particles." Science Citation Index Expanded™ (1900-1981) (1999).

Pileni, M. P. "Reverse Micelles as Microreactors." The Journal of physical chemistry 97: 6961-73, (1993).

Pileni, Marie-Paule, Thomas Zemb, and Christophe Petit. "Solubilization by Reverse Micelles: Solute Localization and Structure Perturbation." Chemical Physics Letters 118.4: 414-20, (1985).

Qi, Limin, Jiming Ma, and Julin Shen. "Synthesis of Copper Nanoparticles in Nonionic Water-in-Oil Microemulsions." Journal of Colloid and Interface Science, 186.2: 498-500, (1997).

Ressler, T., B. L. Kniep, I. Kasatkin, and R. Schlögl. "The Microstructure of Copper Zinc Oxide Catalysts: Bridging the Materials Gap." Angewandte Chemie International Edition 44.30: 4704-7, (2005).

Salzemann, C., I. Lisiecki, A. Brioude, J. Urban, and M. P. Pileni. "Collections of Copper Nanocrystals Characterized by Different Sizes and Shapes: Optical Response of these Nanoobjects." Journal of Physical Chemistry B 108.35: 13242-8, (2004).

Sano, N., K. Limura, H. Wang, I. Alexandrou, M. Chhowalla, and K. B. K. Teo. "Properties of Carbon Onions Produced by an Arc Discharge in Water." Journal of Applied Physics 92.5: 2783-8, (2002).

- Sato, H., T. Hirai, and I. Komasaawa. "Mechanism of Formation of Composite CdS-ZnS Ultrafine Particles in Reverse Micelles." Industrial & Engineering Chemistry Research 34: 2493-8, (1995).
- Schmid, G. (ed ). Clusters and Colloids from Theory to Applications. New York: VCH, 1994.
- Selvan, S. T., J. P. Spatz, H. A. Klok, and M. Moller. "Gold-Polypyrrole Core-Shell Particles in Diblock Copolymer Micelles." Advanced Materials 10.2: 132-4, (1998).
- Shukla, N., C. Liu, P. M. Jones, and D. Weller. "FTIR Study of Surfactant Bonding to FePt Nanoparticles." Journal of Magnetism and Magnetic Materials, 266.1-2: 178-84, (2003).
- Siegel, R. W., and G. E. Fougere. Mechanical Properties of Nanophase Materials. Ed. G. C. Hadjipanayis and R. W. Siegel. Dordrecht: Kluwer Academic Publishers, 1994.
- Siegel, R. W., E. Hu, and M. C. Roco. Nanostructure Science and Technology: R & D Status and Trends in Nanoparticles, Nanostructured Materials, and Nanodevices. Dordrecht: Kluwer, 1999.
- Sihai Chen, and D. L. Carroll. "Synthesis and Characterization of Truncated Triangular Silver Nanoplates." Nano Letters 2.9: 1003-7, (2002).
- Swami, A., A. Kumar, R. Pasricha, M. Sastry, and M. D'Costa. "Variation in Morphology of Gold Nanoparticles Synthesized by the Spontaneous Reduction of Aqueous Chloroaurate

- Ions by Alkylated Tyrosine at a Liquid-Liquid and Air-Water Interface." Journal of Materials Chemistry 14.17: 2696-702, (2004).
- Tanori, J., and M. P. Pileni. "Control of the Shape of Copper Metallic Particles by using a Colloidal System as Template." Langmuir 13.4: 639-46, (1997).
- Towey, T. F., A. Khanlodhi, and B. H. Robinson. "Kinetics and Mechanism of Formation of Quantum-Sized Cadmium-Sulfide Particles in Water Aerosol-Oil Microemulsions." Journal of the Chemical Society, Faraday Transactions 86.22: 3757-62, (1990).
- Turton, R. The Quantum Dot: A Journey into the Future of Microelectronics. New York: Oxford University Press, 1995.
- Ung, T., L. M. Liz-Marzan, and P. Mulvaney. "Optical Properties of Thin Films of Au@SiO<sub>2</sub> Particles." Journal of Physical Chemistry B 105.17: 3441-52, (2001).
- Vidoni, O., K. Philippot, C. Amiens, B. Chaudret, O. Balmes, J. O. Malm, J. O. Bovin, F. Senocq, and M. J. Casanove. "Novel, Spongelike Ruthenium Particles of Controllable Size Stabilized Only by Organic Solvents." Science Citation Index Expanded™ (2000-2004) (1999).
- Vukojević, S., O. Trapp, C. Kiener, F. Schüth, and J.-D. Grunwaldt. "Quasi-Homogeneous Methanol Synthesis Over Highly Active Copper Nanoparticles." Angewandte Chemie - International Edition 44.48: 7978-81, (2005).

- Wang X, and Q. Gao. "Synthesis of Copper(0) Nanoparticles in Nanoporous Nickel Phosphate VSB-1." Solid State Phenomena 121-123: 479-482, (2007).
- Wang, Y. H., P. L. Chen, and M. H. Liu. "Synthesis of Well-Defined Copper Nanocubes by a One-Pot Solution Process." Science Citation Index Expanded™ (2005-current) (2006).
- Wang, Z. L. "Transmission Electron Microscopy of Shape-Controlled Nanocrystals and their Assemblies." Journal of Physical Chemistry B 104.6: 1153-75, (2000).
- Weertman, J. R. "Hall-Petch Strengthening in Nanocrystalline Metals." Materials Science and Engineering A, 166.1-2: 161-7, (1993).
- Wu, Ming-Li , Dong-Hwang Chen, and Ting-Chia Huang. "Synthesis of Au/Pd Bimetallic Nanoparticles in Reverse Micelles." Langmuir 17.13: 3877-83, (2001).
- Wu, Szu-Han, and Dong-Hwang Chen. "Synthesis of High-Concentration Cu Nanoparticles in Aqueous CTAB Solutions." Journal of Colloid and Interface Science, 273.1: 165-9, (2004).
- Xie, Su-Yuan, Zhi-Jie Ma, Chin-Fang Wang, Shui-Chao Lin, Zhi-Yuan Jiang, Rong-Bin Huang, and Lan-Sun Zheng. "Preparation and Self-Assembly of Copper Nanoparticles Via Discharge of Copper Rod Electrodes in a Surfactant Solution: A Combination of Physical and Chemical Processes." Journal of Solid State Chemistry, 177.10: 3743-7, (2004).

Yanase, A., and H. Komiyama. "In Situ Observation of Oxidation and Reduction of Small Supported Copper Particles using Optical Absorption and X-Ray Diffraction." Surface Science 248.1-2: 11-9, (1991).

Yeh, M. -S., Y.-S. Yang, Y.-P. Lee, H.-F. Lee, Y.-H. Yeh, and C.-S. Yeh. "Formation and Characteristics of Cu Colloids from CuO Powder by Laser Irradiation in 2-Propanol." Journal of Physical Chemistry B 103.33: 6851-7, (1999).

Zhang, J. Z. Self-Assembled Nanostructures. New York: Kluwer Academic/Plenum Publishers, 2003.

Zhou, Y., S. H. Yu, X. P. Cui, C. Y. Wang, and Z. Y. Chen. "Formation of Silver Nanowires by a Novel Solid-Liquid Phase Arc Discharge Method." Chemistry of Materials 11.3: 545-6, (1999).